

CURRICULUM VITAE ABREVIADO (CVA)

IMPORTANT – The Curriculum Vitae cannot exceed 4 pages. Instructions to fill this document are available in the website.

Part A. PERSONAL INFORMATION

First name	José Luis		
Family name	Crespo González		
Gender (*)	Male	Birth date (dd/mm/yyyy)	
Social Security, Passport, ID number			
e-mail		URL Web	
Open Researcher and Contributor ID (ORCID) (*)			

(*) Mandatory

A.1. Current position

Position	Investigador Científico - Director of IBVF		
Initial date	17/02/2021		
Institution	Consejo Superior de Investigaciones Científicas (CSIC)		
Department/Center	IBVF	Instituto de Bioquímica Vegetal y Fotosíntesis	
Country	Spain	Teleph. number	954489574
Key words	TOR signaling, autophagy, CO ₂ , stress, Chlamydomonas, alga		

A.2. Previous positions (research activity interruptions, indicate total months)

Period	Position/Institution/Country/Interruption cause
2008-2021	Científico Titular (CSIC) at IBVF
2003-2008	Ramón y Cajal researcher at IBVF
1999-2003	FEBS postdoctoral fellow at the Prof. Michael Hall lab (Biozentrum, Basel, Switzerland)

A.3. Education

PhD, Licensed, Graduate	University/Country	Year
PhD in Biology	Universidad de Sevilla (US)	1999
Degree in Biology	Universidad de Sevilla (US)	1993

Part B. CV SUMMARY (max. 5000 characters, including spaces)

Research career: My research career was initiated with the study of nitrogen metabolism in cyanobacteria during my PhD at the University of Sevilla. After completing my PhD, I performed a postdoctoral stay (1999-2003) at the Biozentrum (University of Basel, CH) to investigate the TOR signaling pathway under the supervision of Prof. Michael Hall with the support of a FEBS long-term fellowship. In 2003 I got a *Ramón y Cajal* research position at the IBVF to investigate the TOR signaling pathway in photosynthetic organisms using the single-celled green alga *Chlamydomonas reinhardtii* as model system. In 2008, I got a permanent position at CSIC as *Científico Titular* to continue my research work on the TOR pathway and autophagy, a TOR-controlled process highly conserved in all eukaryotes. In 2021, I was promoted to *Investigador Científico* at CSIC, and since March 2022 I am the Director of IBVF.

Main research achievements: During my postdoctoral stay at the Prof. Hall's lab, we found that Gln regulates the yeast TOR signaling pathway (Crespo et al. 2002 PNAS) and described for the first time the localization of the TOR kinase in two complexes, TORC1 and TORC2 (Loewith et al. 2002 Mol Cell). Since 2003, I am responsible of the research group "TOR signaling and autophagy in microalgae" at IBVF. Our group has been a pioneer in the study of

the TOR pathway and autophagy in microalgae (Crespo et al. 2005 Plant Physiol; Pérez-Pérez et al. 2010 Plant Physiol; Díaz-Troya et al. 2011 Plant Physiol; Pérez-Pérez et al. 2012 Autophagy). We have described the process of autophagy in algae and demonstrated that TOR negatively regulates this catabolic process for the first time in photosynthetic organisms (Pérez-Pérez et al. 2010 Plant Physiol). Our studies have shown that autophagy is subjected to redox regulation (Pérez-Pérez et al. 2012 Autophagy; Pérez-Pérez et al. 2014 Autophagy; Pérez-Martín et al. 2014 Plant Physiol; Pérez-Pérez et al. 2016 Plant Physiol; Pérez-Pérez et al. 2021 JXB) and maintains chloroplast homeostasis (Heredia-Martínez et al. 2018 Plant Physiol). More recently, our group has made significant contributions to understand the nutrient regulation of TOR and the underlying mechanisms in photosynthetic organisms. We have established that phosphorous availability regulates TOR activity in *Chlamydomonas* via LST8, a TORC1 core protein essential for TOR function (Couso et al. 2020 Plant Cell). Moreover, our group has demonstrated that photosynthetic assimilation of CO₂ activates TOR (Mallén-Ponce et al. 2022 PNAS; Mallén-Ponce et al. 2022 JXB; Mallén-Ponce et al. 2022 New Phytol). This study revealed for the first time a direct link between CO₂ fixation, photosynthesis and TOR. Recently, we identified dihydroxyacetone phosphate (DHAP) generated in the chloroplast as the key metabolite mediating CO₂ and light signals to TOR in photosynthetic cells (Mallén-Ponce, et al. Science Advance). Moreover, we have initiated a new research line to investigate TOR signaling and autophagy in extremophilic organisms (Pérez-Pérez et al. 2024 New Phytol) and their biotechnological and ecological potential. My current research work aims to unravel the nutrient regulation of the TOR kinase in photosynthetic cells, the TOR-target interactome as well as the potential biotechnological implications of this signaling pathway in microalgae.

Research training experience: I have supervised the research work of 3 PhD researchers: Sandra Díaz-Troya (2009), currently professor at the University of Sevilla, Marta Pérez-Martín (2016), currently postdoc at University of Texas, Luis Heredia-Martínez (2022), who is a postdoc at University of Seville. Currently, I am supervising 2 Theses: Yosú Odriozola, supported by an FPI fellowship; and Irene Muñoz granted by the *Garantía Juvenil* program. I have also supervised the work of several PhD researchers during short-term stays performed in my lab in the frame of international collaborations: S. Schmolinger and P. Muller (from Dr Schroda lab), and S. Morisse (from Dr Lemaire lab).

I have also mentored the work of several postdocs in my group: Emilio Gutiérrez-Beltrán, first as Marie Curie-Sklodowska fellow (H2020-MSCA-IF-2015) and then as *Juan de la Cierva-Incorporación* researcher (2018-2019), Inmaculada Couso-Liañez as Comfuturo researcher and Marie Curie-Sklodowska fellow (H2020-MSCA-IF-2016), Águila Ruiz-Sola (2019) and Manuel Mallén-Ponce (2021), both as *Juan de la Cierva-Incorporación* researchers in my group. Moreover, I have supervised international postdoc researchers for short-term stays: M. Bedhome (France), M. Carbó (Czech Republic) and C. Paliwal (Czech Republic).

Internationalization: My research allowed me to establish a solid network of international collaborators: Dr Grossman, Stanford; Dr Field, CEA Marseille; Dr Lemaire, CNRS Paris; Dr Schroda, Kaiserslautern; Dr Merchant, Berkeley; Dr Umen, Danford; Dr Hicks, U North Carolina. I have publications led by our group with most of them. In addition, I have been enrolled in a European consortium to set up Synthetic Biology tools in *Chlamydomonas* (Crozet et al 2018 ACS Synth Biol; Crozet et al in preparation).

Reviewer experience: Member of the Evaluation Panel (PID2022) in the Biosciences and Biotechnology Section (Research National Agency). External reviewer for research programs from international institutions (ERC, Europe; ANR, France; SNF, USA; SNSF, Switzerland; BARD, Israel-USA; GIF, Germany-Israel; FONCYT, Argentina). Manuscript reviewer for different journals including The Plant Cell, Autophagy, Nature Comm, Plant Physiology, New Phytologist, J Exp Botany, etc.

Part C. RELEVANT MERITS (sorted by typology)

C.1. Publications (10 selected contributions from a total of 30 in last 10 years). ^{CA}, corresponding author.

Research productivity (WoS): total number of publications in indexed journals: 61; total citations: 13.484; h index: 34.

1. Mallén-Ponce MJ, Quintero-Moreno A, Gámez-Arcas S, Grossman AR, Pérez-Pérez ME, Crespo JL^{CA} (2025) Dihydroxyacetone phosphate generated in the chloroplast mediates the activation of TOR by CO₂ and light. **Science Advances** 11(16):eadu1240. IF: 11.7. D1. <https://doi.org/10.1126/sciadv.adu1240>
2. Pérez-Pérez ME^{CA}, Mallén-Ponce MJ, Odriozola-Gil Y, Rubio A, Salas JJ, Martínez-Force E, Pérez-Pulido AJ, Crespo JL^{CA} (2024) Lipid turnover through lipophagy in the newly identified extremophilic green microalga *Chlamydomonas urium*. **New Phytologist** 243: 284-298 IF: 9.4. D1. <https://doi.org/10.1111/nph.19811>.
3. Mallén-Ponce MJ, Pérez-Pérez ME, Crespo JL^{CA} (2022) Photosynthetic assimilation of CO₂ regulates TOR activity. **Proc Natl Acad Sci USA** 119 (2): e2115261119. IF: 11.205. D1 <https://doi.org/10.1073/pnas.2115261119>.
4. Mallén-Ponce MJ, Pérez-Pérez ME, Crespo JL^{CA} (2022) Analyzing the impact of autotrophic and heterotrophic metabolism on the nutrient regulation of TOR. **New Phytologist** 236: 1261-1266. IF: 9.4. D1 <https://doi.org/10.1111/nph.18450>.
5. Mallén-Ponce MJ, Pérez-Pérez ME, Crespo JL^{CA} (2022) Deciphering the function and evolution of the target of rapamycin signaling pathway in microalgae. **J Exp Botany** 73: 6993-7005. IF:6.992. D1. <https://doi.org/10.1093/jxb/erac264>.
6. Gutierrez-Beltran E, Elander PH, Dalman K, Dayhoff GW 2nd, Moschou PN, Uversky VN, Crespo JL, Bozhkov PV (2021) Tudor staphylococcal nuclease is a docking platform for stress granule components and is essential for SnRK1 activation in Arabidopsis. **EMBO J** 40:e105043. IF: 11.598. D1 doi.org/10.15252/embj.2020105043.
7. Couso I, Pérez-Pérez ME, Ford MM, Martínez-Force E, Hicks LM, Umen JG, Crespo JL^{CA} (2020) Phosphorus availability regulates TORC1 signaling in *Chlamydomonas*. **The Plant Cell** 32: 69-80. IF:11.277. D1 <https://doi.org/10.1105/tpc.19.00179>.
8. Laureano-Marín AM, Aroca A, Pérez-Pérez ME, Yruea I, Jurado-Flores A, Moreno I, Crespo JL, Romero LC, Gotor C (2020) Absciscic Acid-Triggered Persulfidation of the Cys Protease ATG4 Mediates Regulation of Autophagy by Sulfide. **The Plant Cell** 32(12): 3902-3920. IF:11.277. D1 <https://doi.org/10.1105/tpc.20.00766>.
9. Heredia-Martínez LG, Andrés-Garrido A, Martínez-Force E, Pérez-Pérez ME^{CA}, Crespo JL^{CA} (2018) Chloroplast damage induced by the inhibition of fatty acid synthesis triggers autophagy in *Chlamydomonas*. **Plant Physiol** 178(3): 1112-1129. IF: 6.305. D1. **Selected for journal cover** <https://doi.org/10.1104/pp.18.00630>.
10. Pérez-Pérez ME^{CA}, Lemaire SD, Crespo JL (2016) Control of autophagy in *Chlamydomonas* is mediated through redox-dependent inactivation of the ATG4 protease. **Plant Physiol** 172: 2219-2234. IF: 6.456. D1 <https://doi.org/10.1104/pp.16.01582>.

C.2. Congress

Organizer:

- EMBO Workshop Target of Rapamycin signaling in photosynthetic organisms. October 2021.
- Sociedad Española de Autofagia (SEFAGIA) 2022. Toledo, November 2022.
- Sociedad Española de Autofagia (SEFAGIA) 2020. Cáceres, March 2020.
- Sociedad Española de Autofagia (SEFAGIA) 2018. Miraflores de la Sierra, November 2018.
- Spanish Network for Autophagy Research (NEAR) 2017. Miraflores de la Sierra, Nov 2017.
- Spanish Network for Autophagy Research (NEAR) 2016. Miraflores de la Sierra, June 2016.
- First Joint Meeting of Nordic, Spanish and French Autophagy Networks. Toulouse, France September 2014.

Scientific committee:

- Plant Autophagy: Improving Crop and Energy Production. Transautophagy COST. Madrid, March 2017.
- 16th International Conference on the Cell and Molecular Biology of *Chlamydomonas*. Asilomar, Pacific Grove, USA, June 2014.

Keynote/invited at international conferences:

- French Society of Photosynthesis. Paris, France, May 2025.
- Plant Energy Management: Molecular Mechanisms and Signaling. Umea, Sweden, Aug 2024.

- 20th International Conference on the Cell and Molecular Biology of Chlamydomonas. Princeton, USA June 2023.
- 19th International Conference on the Cell and Molecular Biology of Chlamydomonas. Ile des Embiez, France, August 2021.
- 9th European Symposium on Plant Lipids. Marseille, July 2019.
- EMBO Workshop Target of rapamycin (TOR) signaling in photosynthetic organisms. Bischoffsheim, France, May 2018.

C.3. Research projects, indicating your personal contribution.

International grants as Principal Investigator:

- “Understanding how Inositol Polyphosphates regulate autophagy and lipid body formation in photosynthetic organisms: crosstalk with TOR signaling”. European Commission H2020-MSCA-IF-2016. Duration: 2018-2020. Budget: 170.121 €.
- “Functional analysis of Stress Granules formation in plant adaptation to stress”. European Commission H2020-MSCA-IF-2015. Duration: 2017-2019. Budget: 170.121 €.
- “Molecular mechanism of autophagy in algae and its application in algal fuels”. Korean Research Institute of Bioscience & Biotechnology (KRIBB). Duration: 2015-2019. Budget: 190.023 €.

National grants as Principal Investigator:

- “New insights in the molecular regulation of TOR by light and CO₂ signals (RegulaTOR). Ministerio de Ciencia e Innovación (PID2024-162302NB-I00). Duration: 2025-2028. Budget: 268.750 € (plus FPI fellow).
- “Modulating the TOR signaling pathway to improve CO₂ assimilation into biomass (TORCO₂)”. Ministerio de Ciencia e Innovación (TED2021-130912-B-100). Duration: 2022-2025. Budget: 230.000 €.
- “Elucidating the nutrient regulation of TOR signaling in photosynthetic organisms (GREENTOR)”. Ministerio de Ciencia e Innovación (PID2021-123500-NB-100). Duration: 2022-2025. Budget: 217.800 € (plus FPI fellowship).
- “Elucidating the mechanisms for selective autophagy in the alga *Chlamydomonas*”. Ministerio de Economía y Competitividad (PGC2018-099048-B-100). Duration: 2019-2021. Budget: 137.698 €.
- “Redox control of autophagy”. Ministerio de Economía y Competitividad (BFU2015-68216-P). Duration: 2016-2018. Budget: 201.586 € (plus FPI fellowship).
- “Control of autophagy by TOR signaling and ROS in *Chlamydomonas*”. Ministerio de Economía y Competitividad (BFU2012-35913). Duration: 2013-2015. Budget: 138.060 €.

Regional grants as Principal Investigator:

- “Application of extremophilic microalgae for wastewater bioremediation (ALGAclean)”. Junta de Andalucía (DGP_PIDI_2024_01534). *Under evaluation*.
- “Autophagy in a new extremophilic microalgae”. Junta de Andalucía/Proyectos de Excelencia (P20-00057). Duration: 01/01/2021-31/12/2022. Budget: 80.000 €.
- “Autophagy as a cell adaptation process to stress in photosynthetic organisms”. Junta de Andalucía (CVI-7336). Duration: 01/02/2013-30/09/2016. Budget: 158.705 €.

C.4. Contracts, technological or transfer merits

Research transfer to society:

- Elaboration of the CSIC White Paper on Sustainable Primary Production-Biotechnology and Plant Breeding (CSIC SCIENTIFIC CHALLENGES: TOWARDS 2030).
- Collaboration with the company AGRISERA for the generation of ATG8 and ATG4 antibodies.
- Participation in the project GENETDIESEL (960.000 €) with the company ALGAENERGY.

Outreach activities:

- Participation in Feria de la Ciencia, Café con Ciencia, and European Researchers Night.
- Management of social media (X: @ChlamyAutophagy).

C.5. Teaching activity

- External prof. Master Molecular Genetics and Biotechnology (Univ. Sevilla), 2018-present
- Degree in Biology (Univ. Sevilla), 2003-2008
- Accreditation as “Profesor Contratado Doctor” (ANECA), 2008

PLANT SCIENCES

Dihydroxyacetone phosphate generated in the chloroplast mediates the activation of TOR by CO₂ and light

Manuel J. Mallén-Ponce¹, Andrea M. Quintero-Moreno¹, Samuel Gámez-Arcas¹, Arthur R. Grossman^{2,3}, María Esther Pérez-Pérez¹, José L. Crespo^{1*}

Light and CO₂ assimilation activate the target of rapamycin (TOR) kinase in photosynthetic cells, but how these signals are transmitted to TOR is unknown. Using the green alga *Chlamydomonas reinhardtii* as a model system, we identified dihydroxyacetone phosphate (DHAP) as the key metabolite regulating TOR in response to carbon and light cues. Metabolomic analyses of synchronized cells revealed that DHAP levels change more than any other metabolite between dark- and light-grown cells and that the addition of the DHAP precursor, dihydroxyacetone (DHA), was sufficient to activate TOR in the dark. We also demonstrated that TOR was insensitive to light or inorganic carbon but not to exogenous DHA in a *Chlamydomonas* mutant defective in the export of DHAP from the chloroplast. Our results provide a metabolic basis for the mode of TOR control by light and inorganic carbon and indicate that cytoplasmic DHAP is an important metabolic regulator of TOR.

INTRODUCTION

The highly conserved target of rapamycin (TOR) is a serine-threonine protein kinase that is a member of the phosphatidylinositol 3-kinase-related protein kinase family. This kinase integrates nutrient, energy, and environmental signals to promote cell growth in all eukaryotes. This nutrient sensor binds to the key proteins regulatory-associated protein of TOR (Raptor) and lethal with SEC13 protein 8 (LST8) to constitute the TOR complex 1 (TORC1), which is conserved through evolution (1). Control of TOR signaling by nutrients has been extensively investigated in yeasts and mammals (2, 3). In these organisms, TOR responds to glucose and amino acids, particularly glutamine, leucine, and arginine, as main nutrient-activation signals with the underlying regulatory mechanisms connecting these nutrients to TOR activity partially elucidated (2, 3).

TOR and its associated proteins Raptor and LST8 are functionally and structurally conserved in the green lineage (4–7). In plants, TOR coordinates hormone, nutrient, and energy signals to regulate fundamental processes including translation, transcription, cell expansion, autophagy, metabolism, and nutrient assimilation. Carbon and nitrogen availability is the primary nutrient signal acting upstream of TOR in plants (8). Glucose has been shown to activate TOR kinase activity in the root apex through glycolysis and mitochondrial energetics (9), but light inputs are also required for full TOR activation in photosynthetic tissues (10). The mechanisms by which glucose and light cues are transmitted to TOR in plants are starting to be elucidated, with mounting evidence indicating that the Rho-related protein from plants 2 (ROP2) guanosine triphosphatase acts as a key regulator of TOR in plants. ROP2 binds to and activates TOR in response to both light and auxin signals (10, 11). However, glucose signaling does not appear to be mediated via ROP2, suggesting that glucose and light activation of TOR are elicited by different regulatory pathways (10). Plant TOR signaling is also regulated by inorganic nitrogen and amino acids such as glutamine and

branched-chain amino acids (12–15). Although the precise underlying mechanism linking nitrogen to TOR is not fully understood, it has been shown that nitrate, ammonium, and glutamine stimulate ROP2 to activate TOR (12).

The TOR pathway has also been investigated in microalgae, mostly in the model green alga *Chlamydomonas reinhardtii* (hereafter *Chlamydomonas*). Chemical inhibition of TOR mimics a nutrient starvation response, which includes activation of autophagy and an increase in the levels of triacylglycerol and starch, the main intracellular carbon reservoirs (16–18). Under photosynthetic growth, microalgae use light energy to fix atmospheric carbon (CO₂) through the Calvin-Benson-Bassham (CBB) cycle. Photosynthetic CO₂ assimilation provides carbon skeletons for all reactions in the cell, including the mitochondrial tricarboxylic acid (TCA) cycle and the synthesis of starch and lipids (Fig. 1A) [reviewed in (19)]. In microalgae such as *Chlamydomonas*, fixed carbon is exported from the chloroplast mostly as triose phosphate [dihydroxyacetone phosphate (DHAP) and glyceraldehyde 3-phosphate (GAP)], which are then used for the biosynthesis of other metabolites and to drive respiratory activity (Fig. 1A). Metabolomic, transcriptomic, and proteomic studies revealed that TOR operates as a central hub regulating primary metabolism and integrating nutrient signals including phosphorus, nitrogen, amino acids, and inorganic carbon in microalgae (5, 20–24). The intracellular level of phosphorus regulates TOR activity in *Chlamydomonas* via LST8, with phosphorus limitation causing a decrease in LST8 protein abundance and TOR activity (24). Nitrogen is an important nutrient acting upstream of TOR in *Chlamydomonas*, although the underlying mechanism remains unknown (23). Amino acids are also major regulators of TOR activity in microalgae. A metabolomic analysis of *Chlamydomonas* cells treated with inhibitors of the synthesis of alanine or the branched-chain amino acids leucine and valine showed that TOR responds to the intracellular abundance of these amino acids (5). Furthermore, the photosynthetic assimilation of CO₂ has also been demonstrated to regulate TOR activity in *Chlamydomonas* (5). Inhibition of CO₂ fixation or photosynthetic electron transport inactivates TOR, but how carbon and light signals are linked to TOR in photosynthetic cells is unknown. In this study, we identify a central metabolite connecting

Copyright © 2025 The Authors, some rights reserved; exclusive licensee American Association for the Advancement of Science. No claim to original U.S. Government Works. Distributed under a Creative Commons Attribution NonCommercial License 4.0 (CC BY-NC).

¹Instituto de Bioquímica Vegetal y Fotosíntesis (CSIC-Universidad de Sevilla), 41092 Sevilla, Spain. ²Biosphere Sciences & Engineering, Carnegie Institution for Science, Stanford, CA 94305, USA. ³Biology Department, Stanford University, Stanford, CA 94305, USA.

*Corresponding author. Email: crespo@ibvf.csic.es

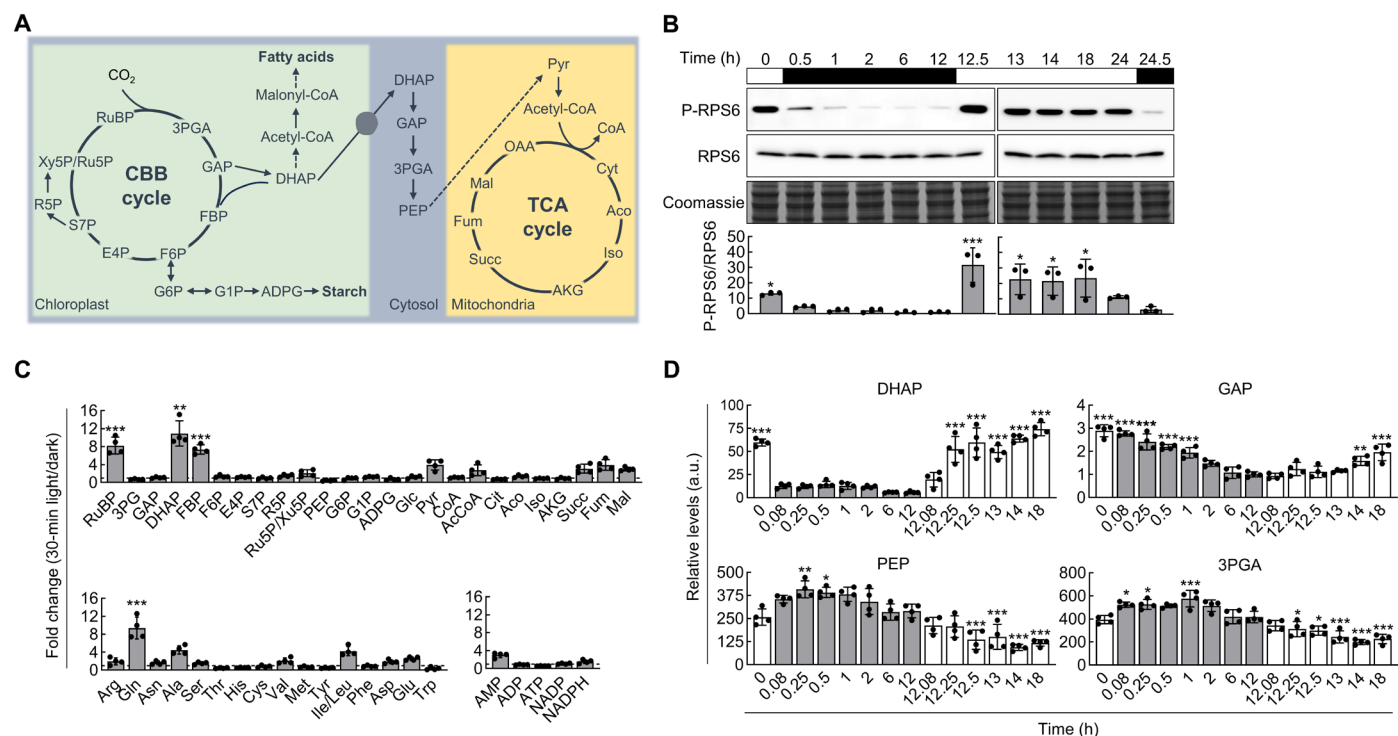


Fig. 1. Overview of TOR activity and central metabolism over the diurnal cycle in synchronized *Chlamydomonas* cells. (A) Schematic representation of CBB and TCA cycles in *Chlamydomonas* [adapted from (19)]. (B) Immunoblot analysis of P-RPS6/RPS6 in *Chlamydomonas* cells over one diurnal cycle. Coomassie brilliant blue–stained gels were used as loading control (19). h, hours. (C) Bar graph representation of fold change for CBB and TCA cycle intermediates, central metabolites, amino acids, and energy- and reducing power–related metabolites. Data were calculated using the relative levels in darkness (12 hours) and after 30 min of reillumination (12.5 hours). A fold change of 1 (no change) is indicated with a dashed line. (D) Relative abundance of central carbon intermediates (DHAP, GAP, PEP, and 3PGA) over one diurnal cycle. *Chlamydomonas* cells were grown in TP medium. Error bars in (B) to (D) correspond to SD from at least three biological replicates. Asterisks represent significant differences according to one-way ANOVA and Bonferroni's test: *** $P < 0.001$; ** $P < 0.01$; * $P < 0.05$; not significant, ≥ 0.05 . The statistical analyses described apply to all statistical analyses in this figure (detailed in table S8). F6P, fructose 6-phosphate; E4P, erythrose 4-phosphate; S7P, sedoheptulose 7-phosphate; R5P, ribose 5-phosphate; Xy5P/Ru5P, xylulose 5-phosphate/ribulose 5-phosphate; G1P, glucose 1-phosphate; ADPG, adenosine diphosphate glucose; Pyr, pyruvate; Cit, citrate; Aco, aconitate; Iso, isocitrate; Succ, succinate; Fum, fumarate; Mal, malate; OAA, oxaloacetate. Arg, arginine; Gln, glutamine; Asn, asparagine; Ala, alanine; Ser, serine; Thr, threonine; His, histidine; Cys, cysteine; Val, valine; Met, methionine; Tyr, tyrosine; Ile/Leu, isoleucine/leucine; Phe, phenylalanine; Asp, aspartate; Glu, glutamate; Trp, tryptophan. a.u., arbitrary units. White and black bars indicate light and dark phases, respectively.

carbon and light signals to TOR using metabolomic, chemical, and genetic approaches in *Chlamydomonas* cells.

RESULTS

DHAP regulates TOR activity in response to light and inorganic carbon

We have previously demonstrated that TOR is activated by light and inactivated in the dark in *Chlamydomonas* cells (5). To understand the effect of light on TOR activity, we monitored RPS6 phosphorylation in synchronized cells (fig. S1A). TOR was markedly and progressively inactivated following transfer of the cells to the dark, whereas a sharp reactivation was observed upon illumination (Fig. 1B). The dark-mediated inactivation of TOR did not occur when the synchronized cells were maintained in continuous light following the dark period (fig. S1B), suggesting that TOR activity is not subjected to circadian regulation in *Chlamydomonas*. The fast and strong activation of TOR by light prompted us to further characterize this process. We initiated this characterization with an in-depth metabolomic analysis of synchronized *Chlamydomonas* cells over a diurnal cycle. The abundance of more than 50 primary metabolites was determined,

including amino acids, energy-related metabolites, and intermediates from the CBB and TCA cycles. Our results revealed a pronounced increase in some metabolites when cells enter the light phase of the diurnal cycle. The most highly up-regulated metabolites included the CBB cycle intermediates DHAP, ribulose 1,5-bisphosphate (RuBP), and fructose 1,6-bisphosphate (FBP), and the amino acid glutamine (Fig. 1C; fig. S2, A and B; and table S1). The levels of these metabolites were elevated in the light and diminished in the dark phase of the diurnal cycle (Fig. 1D, fig. S2A, and table S1). In *Chlamydomonas*, FBP and RuBP are generated and metabolized in the chloroplast through the CBB cycle (19, 25), whereas DHAP is mostly synthesized in this organelle and actively exported to the cytoplasm (26). DHAP is converted to GAP, 3-phosphoglycerate (3PGA), and phosphoenolpyruvate (PEP), which feeds the TCA cycle through the synthesis of pyruvate and acetyl-CoA in mitochondria (Fig. 1A). Our metabolomic analysis indicated that the levels of GAP, 3PGA, and PEP did not increase in response to light (Fig. 1D and table S1). However, in notable contrast, the abundance of DHAP rose 20 times within 15 min of exposure to the light (Fig. 1D and table S1).

On the basis of these results, we speculated that DHAP might have a positive impact on TOR activity in *Chlamydomonas*. To test

this hypothesis, we analyzed the effect of dihydroxyacetone (DHA), the triose precursor to DHAP (fig. S3), on TOR in *Chlamydomonas* cells after being kept in the dark for 6 hours, when TOR activity reached its lowest level (Fig. 1B). We first confirmed that exogenously added DHA was efficiently converted to DHAP in *Chlamydomonas*. DHAP was readily detected following DHA addition (Fig. 2A and table S2). Conversion of DHA to DHAP is catalyzed by the enzyme dihydroxyacetone kinase 1, whose expression has been confirmed in *Chlamydomonas* (27). Moreover, a rapid rise in TCA cycle intermediates and other metabolites was detected upon DHA addition (fig. S4A and table S2), indicating that DHA is first converted to DHAP and then further metabolized. The analysis of RPS6 phosphorylation in DHA-treated cells revealed a marked and rapid activation of TOR in the dark (Fig. 2A). Our results indicated that 2 mM DHA was sufficient to activate TOR within 30 min under dark conditions and higher concentrations of DHA did not further increase TOR activity (fig. S4B). The DHA-mediated induction of TOR was transient and TOR activity decreased within 60 min of DHA addition, likely as a consequence of the decrease in DHAP (Fig. 2A).

Given that DHAP also participates in the synthesis of fatty acids in the chloroplast, and lipids represent a major sink of fixed carbon in algae (28), we examined the effect of blocking fatty acid synthesis on both DHAP abundance and TOR activity by using the fatty acid synthase inhibitor cerulenin (Fig. 1A and fig. S3) (29). Treatment of *Chlamydomonas* cells with cerulenin in the light phase of the diurnal cycle caused an increase in the abundance of DHAP (Fig. 2B) and other metabolites (fig. S5A and table S3), particularly the fatty acid precursor malonyl-CoA, which displayed a 100-fold boost resulting

from the efficient inhibition of fatty acid synthase activity (fig. S5, A and B). We detected rapid activation of TOR in cerulenin-treated cells (Fig. 2B), supporting a potential link between the level of DHAP and TOR activity.

TCA cycle intermediates and glutamine are not required for the activation of TOR by light

In plants, glucose activates TOR through glycolysis and mitochondrial function (9). To investigate whether TOR may respond to an increase in the level of TCA cycle intermediates in *Chlamydomonas*, cells maintained in the dark were supplemented with dimethyl- α -ketoglutarate (DMKG), an esterified analog of α -ketoglutarate (AKG) that permeates the cell membranes and is hydrolyzed to α -ketoglutaric acid (30). Addition of DMKG to *Chlamydomonas* cells resulted in a rapid increase in AKG along with other TCA cycle intermediates including malate, fumarate, and succinate (fig. S6, A and B, and table S4). DMKG had no significant effect on TOR activity (Fig. 2C), indicating that TOR does not respond to changes in the abundance of TCA cycle metabolites under these experimental conditions. In addition, the DMKG treatment did not alter the abundance of DHAP (Fig. 2C). Together, these results suggested that activation of TOR by DHA is not due to the increase in TCA cycle intermediates detected following DHA supplementation.

The metabolomic analysis of synchronized *Chlamydomonas* cells showed that, like DHAP, glutamine abundance increased in the light and decreased in the dark (fig. S2A and table S1). Because this amino acid regulates TOR in different organisms including microalgae (5, 31, 32), we investigated whether glutamine participates in the

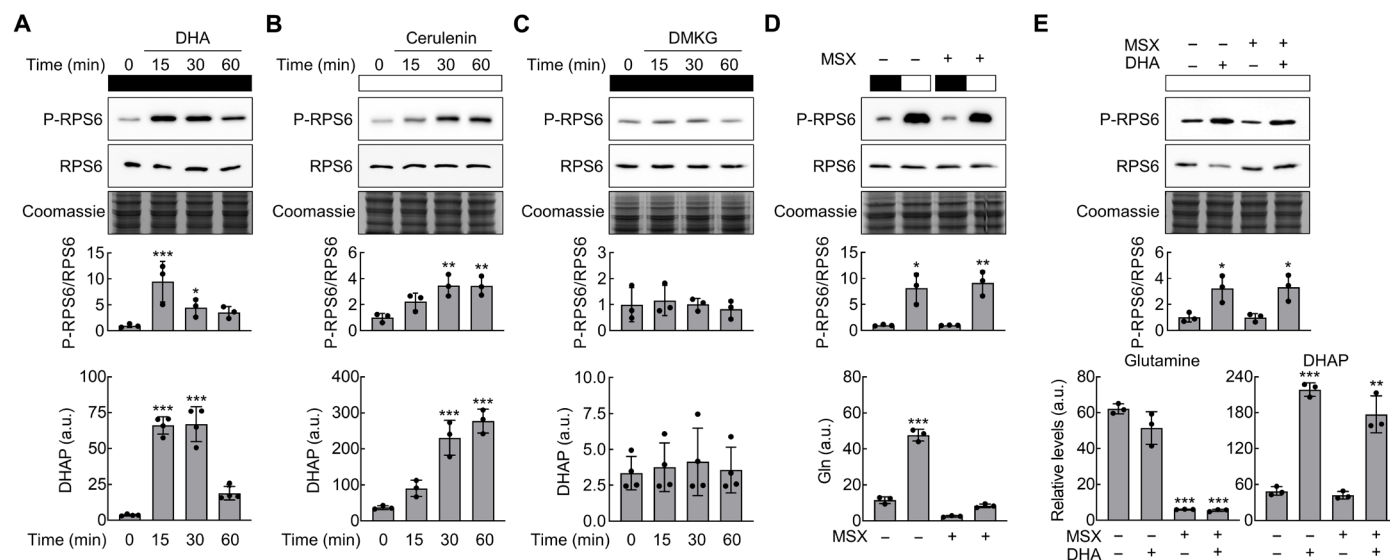


Fig. 2. Effect of DHA, cerulenin, DMKG, or MSX on TOR activity. (A) Immunoblot (upper panel) of P-RPS6/RPS6 in *Chlamydomonas* cells treated with 2 mM DHA (0, 15, 30, and 60 min) over the night part of the diurnal cycle. Relative abundance (lower panel) of DHAP in cells treated with 2 mM DHA (0, 15, 30, and 60 min). (B) Immunoblot (upper panel) of P-RPS6/RPS6 in cells treated with 20 μ M cerulenin (0, 15, 30, and 60 min) over the day part of the diurnal cycle. Relative abundance (lower panel) of DHAP in cells treated with 20 μ M cerulenin (0, 15, 30, and 60 min). (C) Immunoblot (upper panel) of P-RPS6/RPS6 in cells treated with 2 mM DMKG (0, 15, 30, and 60 min) over the night part of the diurnal cycle. Relative abundance (lower panel) of DHAP in cells under the same conditions. (D) Immunoblot (upper panel) of P-RPS6/RPS6 and relative abundance (lower panel) of Gln in cells treated or not with 5 mM MSX for 2 hours over the night part of the diurnal cycle and then reilluminated for 30 min. (E) Immunoblot (upper panel) of P-RPS6/RPS6 and relative abundance (lower panel) of Gln and DHAP in cells treated or not with 5 mM MSX for 2 hours and then 2 mM DHA for 30 min over the day part of the diurnal cycle. Coomassie brilliant blue–stained gels were used as a loading control. *Chlamydomonas* cells were grown in TP medium. Error bars correspond to SD from at least three biological replicates. Asterisks represent significant differences according to one-way ANOVA: *** $P < 0.001$; ** $P < 0.01$; * $P < 0.05$; not significant, ≥ 0.05 . The statistical analyses described apply to all statistical analyses in this figure (detailed in table S8). White and black bars indicate light and dark phases, respectively.

up-regulation of TOR mediated by light and carbon. For this, we analyzed TOR activity and the metabolomic profile of *Chlamydomonas* cells upon illumination in the presence or absence of the glutamine synthetase inhibitor L-methionine sulfoximine (MSX) (fig. S3). In these assays, MSX was added before illumination to prevent the light-mediated induction of glutamine when cells are shifted from dark to light conditions. Our results revealed a similar activation of TOR by light in control and MSX-treated cells (Fig. 2D). As expected, MSX largely suppressed the light-triggered up-regulation of glutamine levels (Fig. 2D and table S5). Furthermore, we investigated whether glutamine participates in the activation of TOR by DHA. These experiments were performed during the light part of the diurnal cycle because glutamine synthesis is repressed under dark conditions (fig. S2A). To study the role of glutamine in TOR activation by DHA, cells were treated with MSX before the addition of DHA. Metabolomic analysis of these cells showed that MSX treatment resulted in a pronounced drop of the cellular glutamine level, whereas the addition of DHA raised the DHAP level in both untreated and MSX-treated cells (Fig. 2E; fig. S7, A and B; and table S6). Under these conditions, TOR was similarly activated by DHA regardless of the glutamine level (Fig. 2E). Together, these results strongly suggested that the intracellular abundance of glutamine does not play a major role in activation of TOR by light or DHA.

The cytoplasmic level of DHAP generated in the chloroplast regulates TOR activity

Our results indicated that DHAP is a key metabolite for light-driven up-regulation of TOR in *Chlamydomonas*. To further test whether DHAP controls TOR, we examined TOR activity in the *t3ko2* mutant, which lacks the chloroplast triose-phosphate translocator TPT3 (fig. S3) (26). This protein resides in the inner chloroplast envelope membrane and is responsible for the export of photosynthetically synthesized DHAP to the cytoplasm while enabling the import of inorganic phosphate into the chloroplast (26). TPT3 is required for growth of *Chlamydomonas* under moderate or high light conditions, but the *t3ko2* mutant can grow in low light in either tris-acetate-phosphate (TAP) or acetate-free tris-phosphate (TP) medium (26). First, we determined TOR activity in wild-type (WT), *t3ko2*, and complemented (*C_T3KO2*) cells grown in TAP medium and low light because acetate stimulates TOR under mixotrophic conditions in *Chlamydomonas* (5). Our results revealed similar TOR activity in WT, *t3ko2*, and *C_T3KO2* cells under these conditions (fig. S8A). Next, to investigate TOR regulation by light and DHAP in the *t3ko2* mutant, cells growing in TAP and low light were shifted to TP medium and the dark for 8 hours and then exposed to light for 15, 30, or 60 min. As expected, TOR was down-regulated in the dark and quickly reactivated by light in WT and *C_T3KO2* cells (Fig. 3A). However, although TOR activity decreased in *t3ko2* cells shifted to the dark, no reactivation of TOR was detected upon illumination (Fig. 3A), indicating that TOR is not properly regulated by light in this mutant.

To understand why the *t3ko2* mutant failed to activate TOR upon reillumination, we performed a detailed metabolomic analysis of these cells. We found that DHAP decreased in the dark and rapidly increased in the light in WT, *t3ko2*, and *C_T3KO2* cells, although the mutant accumulated higher levels of this and other metabolites in the light (fig. S8B and table S7). Significantly larger pools of intermediates of the CBB cycle and precursors of starch synthesis such as adenosine diphosphate glucose (ADPG) were also detected in the

mutant compared with WT and complemented cells following reillumination (fig. S8B). In contrast, we observed a decreased level of metabolites located outside the chloroplast such as pyruvate (fig. S8B and table S7).

We previously showed that the stimulation of CO₂ fixation by supplementation of *Chlamydomonas* cultures with HCO₃[−] boosts TOR activity (5). Thus, we investigated whether the addition of HCO₃[−] could enhance TOR activity in the *t3ko2* mutant using the same experimental setup described above but with the addition of HCO₃[−] followed by 15 and 30 min of illumination. In WT and *C_T3KO2* cells, TOR was further activated upon HCO₃[−] addition in the light (Fig. 3B), confirming the positive impact of CO₂ fixation on TOR. By contrast, HCO₃[−] had no effect on TOR activity in the *t3ko2* mutant (Fig. 3B). Metabolomic analysis of these cells revealed a more pronounced accumulation of CBB cycle intermediates with HCO₃[−] than their accumulation in response to light alone (fig. S8B and table S7). Together, these results indicated that light/CO₂-derived signals cannot activate TOR in a mutant impaired in the export of DHAP from the chloroplast to the cytoplasm. On the basis of the findings that *Chlamydomonas* cells efficiently converted exogenous DHA to DHAP and this compound was sufficient to activate TOR (Fig. 2A), we hypothesized that the addition of DHA may restore the regulation of TOR in the *t3ko2* mutant. Our results demonstrated that the addition of DHA resulted in full activation of TOR in WT, *t3ko2*, and *C_T3KO2* cells in the dark-to-light assays (Fig. 3C). The metabolomic analysis of these cells showed that most of the CBB cycle intermediates accumulated to lower levels following the addition of DHA compared with HCO₃[−] in the *t3ko2* mutant (fig. S8B and table S7). Moreover, a larger amount of starch was detected in the *t3ko2* mutant within 60 min of illumination, which was even higher with HCO₃[−] but not with DHA (fig. S9). Last, we found that the presence of DHA in the medium rescued the growth defect phenotype of *t3ko2* cells in TP medium (Fig. 3D), showing that the inability to export DHAP outside the chloroplast impaired the cell growth of this mutant.

DISCUSSION

Although our current knowledge of the TOR signaling pathway as a plant energy master regulator has notably increased in the past years, the mechanisms by which light and carbon availability regulate TOR in photosynthetic organisms are largely unknown. In plants, TOR activity has been shown to be modulated by glucose via mitochondrial function (9) and light through the chloroplast electron transport chain (33). In microalgae, CO₂ fixation is a primary activation signal connecting carbon and light to TOR (5), although the underlying mechanism is still unclear. In this study, we performed a detailed metabolomic analysis of synchronized *Chlamydomonas* cells to understand how carbon and light regulate TOR in photosynthetic cells.

Our results uncovered DHAP, which is synthesized in the chloroplast and exported to the cytoplasm (26), as a key metabolite connecting carbon availability and light signals to TOR (Fig. 3E). Supporting this hypothesis, we found that the addition of the DHAP precursor DHA to *Chlamydomonas* cells was sufficient to highly activate TOR in the dark (Fig. 2A), bypassing any chloroplast function for this activation. Moreover, the experiments carried out in the *t3ko2* mutant demonstrated that the transport of DHAP from the chloroplast to the cytoplasm is required for the proper regulation of

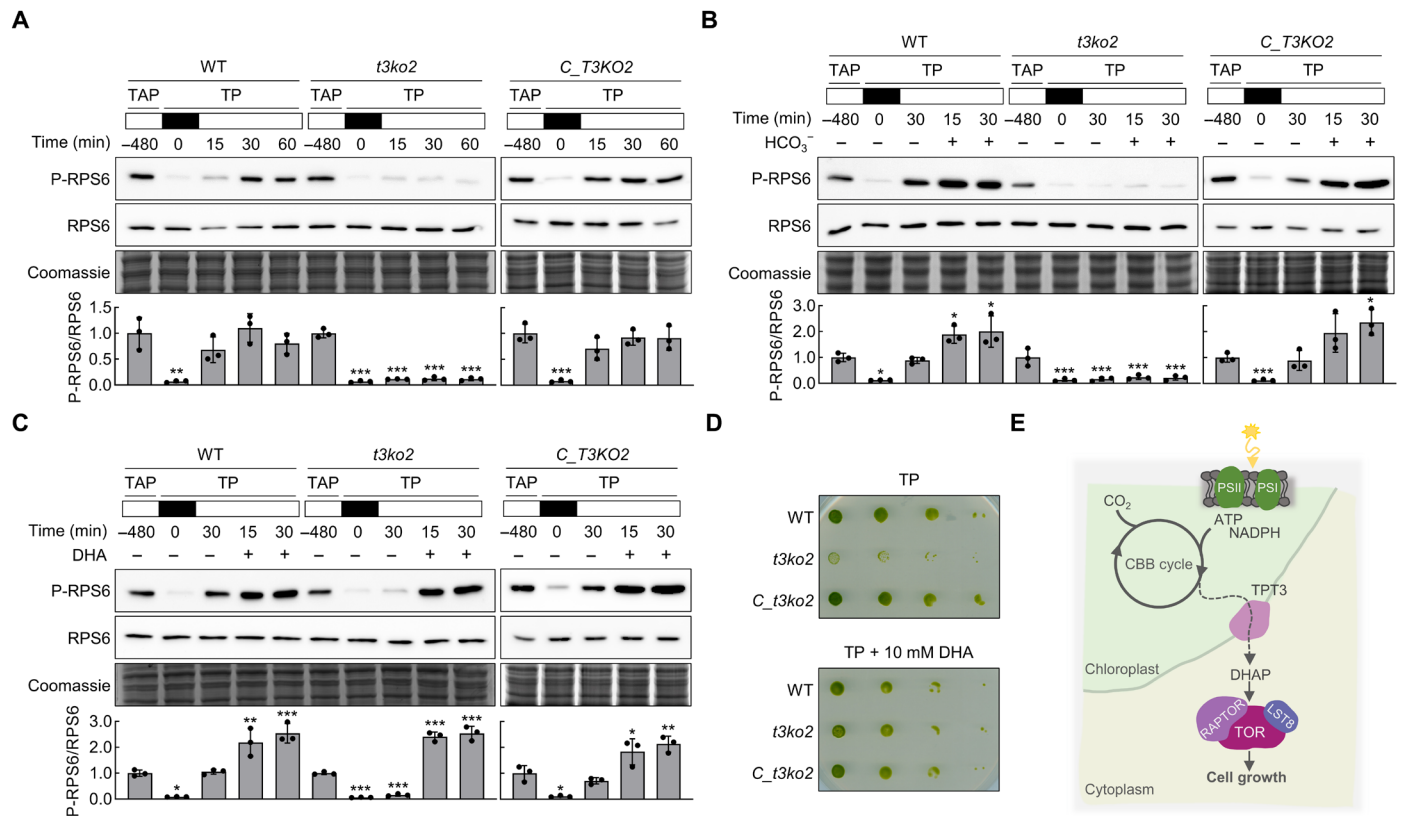


Fig. 3. TOR activity does not respond to inorganic carbon and light in the *Chlamydomonas* mutant lacking the DHAP transporter TPT3. (A) Immunoblot of P-RPS6/RPS6 in WT, *t3ko2*, and *C_T3KO2* *Chlamydomonas* cells transferred from TAP to acetate-free TP medium and darkness for 8 hours and then reilluminated for 15, 30, and 60 min. (B) Immunoblot of P-RPS6/RPS6 in WT, *t3ko2*, and *C_T3KO2* *Chlamydomonas* cells processed as described in (A) but reilluminated for 15 and 30 min in the presence (+) or absence (–) of 10 mM HCO₃[–]. (C) Immunoblot of P-RPS6/RPS6 in WT, *t3ko2*, and *C_T3KO2* *Chlamydomonas* cells processed as described in (A) but reilluminated for 15 and 30 min in the presence (+) or absence (–) of 2 mM DHA. Coomassie brilliant blue–stained gels were used as a loading control in (A) to (C). (D) Serial spot dilutions (10-fold) of WT, *t3ko2*, and *C_T3KO2* *Chlamydomonas* cells on TP plates containing 10 mM DHA. Growth was recorded after 7-day incubation at 25°C under continuous illumination. (E) Proposed model for the regulation of TOR activity by DHAP in *Chlamydomonas*. Photosynthesis provides reducing power [NADPH (reduced form of nicotinamide adenine dinucleotide phosphate)] and energy [ATP (adenosine 5′-triphosphate)] for CO₂ fixation and the biosynthesis of organic carbon compounds. DHAP is synthesized in the chloroplast and exported to the cytoplasm through the TPT3 transporter. The abundance of cytoplasmic DHAP is transmitted to TOR to modulate its activity. Error bars correspond to SD from three biological replicates in (A) to (C). Asterisks represent significant differences according to one-way ANOVA and Bonferroni’s test: ****P* < 0.001; ***P* < 0.01; **P* < 0.05; not significant, ≥0.05. The statistical analyses described apply to all statistical analyses in this figure (detailed in table S8). White and black bars indicate light and dark phases, respectively.

TOR by light (Fig. 3, A to C). This mutant was unable to activate TOR in response to light or HCO₃[–] but exhibited the full capacity for TOR induction with the addition of exogenous DHA. The misregulation of TOR by light or HCO₃[–] in the *t3ko2* mutant was not due to a defect in DHAP synthesis, as we found that this mutant accumulates large amounts of DHAP and all intermediates of the CBB cycle upon illumination of cells (fig. S8B and table S7). The larger abundance of these metabolites in the *t3ko2* mutant is in close agreement with a previous study showing higher levels of DHAP, 3PGA, FBPA, glucose 6-phosphate (G6P), and PEP in the chloroplast stroma of *t3ko2* cells because of the decreased ability of the mutant chloroplast to export fixed carbon (26). The *t3ko2* mutant has been instrumental to dissect the regulation of TOR by light and inorganic carbon because of the high compartmentalization of the glycolytic pathway in green algae such as *C. reinhardtii*. In these organisms, the first part of glycolysis (from glucose to G3P) is exclusively chloroplastic, while the second part (from 3PGA to pyruvate and acetyl-CoA) is localized in the cytoplasm (19, 34). In contrast, plants have the entire

glycolytic pathway in both the chloroplast and cytoplasm, and plant chloroplasts also have an efficient export system for hexose and triose phosphate to feed glycolysis in the cytoplasm (35).

In the cytoplasm, DHAP is converted to downstream metabolites such as GAP, 3PGA, or PEP, which feeds the TCA cycle in the mitochondria. Given that activation of TOR by glucose in *Arabidopsis* depends on glycolysis-mitochondria-mediated energy and metabolic relays (9), it might be speculated that DHAP-derived metabolites promote the activation of TOR by light in *Chlamydomonas*. However, unlike DHAP levels, the abundances of GAP, 3PGA, or PEP were not sharply controlled by light/dark oscillations (Fig. 1D). On this basis, we propose that these metabolites are unlikely to play a role in promoting TOR activation. Furthermore, feeding of the TCA cycle by exogenous DMKG had no impact on TOR activity in *Chlamydomonas* (Fig. 2C), suggesting that TCA cycle intermediates do not mediate light signaling to TOR under autotrophic growth. Nevertheless, we cannot rule out the notion that other metabolites, in addition to DHAP, might regulate TOR when *Chlamydomonas* cells are grown

with a reduced carbon source such as acetate. In plants, the sugar small-molecule signal trehalose 6-phosphate has been shown to control root branching via SnRK1 and TOR kinases (36), but the contribution of this sugar to the regulation of the TOR pathway in microalgae has not been addressed yet. As unicellular autotrophic organisms, microalgae may have evolved signaling mechanisms connecting carbon and light inputs to TOR that are different from those described in plants, which have heterotrophic and autotrophic tissues (5). Root and shoot apices display distinct regulation of TOR activity by glucose and light (10). Whether DHAP or other specific metabolites regulate TOR in plant photosynthetic tissues remains to be explored.

Amino acids are key upstream signals for TOR regulation in all eukaryotes. Among them, glutamine plays a prominent role as a TOR regulator in different organisms including microalgae and plants (5, 13). Our results revealed that glutamine is not required for the activation of TOR by light or DHA (Fig. 2, D and E), strongly suggesting that amino acids and inorganic carbon have distinct impacts on TOR. This hypothesis is in consonance with the presence of specific mechanisms that convey amino acid and glucose availability to TOR in yeasts and mammals (2). A recent study identified three different pathways through which glucose activates TORC1 in yeasts, demonstrating that FBP, G6P, and complete glycolysis are required for this activation (37). In mammals, glucose signaling to mechanistic TORC1 (mTORC1) has been shown to be mediated by DHAP rather than by glucose itself (38). Similar to what we have observed in light/dark synchronized *Chlamydomonas* cells (Fig. 1D), DHAP levels change more than any other glycolytic intermediate between high and low glucose conditions in mammalian cells (38). Moreover, DHA is sufficient to activate mTORC1 in the absence of glucose (38), in close agreement with our findings in *Chlamydomonas* showing full activation of TOR by exogenous DHA under dark conditions (Fig. 2A). Although there is no known plasma membrane transporter for DHAP in mammals (38), our study in *Chlamydomonas* using a mutant defective in the chloroplast DHAP transporter TPT3 provided genetic evidence connecting this central metabolite to TOR regulation. Thus, we conclude that DHAP might be a conserved regulatory metabolite connecting carbon availability to TOR activity in autotrophic and heterotrophic eukaryotes. However, the precise molecular machinery involved in DHAP sensing by TOR remains to be elucidated. In mammals, the GATOR-Rag pathway has been proposed to convey the DHAP signal to mTORC1 at the lysosomal surface (38, 39). Upstream regulators of mTORC1 such as the amino acid sensor GATOR or Rag guanosine triphosphatases are not conserved in the green lineage (40), but it is plausible that yet-to-be identified proteins with similar function may transmit DHAP availability to TOR in *Chlamydomonas*.

MATERIALS AND METHODS

C. reinhardtii strains and growth conditions

C. reinhardtii strains used in this study were WT 4A+ (CC-4051) and M10 (CC-4403, isogenic line derived from CC-124), *t3ko2*, and complemented *t3ko2* (termed as *C_T3KO2*) (26). *Chlamydomonas* cells were grown under standard (50 $\mu\text{mol photons m}^{-2} \text{ s}^{-1}$) illumination from light-emitting diode lamps in TP or TAP medium (41) on an orbital shaker (100 rpm) at 25°C. When required, TAP or TP medium was solidified with 1.2% Bacto agar (Difco). For synchronous diurnal cycles (12-hour light/12-hour dark), cells were inoculated from TP

precultures at a starting optical density at 750 nm ($\text{OD}_{750\text{nm}}$) of 0.05 in an Innova 42 incubator (New Brunswick Scientific) and maintained for 5 days under entraining conditions at an $\text{OD}_{750\text{nm}}$ of 0.4 to 0.5. When required, cells were treated with DHA (Sigma-Aldrich, 8.20482), DMKG (Sigma-Aldrich, 349631), MSX (Sigma-Aldrich, M5379), cerulenin (Sigma-Aldrich; C2389), or HCO_3^- (Sigma-Aldrich, S5761) at the indicated concentrations and times. For light-to-dark transition assays or when acetate was removed from the medium, cells growing in TAP medium were washed three times with TP, transferred from standard illumination to complete darkness for 8 hours, and then reilluminated for 15, 30, or 60 min.

Protein preparation, Western blot assays, and TOR activity determination

Chlamydomonas cells from liquid cultures were collected by centrifugation (4000g, 2 min), washed in lysis buffer [50 mM Tris-HCl (pH 7.5)], and resuspended in 100 μl of the same buffer. Cells were lysed by two cycles of slow freezing to -80°C followed by thawing at room temperature. The soluble protein cell extract was separated from the insoluble fraction by centrifugation (15,000g, 20 min, 4°C). Proteins were quantified using the Coomassie dye binding method (Bio-Rad, 500-0006). For immunoblot analyses, total protein extracts (30 μg) were subjected to denaturing gel electrophoresis and then transferred to either polyvinylidene fluoride membranes (Amersham, 10600023) that were previously activated in methanol for phosphorylated RPS6 (P-RPS6) detection or to nitrocellulose membranes (Amersham, 10600003) for RPS6 detection. Primary antibodies raised against *Chlamydomonas* P-RPS6 and RPS6 (24) and secondary anti-rabbit antibodies (Sigma-Aldrich, A6154) were diluted 1:3,000, 1:3,000, and 1:10,000, respectively, in phosphate-buffered saline containing 0.1% (v/v) Tween-20 (Applichem, A4974) and 5% (w/v) milk powder (Applichem, A0830). Proteins were detected with the Lumina Crescendo Merck Millipore immunoblotting detection system (Millipore, WBLUR0100) and visualized using an ImageQuant 800 molecular imaging system (Amersham). Coomassie brilliant blue-stained gels were used as protein loading controls. TOR activity was analyzed by monitoring the phosphorylation state of the RPS6 ribosomal protein with antibodies that specifically recognize phosphorylation of this protein at Ser²⁴⁵ (24). We have previously reported that phosphorylation of Ser²⁴⁵ in RPS6 is regulated by TOR in *Chlamydomonas* (24). The phosphorylation state of RPS6 has been widely used to monitor TOR activity in different systems including plants (33, 42–44). To determine the phosphorylation state of RPS6, P-RPS6 and total RPS6 signals were quantified using ImageQuant TL analysis software (Amersham). The P-RPS6/RPS6 ratio was calculated as the P-RPS6 intensity divided by the RPS6 intensity. This value was normalized to the mean control ratio for each treatment or condition analyzed (24).

Metabolomic analysis

Metabolites were analyzed as previously described (45). Briefly, *Chlamydomonas* cells growing under the indicated conditions were collected by centrifugation (4000g, 2 min, 4°C) and pellets were rapidly frozen in liquid nitrogen and immediately stored at -80°C . Frozen pellets were resuspended in ice-cold 70:30 (v/v) methanol:chloroform and homogenized by 15 cycles of 30 s of vortexing followed by immersion in liquid nitrogen to keep the samples cool. Subsequently, Milli-Q water was added to the samples and, after centrifugation (15,000g, 20 min, 4°C), the polar phase was transferred to a new

tube to evaporate all of the solvent using a vacuum concentrator overnight. Last, metabolites were resuspended in 50 µl of Milli-Q water and analyzed using a liquid chromatography–tandem mass spectrometry system (Sciex Qtrap 6500+) at the Chromatography Facility of IBVF. For chromatography, a XSELECT HSS T3 XP column (Waters) with an UFLC XR HPLC (Shimadzu) was used. Mobile phases were composed of 10 mM tributylamine, 10 mM acetic acid (pH 6.86), 5% methanol and 2% 2-propanol (mobile phase A) and 2-propanol (mobile phase B). The injection volume was 5 µl with full loop injection. Peak areas of all the metabolites identified were normalized by the peak areas of the internal standard acetaminophen. For mass spectrometry, operating conditions were set up according to the manufacturer's instructions (https://sciex.com/content/dam/SCIEX/pdf/tech-notes/all/quant_qual_Metabolomics_AnalysisQTRAP.pdf).

Starch analysis

Cells were concentrated (OD_{750nm}, 4 to 5), washed twice with Milli-Q water (Merck Millipore), and stored at −20°C until use. Subsequently, starch was obtained from the cell pellet by ethanolic extraction. Briefly, cells were resuspended in 1 ml of 80% ethanol, heated at 70°C for 30 min, and centrifuged for 5 min (15,000g, 4°C). After two additional washing steps, the pellet was resuspended in 200 µl of 0.2 M KOH and heated at 95°C for 30 min, and last, 40 µl of 1 M acetic acid was added. The starch was digested with amyloglucosidase from *Aspergillus niger* (Sigma-Aldrich, A7095), and the glucose level was determined using the glucose oxidase/peroxidase method (Sigma-Aldrich, GAGO20).

Statistical information

Data from at least three biological replicates were analyzed using GraphPad software. Two-tailed Student's *t* tests and one-way analysis of variance (ANOVA) were used to compare different strains or different growth conditions and treatments and to analyze the temporal changes. Metabolites with a false discovery rate <0.05 were assigned as considered statistically significant in the volcano plots. For all other representations, *P* < 0.05 was taken as the threshold for statistical significance. Single (*), double (**), and triple (***) asterisks indicate a significant difference: *P* < 0.05, *P* < 0.01, and *P* < 0.001, respectively. When indicated, Bonferroni correction was applied for multiple comparisons. A summary of the statistical analysis of experiments shown in main and supplementary figures can be found in table S8.

Supplementary Materials

The PDF file includes:

Figs. S1 to S9
Table S8
Legends for tables S1 to S7

Other Supplementary Material for this manuscript includes the following:

Tables S1 to S7

REFERENCES AND NOTES

1. R. Loewith, E. Jacinto, S. Wullschlegler, A. Lorberg, J. L. Crespo, D. Bonenfant, W. Oppliger, P. Jenoe, M. N. Hall, Two TOR complexes, only one of which is rapamycin sensitive, have distinct roles in cell growth control. *Mol. Cell* **10**, 457–468 (2002).
2. A. González, M. N. Hall, Nutrient sensing and TOR signaling in yeast and mammals. *EMBO J.* **36**, 397–408 (2017).
3. G. Y. Liu, D. M. Sabatini, mTOR at the nexus of nutrition, growth, ageing and disease. *Nat. Rev. Mol. Cell Biol.* **21**, 183–203 (2020).
4. T. Dobrenel, C. Caldana, J. Hanson, C. Robaglia, M. Vincentz, B. Veit, C. Meyer, TOR signaling and nutrient sensing. *Annu. Rev. Plant Biol.* **67**, 261–285 (2016).
5. M. J. Mallén-Ponce, M. E. Pérez-Pérez, J. L. Crespo, Photosynthetic assimilation of CO₂ regulates TOR activity. *Proc. Natl. Acad. Sci. U.S.A.* **119**, e2115261119 (2022).
6. J. O. Brunkard, Exaptive evolution of target of rapamycin signaling in multicellular eukaryotes. *Dev. Cell* **54**, 142–155 (2020).
7. Y. Liu, Y. Xiong, Plant target of rapamycin signaling network: Complexes, conservations, and specificities. *J. Integr. Plant Biol.* **64**, 342–370 (2022).
8. A. Artins, M. C. M. Martins, C. Meyer, A. R. Fernie, C. Caldana, Sensing and regulation of C and N metabolism – Novel features and mechanisms of the TOR and SnRK1 signaling pathways. *Plant J.* **118**, 1268–1280 (2024).
9. Y. Xiong, M. McCormack, L. Li, Q. Hall, C. Xiang, J. Sheen, Glucose–TOR signalling reprograms the transcriptome and activates meristems. *Nature* **496**, 181–186 (2013).
10. X. Li, W. Cai, Y. Liu, H. Li, L. Fu, Z. Liu, L. Xu, H. Liu, T. Xu, Y. Xiong, Differential TOR activation and cell proliferation in Arabidopsis root and shoot apices. *Proc. Natl. Acad. Sci. U.S.A.* **114**, 2765–2770 (2017).
11. M. Scheptelinkov, J. Makarian, O. Srour, A. Geldreich, Z. Yang, J. Chicher, P. Hammann, L. A. Ryabova, GTPase ROP2 binds and promotes activation of target of rapamycin, TOR, in response to auxin. *EMBO J.* **36**, 886–903 (2017).
12. Y. Liu, X. Duan, X. Zhao, W. Ding, Y. Wang, Y. Xiong, Diverse nitrogen signals activate convergent ROP2-TOR signaling in Arabidopsis. *Dev. Cell* **56**, 1283–1295.e5 (2021).
13. C. Ingargiola, I. Jéhanno, C. Forzani, A. Marmagne, J. Broutin, G. Clément, A.-S. Leprince, C. Meyer, The Arabidopsis Target of Rapamycin kinase regulates ammonium assimilation and glutamine metabolism. *Plant Physiol.* **192**, 2943–2957 (2023).
14. P. Cao, S.-J. Kim, A. Xing, C. A. Schenck, L. Liu, N. Jiang, J. Wang, R. L. Last, F. Brandizzi, Homeostasis of branched-chain amino acids is critical for the activity of TOR signaling in Arabidopsis. *eLife* **8**, e50747 (2019).
15. B. M. O'Leary, G. G. K. Oh, C. P. Lee, A. H. Millar, Metabolite regulatory interactions control plant respiratory metabolism via target of rapamycin (TOR) kinase activation. *Plant Cell* **32**, 666–682 (2020).
16. J. Jüppner, U. Mubeen, A. Leisse, C. Caldana, A. Wiszniewski, D. Steinhäuser, P. Gialvalisco, The target of rapamycin kinase affects biomass accumulation and cell cycle progression by altering carbon/nitrogen balance in synchronized *Chlamydomonas reinhardtii* cells. *Plant J.* **93**, 355–376 (2018).
17. S. Imamura, Y. Kawase, I. Kobayashi, T. Sone, A. Era, S. Miyagishima, M. Shimajima, H. Ohta, K. Tanaka, Target of rapamycin (TOR) plays a critical role in triacylglycerol accumulation in microalgae. *Plant Mol. Biol.* **89**, 309–318 (2015).
18. M. E. Pérez-Pérez, F. J. Florencio, J. L. Crespo, Inhibition of target of rapamycin signaling and stress activate autophagy in *Chlamydomonas reinhardtii*. *Plant Physiol.* **152**, 1874–1888 (2010).
19. X. Johnson, J. Alric, Central carbon metabolism and electron transport in *Chlamydomonas reinhardtii*: Metabolic constraints for carbon partitioning between oil and starch. *Eukaryot. Cell* **12**, 776–793 (2013).
20. E. G. Werth, E. W. McConnell, I. C. Lianez, Z. Perrine, J. L. Crespo, J. G. Umen, L. M. Hicks, Investigating the effect of target of rapamycin kinase inhibition on the *Chlamydomonas reinhardtii* phosphoproteome: From known homologs to new targets. *New Phytol.* **221**, 247–260 (2019).
21. U. Mubeen, J. Jüppner, J. Alpers, D. K. Hinch, P. Gialvalisco, Target of rapamycin inhibition in *Chlamydomonas reinhardtii* triggers de novo amino acid synthesis by enhancing nitrogen assimilation. *Plant Cell* **30**, 2240–2254 (2018).
22. V. Roustan, W. Weckwerth, Quantitative phosphoproteomic and system-level analysis of TOR inhibition unravel distinct organellar acclimation in *Chlamydomonas reinhardtii*. *Front. Plant Sci.* **9**, 1590 (2018).
23. S. Upadhyaya, S. Agrawal, A. Gorakshakar, B. J. Rao, TOR kinase activity in *Chlamydomonas reinhardtii* is modulated by cellular metabolic states. *FEBS Lett.* **594**, 3122–3141 (2020).
24. I. Couso, M. E. Pérez-Pérez, M. M. Ford, E. Martínez-Force, L. M. Hicks, J. G. Umen, J. L. Crespo, Phosphorus availability regulates TORC1 signaling via LST8 in *Chlamydomonas*. *Plant Cell* **32**, 69–80 (2020).
25. H. Treves, A. Küken, S. Arrivault, H. Ishihara, I. Hoppe, A. Erban, M. Höhne, T. A. Moraes, J. Kopka, J. Szymanski, Z. Nikoloski, M. Stitt, Carbon flux through photosynthesis and central carbon metabolism show distinct patterns between algae, C3 and C4 plants. *Nat. Plants* **8**, 78–91 (2022).
26. W. Huang, A. Krishnan, A. Plett, M. Meagher, N. Linka, Y. Wang, B. Ren, J. Findinier, P. Redekop, N. Fakhimi, R. G. Kim, D. A. Karns, N. Boyle, M. C. Posewitz, A. R. Grossman, *Chlamydomonas* mutants lacking chloroplast TRIOSE PHOSPHATE TRANSPORTER3 are metabolically compromised and light sensitive. *Plant Cell* **35**, 2592–2614 (2023).
27. D. Morales-Sánchez, Y. Kim, E. L. Terng, L. Peterson, H. Cerutti, A multidomain enzyme, with glycerol-3-phosphate dehydrogenase and phosphatase activities, is involved in a chloroplastic pathway for glycerol synthesis in *Chlamydomonas reinhardtii*. *Plant J.* **90**, 1079–1092 (2017).
28. Y. Li-Beisson, J. J. Thelen, E. Fedosejevs, J. L. Harwood, The lipid biochemistry of eukaryotic algae. *Prog. Lipid Res.* **74**, 31–68 (2019).

29. L. G. Heredia-Martínez, A. Andrés-Garrido, E. Martínez-Force, M. E. Pérez-Pérez, J. L. Crespo, Chloroplast damage induced by the inhibition of fatty acid synthesis triggers autophagy in *Chlamydomonas*. *Plant Physiol.* **178**, 1112–1129 (2018).
30. S. J. Parker, J. Encarnación-Rosado, K. E. R. Hollinshead, D. M. Hollinshead, L. J. Ash, J. A. K. Rossi, E. Y. Lin, A. S. W. Sohn, M. R. Philips, D. R. Jones, A. C. Kimmelman, Spontaneous hydrolysis and spurious metabolic properties of α -ketoglutarate esters. *Nat. Commun.* **12**, 4905 (2021).
31. J. L. Crespo, T. Powers, B. Fowler, M. N. Hall, The TOR-controlled transcription activators GLN3, RTG1, and RTG3 are regulated in response to intracellular levels of glutamine. *Proc. Natl. Acad. Sci. U.S.A.* **99**, 6784–6789 (2002).
32. R. V. Durán, W. Oppliger, A. M. Robitaille, L. Heiserich, R. Skendaj, E. Gottlieb, M. N. Hall, Glutaminolysis activates Rag-mTORC1 signaling. *Mol. Cell* **47**, 349–358 (2012).
33. S. Riegler, L. Servi, M. R. Scarpin, M. A. Godoy Herz, M. G. Kubaczka, P. Venhuizen, C. Meyer, J. O. Brunkard, M. Kalyna, A. Barta, E. Petrillo, Light regulates alternative splicing outcomes via the TOR kinase pathway. *Cell Rep.* **36**, 109676 (2021).
34. U. Klein, Compartmentation of glycolysis and of the oxidative pentose-phosphate pathway in *Chlamydomonas reinhardtii*. *Planta* **167**, 81–86 (1986).
35. W. Plaxton, The organization and regulation of plant glycolysis. *Annu. Rev. Plant Biol.* **47**, 185–214 (1996).
36. S. Morales-Herrera, J. Jourquin, F. Coppé, L. Lopez-Galvis, T. De Smet, A. Safi, M. Njo, C. A. Griffiths, J. D. Sidda, J. S. O. Mccullagh, X. Xue, B. G. Davis, J. Van der Eycken, M. J. Paul, P. Van Dijk, T. Beeckman, Trehalose-6-phosphate signaling regulates lateral root formation in *Arabidopsis thaliana*. *Proc. Natl. Acad. Sci. U.S.A.* **120**, e2302996120 (2023).
37. M. Alfatah, L. Cui, C. J. H. Goh, T. Y. N. Cheng, Y. Zhang, A. Naaz, J. H. Wong, J. Lewis, W. J. Poh, P. Arumugam, Metabolism of glucose activates TORC1 through multiple mechanisms in *Saccharomyces cerevisiae*. *Cell Rep.* **42**, 113205 (2023).
38. J. M. Orozco, P. A. Krawczyk, S. M. Scaria, A. L. Cangelosi, S. H. Chan, T. Kunchok, C. A. Lewis, D. M. Sabatini, Dihydroxyacetone phosphate signals glucose availability to mTORC1. *Nat. Metab.* **2**, 893–901 (2020).
39. G. Hoxhaj, J. W. Locasale, I. Ben-Sahra, A spoonful of DHAP keeps mTORC1 running on sugars. *Nat. Metab.* **2**, 801–802 (2020).
40. M. J. Mallén-Ponce, M. E. Pérez-Pérez, J. L. Crespo, Deciphering the function and evolution of the target of rapamycin signaling pathway in microalgae. *J. Exp. Bot.* **73**, 6993–7005 (2022).
41. E. H. Harris, "Chapter 8 - *Chlamydomonas* in the laboratory," in *The Chlamydomonas Sourcebook (Second Edition)*, E. H. Harris, D. B. Stern, G. B. Witman, Eds. (Academic Press, ed. 2, 2009), pp. 241–302.
42. G.-H. Chen, M.-J. Liu, Y. Xiong, J. Sheen, S.-H. Wu, TOR and RPS6 transmit light signals to enhance protein translation in deetiolating *Arabidopsis* seedlings. *Proc. Natl. Acad. Sci. U.S.A.* **115**, 12823–12828 (2018).
43. T. Dobrenel, E. Mancera-Martínez, C. Forzani, M. Azzopardi, M. Davanture, M. Moreau, M. Schepetilnikov, J. Chicher, O. Langella, M. Zivy, C. Robaglia, L. A. Ryabova, J. Hanson, C. Meyer, The *Arabidopsis* TOR kinase specifically regulates the expression of nuclear genes coding for plastidic ribosomal proteins and the phosphorylation of the cytosolic ribosomal protein S6. *Front. Plant Sci.* **7**, 1611 (2016).
44. Y.-K. Kim, S. Kim, Y. Shin, Y.-S. Hur, W.-Y. Kim, M.-S. Lee, C.-I. Cheon, D. P. S. Verma, Ribosomal protein S6, a Target of Rapamycin, is involved in the regulation of rRNA genes by possible epigenetic changes in *Arabidopsis*. *J. Biol. Chem.* **289**, 3901–3912 (2014).
45. M. E. Pérez-Pérez, M. J. Mallén-Ponce, Y. Odriozola-Gil, A. Rubio, J. J. Salas, E. Martínez-Force, A. J. Pérez-Pulido, J. L. Crespo, Lipid turnover through lipophagy in the newly identified extremophilic green microalga *Chlamydomonas urium*. *New Phytol.* **243**, 284–298 (2024).

Acknowledgments: We thank C. Parejo for technical assistance with the analysis of metabolites and R. Durán for helpful discussion. **Funding:** This work was supported in part by Ministerio de Ciencia, Innovación y Universidades (grants PID2021-123500NB-I00 to J.L.C., TED2021-130912B-I00 to J.L.C. and M.E.P.-P., and PID2023-150436NB-I00 to M.E.P.-P.) and a Juan de la Cierva postdoctoral contract (FJC2021-048000-I) to M.J.M.-P. **Author contributions:** Conceptualization: M.J.M.-P., M.E.P.-P., S.G.-A., A.R.G., and J.L.C. Methodology: M.J.M.-P., M.E.P.-P., and J.L.C. Investigation: M.J.M.-P., M.E.P.-P., S.G.-A., A.M.Q.-M., and J.L.C. Visualization: M.J.M.-P., M.E.P.-P., and J.L.C. Validation: M.J.M.-P., M.E.P.-P., S.G.-A., A.M.Q.-M., and J.L.C. Data curation: M.J.M.-P., M.E.P.-P., and J.L.C. Formal analysis: M.J.M.-P., M.E.P.-P., S.G.-A., and J.L.C. Funding acquisition: M.J.M.-P., M.E.P.-P., and J.L.C. Resources: M.J.M.-P., M.E.P.-P., and J.L.C. Project administration: M.E.P.-P. and J.L.C. Supervision: J.L.C. Writing—original draft: J.L.C. Writing—review and editing: M.J.M.-P., M.E.P.-P., S.G.-A., A.R.G., and J.L.C. **Competing interests:** The authors declare that they have no competing interests. **Data and materials availability:** All data needed to evaluate the conclusions in the paper are present in the paper and/or the Supplementary Materials. Metabolomic source data are provided in tables S1 to S7.

Submitted 24 October 2024

Accepted 12 March 2025

Published 18 April 2025

10.1126/sciadv.adu1240

Lipid turnover through lipophagy in the newly identified extremophilic green microalga *Chlamydomonas urium*

María Esther Pérez-Pérez^{1*}, Manuel J. Mallén-Ponce^{1*}, Yosu Odrizola-Gil¹ , Alejandro Rubio², Joaquín J. Salas³, Enrique Martínez-Force³, Antonio J. Pérez-Pulido² and José L. Crespo¹ 

¹Instituto de Bioquímica Vegetal y Fotosíntesis (CSIC-Universidad de Sevilla), 41092, Sevilla, Spain; ²Centro Andaluz de Biología del Desarrollo (CABD, UPO-CSIC-JA), Faculty of Experimental Sciences (Genetics Department), University Pablo de Olavide, 41013, Sevilla, Spain; ³Instituto de la Grasa (CSIC), Ctra Utrera Km1, Ed. 46, 41013, Sevilla, Spain

Summary

- Autophagy is a central degradative pathway highly conserved among eukaryotes, including microalgae, which remains unexplored in extremophilic organisms. In this study, we described and characterized autophagy in the newly identified extremophilic green microalga *Chlamydomonas urium*, which was isolated from an acidic environment.
- The nuclear genome of *C. urium* was sequenced, assembled and annotated in order to identify autophagy-related genes. Transmission electron microscopy, immunoblotting, metabolomic and photosynthetic analyses were performed to investigate autophagy in this extremophilic microalga.
- The analysis of the *C. urium* genome revealed the conservation of core autophagy-related genes. We investigated the role of autophagy in *C. urium* by blocking autophagic flux with the vacuolar ATPase inhibitor concanamycin A. Our results indicated that inhibition of autophagic flux in this microalga resulted in a pronounced accumulation of triacylglycerols and lipid droplets (LDs). Metabolomic and photosynthetic analyses indicated that *C. urium* cells with impaired vacuolar function maintained an active metabolism. Such effects were not observed in the neutrophilic microalga *Chlamydomonas reinhardtii*.
- Inhibition of autophagic flux in *C. urium* uncovered an active recycling of LDs through lipophagy, a selective autophagy pathway for lipid turnover. This study provided the metabolic basis by which extremophilic algae are able to catabolize lipids in the vacuole.

Authors for correspondence:

José L. Crespo

Email: crespo@ibvf.csic.es

María Esther Pérez-Pérez

Email: eperez@ibvf.csic.es

Received: 28 November 2023

Accepted: 19 April 2024

New Phytologist (2024) 243: 284–298

doi: 10.1111/nph.19811

Key words: autophagy, *Chlamydomonas*, extremophile, lipid, lipophagy, metabolism, microalga.

Introduction

Microalgae constitute a highly diverse group of aquatic photosynthetic organisms encompassing green algae (Chlorophyta), red algae (Rhodophyta), diatoms (Stramenopila) and prokaryotic cyanobacteria among the most representative groups. Microalgae produce c. 50% of the planet's oxygen and are present in almost all ecosystems ranging from oceans and freshwater to extreme environments such as snow and acidic waters (Field *et al.*, 1998). However, photosynthesis in acidic environments is performed only by eukaryotic phototrophs since cyanobacteria cannot grow at low pH (Brock, 1973). A number of acidophilic green and red algae, including *Chlamydomonas*, *Chlorella* and *Cyanidium* genus, have been isolated from extremely acidic waters, including mine drainage and geothermal hot springs (Aguilera, 2013; Malavasi *et al.*, 2020). The low pH of this acidic environment (pH < 3.0) facilitates metal solubility and hence acidophilic algae are usually adapted to live with toxic concentrations of heavy metals (Aguilera, 2013).

To respond to metal toxicity, microalgae activate several mechanisms that include the regulated transport of metals into/out of the cell and the storage of metals in acidic vacuoles (Goodenough *et al.*, 2019; Schmollinger *et al.*, 2021), which are responsible for the degradation of damaged material. In the neutrophilic model green alga *Chlamydomonas reinhardtii*, it has been reported that heavy metals activate autophagy (Pérez-Martín *et al.*, 2015), a major degradative process required to maintain cellular homeostasis under stress conditions. Autophagy is characterized by the formation of double-membrane vesicles called autophagosomes that engulf a wide range of intracellular components and transport this cargo to the vacuole for its degradation and recycling (Marshall & Vierstra, 2018; Soto-Burgos *et al.*, 2018). This complex catabolic process is catalyzed by > 40 autophagy-related (*ATG*) genes. A subset of these *ATG* genes constitutes the autophagy core machinery and is highly conserved in all eukaryotes with the remarkable exception of red microalgae, which likely lost *ATG* genes before diversification (Shemi *et al.*, 2015; Mallén-Ponce *et al.*, 2023). Under optimal growth, eukaryotic cells recycle unnecessary cytoplasmic constituents by maintaining a basal level of autophagy. However, this catabolic process is upregulated in response to a wide range of stresses such

*These authors contributed equally to this work.

as nutrient limitation, oxidative damage and energy deficit to maintain cellular homeostasis (Marshall & Vierstra, 2018).

Autophagy was originally described as an unspecific degradation system but the identification of receptor and adaptor proteins involved in the selective degradation of cellular material via autophagy demonstrated that this degradative process can also be highly specific. Autophagy selectively eliminates specific proteins, protein aggregates, ribosomes, proteasomes, fragments of endoplasmic reticulum or nuclei, and even entire organelles such as peroxisomes, mitochondria and chloroplasts (Marshall & Vierstra, 2018; Stephani & Dagdas, 2020). Autophagy has also been reported to mediate lipid degradation in mammals, yeasts and plants through a process known as lipophagy (Singh *et al.*, 2009; van Zutphen *et al.*, 2013; Fan *et al.*, 2019). Eukaryotic cells can store lipids, mostly triacylglycerol (TAG), in specialized organelles called lipid droplets (LDs) (Barros *et al.*, 2020; Masclaux-Daubresse *et al.*, 2020). LDs are composed of a core of neutral lipids surrounded by a phospholipid monolayer that includes peripheral and integral proteins. Although initially considered as mere cytoplasmic inclusions of fat, LDs are now recognized to play key functions in lipid and energy homeostasis (Olzmann & Carvalho, 2019). Indeed, LDs are dynamic organelles that reflect the status of cellular metabolism since lipids are stored in LDs during excess nutrient availability and mobilized for energy production under nutrient stress. LDs can be degraded through enzymatic hydrolysis mediated by lipases or via lipophagy, which requires the participation of ATG proteins (Fan *et al.*, 2019; Barros *et al.*, 2020; Li-Beisson *et al.*, 2021). Lipophagy has been described in mammalian cells as a mechanism by which small LDs are wrapped by autophagosomes and delivered to the lysosome for degradation (Singh *et al.*, 2009). Eukaryotic cells also degrade LDs through microlipophagy, a process by which lysosomes/vacuoles and LDs form stable contacts that allow the transfer of lipid contents into these lysosomes. Microlipophagy has been well characterized in the budding yeast *Saccharomyces cerevisiae*, and several studies indicate that the direct engulfment of LDs by vacuoles requires the autophagy machinery (van Zutphen *et al.*, 2013; Seo *et al.*, 2017).

Lipophagy has been described in plants and algae. In plants, lipophagy is involved in pollen germination and contributes to the degradation of LDs during seed germination and seedling growth (Kurusu *et al.*, 2014). Mounting studies in green algae indicate that lipophagy may be involved in LD degradation. A microlipophagy-like process has been described in *Auxenochlorocella protothecoides* (Zhao *et al.*, 2014), *Nannochloropsis oceanica* (Zienkiewicz *et al.*, 2020) and *C. reinhardtii* (Tsai *et al.*, 2018; Tran *et al.*, 2019). Direct interaction between LDs and ATG8-labeled structures has been shown in *C. reinhardtii* cells under nitrogen starvation (Tran *et al.*, 2019). Our previous results in *C. reinhardtii* reveal that inhibition of the autophagic flux prevented the accumulation of TAGs and the formation of LDs in nitrogen- or phosphate-starved cells, suggesting that a vacuolar lytic function is needed for the synthesis of lipids under nutrient limitation (Couso *et al.*, 2018). Moreover, a functional

study performed in *C. reinhardtii* indicates that ATG8 is involved in the degradation of TAGs (Kajikawa *et al.*, 2019). Finally, a lipophagy pathway seems to operate in the large unicellular green alga *Micrasterias denticulata* by trapping LDs in autophagosome-like vesicles that are delivered into vacuoles (Schwarz *et al.*, 2017).

Current knowledge of autophagy in extremophiles is very limited. Despite these organisms live under severe conditions that usually trigger autophagy in other eukaryotes, little attention has been paid to the role of this catabolic process in regulating the physiology of extremophiles. To learn about the function of autophagy in extremophilic organisms, in this study we blocked autophagic flux with the vacuolar ATPase inhibitor concanamycin A (ConcA) in *Chlamydomonas urium*, a new unicellular green alga isolated from a highly acidic river from Spain. Our results indicated that the core autophagy machinery is conserved in the genome of *C. urium* and other acidophilic microalgae. Moreover, transmission electron microscopy and metabolomic studies revealed an active recycling of LDs via lipophagy upon inhibition of autophagic flux in *C. urium* that does not seem to operate in *C. reinhardtii*.

Materials and Methods

Strains, media and growth conditions

Samples from the source of the Río Tinto (37°43'18"N, 6°33'2"W) were collected in spring 2015. *Chlamydomonas urium* strain was isolated and identified in this study as described in the Results and Discussion section. *Chlamydomonas reinhardtii* wild-type 4A+ (WT4A+) strain (CC-4051) was obtained from the Chlamydomonas Resource Center (www.chlamycollection.org).

Typically, both *Chlamydomonas* strains were grown under standard illumination ($c. 50 \mu\text{mol m}^{-2} \text{s}^{-1}$ from led lamps) at 25°C in high salt medium (HSM) as described previously (Harris, 1989). When required, cells in exponential growth phase ($c. 10^6 \text{ cells ml}^{-1}$) were treated with different metals including Cu^{2+} and Ni^{2+} or with ConcA (sc-202111A; Santa Cruz Biotechnology, Heidelberg, Germany) at the indicated concentrations. Stock solutions of ConcA (100 μM) were prepared in dimethyl sulfoxide (DMSO) and kept at -20°C , whereas stock solutions of the different metals were freshly prepared 1000-times concentrated in redistilled water. For experiments at low pH, the HSM medium was acidified with the required concentration of HCl during its preparation. When required, ammonium chloride was added to HSM medium which typically contains 7.5 mM NH_4Cl . For nitrogen limitation experiments, cells growing exponentially in HSM medium were washed twice and then transferred to N-free HSM medium. When required, cells were grown mixotrophically or heterotrophically in Tris–acetate–phosphate (TAP) medium as described previously (Harris, 1989). Growth curves were constructed using mean values of $\text{OD}_{750 \text{ nm}}$ or cell number per mL measurements performed at least in triplicate. For growth on plates, 1.2% (w/v) bacto agar (214010; Becton, Dickinson and Company, Le Pont de Claix, France) was added to the medium.

Optical microscopy

Chlamydomonas urium cells were collected by centrifugation and resuspended in 1 ml of phosphate-buffered saline (PBS). Cells were fixed with 2.5% (v/v) glutaraldehyde (G5882; Sigma-Aldrich) in 50 mM Tris-HCl (pH 7.5) for 1 h at 25°C. After fixing, cells were washed four times with 50 mM Tris-HCl (pH 7.5) and resuspended in the same buffer. Cells were examined with an optical microscope (AXIO Scope A1; Zeiss) equipped with DIC optics. Images were registered with an Axiocam 105 camera (Zeiss) and processed with ZEN v.2.3 software (Zeiss).

Electron microscopy

Chlamydomonas urium cells ($c. 2 \times 10^6$ cells ml^{-1}) treated with 0.2 μM ConA for 8 h were fixed with 2.5% glutaraldehyde (G5882; Sigma-Aldrich) in 0.1 M sodium cacodylate buffer (pH 7.4) for 2 h at 25°C. After fixing, cells were washed five times with 1 ml of the same buffer at 25°C. Then, samples were postfixed in 1% osmium tetroxide in 0.1 M cacodylate buffer (pH 7.4) for 1 h at 4°C. After washing, samples were immersed in 2% uranyl acetate, dehydrated through a gradient acetone series (50%, 70%, 90% and 100%, v/v) and embedded in Spurr resin (Spurr, 1969). Semithin sections (300 nm thickness) were obtained with a glass knife and stained with 1% (w/v) Toluidine Blue for cell localization and reorientation using a conventional optical microscope. Once a suitable block face of the selected area was trimmed, several ultrathin sections (70 nm) were obtained using an ultramicrotome (UC7; Leica, Wetzlar, Germany) equipped with a diamond knife (Diatome, Nidau, Switzerland) and collected on 200-mesh copper grids. Sections were examined in a Zeiss Libra 120 transmission electron microscope and digitized ($2048 \times 2048 \times 16$ bits) using an on-axis mounted TRS camera.

Genomic DNA isolation and sequencing

Chlamydomonas urium cells growing autotrophically at the exponential phase were collected by centrifugation (4000 g for 5 min) and washed once in 50 mM Tris-HCl (pH 7.5) buffer, and then, pellets were frozen in liquid nitrogen and immediately stored at -80°C . Total DNA was isolated from frozen cell pellets using the Qiagen kit (69104; Qiagen) following the instructions of the manufacturer. For genomic DNA sequencing, 200 ng of total DNA was used to prepare genomic libraries with Illumina DNA Prep. Paired-end (150-bp) libraries were sequenced with Illumina NextSeq 500 Mid Output. Quality control of DNA reads was performed with BASESPACE Onsite v.3.22.91.158 (Illumina).

Genome assembly and annotation

The quality of the reads was evaluated by FASTQC v.0.11.9 (www.bioinformatics.babraham.ac.uk/projects/fastqc). Reads with low quality or length were removed (parameters, LEADING = 5, TRAILING = 5, SLIDINGWINDOW = 3 : 15, MINLEN =

80), as well as the sequencing adaptors using TRIMMOMATIC v.0.35 (ILLUMINACLIP:adapters_nextera.fa:2:30:10) (Bolger *et al.*, 2014). The remaining reads were normalized by the tool bbnorm (<https://sourceforge.net/projects/bbmap>) and assembled by the tool ABYSS v.2.2.5 with a k -mer interval optimized to 127, $P = 0.95$ and $b = 1000\ 000$ (Jackman *et al.*, 2017). Resulting contigs with length shorter than 1000 bp were discarded, and low-complexity regions were filtered using REPEATMASKER release v.4.1.1 and default parameters (with Dfam database) (www.repeatmasker.org). Then, protein-coding genes were predicted by AUGUSTUS v.3.3.2 (parameters, --strand=both --genemodel=partial --protein=on --introns=on --codingseq=on --gff3=on --sample=100), and the corresponding protein sequences were obtained (using the script getAnnoFasta.pl from the AUGUSTUS repository) (Stanke & Morgenstern, 2005). These sequences were functionally annotated using SMA3S v.2 and UNIREF90 database (release 05/2017) (Casimiro-Soriguer *et al.*, 2017). The assembly was deposited in GenBank (BioProject PRJNA1037726).

Molecular phylogeny

The chloroplast genome of *C. reinhardtii* was used as reference sequence (GenBank: BK000554.2). Both 16S and 23S ribosomal RNA sequences were searched using the tool BARRNAP v.0.9 and a reject threshold of 0.9 (www.github.com/tseemann/barrnap). Then, these were used as query sequences in a similarity search with BLASTN (filtering by identity 80% and query coverage lower than 80%) (Altschul *et al.*, 1997) against the chloroplast genomes of the species listed in Supporting Information Table S1. Both sequences were concatenated in the same order by species, and a multiple alignment was performed using MAFFT v.7.271 (--globalpair --maxiterate 16 --phylopout) (Katoh & Standley, 2013), where regions with gaps in at least 10% of the sequences were removed using TRIMAL v.1.2 (Capella-Gutiérrez *et al.*, 2009). Finally, the molecular phylogeny was constructed using the multiple alignment and the tool RAXML v.8.2.9 with the method GTRCAT (proposed by MODELINDER from the package IQTREE v.2.0.3) and bootstrap 1000 (Stamatakis, 2014). The phylogeny was displayed using the R package GGTREE v.1.10.5.

Comparison of genes involved in autophagy

Genes related to autophagy of *S. cerevisiae* were used to search in *C. reinhardtii* and *A. thaliana*, using BLASTP with low-restricted parameters (e -value threshold = 0.0005, query coverage = 30%) (Altschul *et al.*, 1997), due to the expected low sequence conservation. Then, sequences of each autophagy protein were aligned using MAFFT v.7.271 with default parameters (Katoh & Standley, 2013). Alignments with orthologous proteins were converted to HMM profiles with hmmbuild (package HMMER v.3.3.2) (Eddy, 1998). Thus, these profiles were used to search for these new orthologous proteins in the other species using HMMSEARCH (parameters -E 0.00001 and -noali). Proteomes were downloaded from JGI database (Table S1). To calculate a comparable

identity percent for every found protein sequence, the *S. cerevisiae* sequence was used as reference using the program ESL-ALIPID (Eddy, 1998).

Modeling of *C. urium* and *C. reinhardtii* ATG8 proteins

Chlamydomonas urium ATG8 and *C. reinhardtii* ATG8 models were created using Swiss-Model (Waterhouse *et al.*, 2018). The best model was selected based on QMEAN and sequence identity. Subsequently, the UCSF Chimera Modeller interface was used for *de novo* modeling of N- and C-terminal regions based on two different statistical scores (GA341 and zDOPE) (Šali & Blundell, 1993; Melo *et al.*, 2002; Shen & Sali, 2006). Electrostatic potential surfaces were calculated using the APBS-PDB2PQR software (Dolinsky *et al.*, 2004; Jurrus *et al.*, 2018).

Lipid analysis

For the TAG analysis under N starvation, *C. urium* cells growing exponentially ($c. 2 \times 10^6$ cells ml⁻¹) in a N-replete HSM medium were transferred to a N-depleted HSM medium (HSM-N) or kept at the same medium (HSM) as control for 24 h. Then, cells were collected by centrifugation (4000 g for 2 min), washed once in 50 mM Tris-HCl (pH 7.5) buffer and immediately frozen at -80°C until use. The frozen cell pellets were dried using a SP VirTis BenchTop Pro Freeze Drier, and dry weight was measured using a Sartorius precision balance. For the TAG analysis under ConcA treatment, *C. urium* in the absence (control) or presence of 0.2 µM ConcA for 16 h in HSM or HSM-N were collected as described previously. TAGs were analyzed as described previously (Couso *et al.*, 2018). The analysis of TAGs was carried out by injecting 1 µl of the lipid extraction into the GC (6890 GC; Agilent, Santa Clara, CA, USA), using hydrogen as the carrier gas. The injector and detector temperatures were both 370°C, the oven temperature was 335°C, and a head pressure gradient from 70 to 120 kPa was applied. The GC column used was a Quadrex Aluminium-Clad 400-65HT (30 m length, 0.25 mm id, 0.1 µm film thickness; Woodbridge, USA), and a linear gas rate of 50 cm s⁻¹, a split ratio 1 : 80, and a flame ionization detector (FID) were used. The TAG species were identified and quantified according to Fernandez-Moya *et al.* (2000). Four biological replicates were analyzed for each condition. Errors bars indicate SD of the values.

Metabolomic analysis

Chlamydomonas urium and *C. reinhardtii* cells growing autotrophically at the exponential phase ($c. 2 \times 10^6$ cells ml⁻¹) in HSM medium were treated with 0.2 µM ConcA or drug vehicle for 16 h. Then, cells were collected by centrifugation (4000 g for 2 min at 4°C) and pellets were rapidly frozen in liquid nitrogen and immediately stored at -80°C. Frozen pellets were resuspended in ice-cold 70 : 30 methanol : chloroform (v/v) and homogenized by 15 cycles of 30'' vortex followed by immersion in liquid nitrogen to keep the samples cool. Subsequently, milliQ water was added to the samples and after centrifugation

(15 000 g for 20 min at 4°C), the polar phase was transferred to a new tube to evaporate all the solvent using a vacuum concentrator overnight. Finally, metabolites were resuspended in 50 µl milliQ water and analyzed using a LC-MS/MS system (Sciex Qtrap 6500+). Peak areas of all the metabolites identified were normalized by the peak areas of internal standard acetaminophen. For amino acids, cells were collected by centrifugation (4000 g for 2 min at 4°C), lyophilized and 2 mg of dried weight was used to extract amino acids as previously described (Mallén-Ponce *et al.*, 2022a). Amino acid content was analyzed by LC-MS/MS system (Sciex Qtrap 6500+). Four biological replicates were analyzed for each condition. Metabolites and amino acids were analyzed at the Chromatography Facility of IBVF.

Protein preparation and immunoblot analysis

Chlamydomonas urium and *C. reinhardtii* cells from liquid cultures were collected by centrifugation (4000 g for 5 min), washed in 50 mM Tris-HCl (pH 7.5) buffer and resuspended in a minimal volume of the same solution. Cells were lysed by two cycles of slow freezing to -80°C followed by thawing at room temperature. The soluble cell extract was separated from the insoluble fraction by centrifugation (15 000 g for 20 min) in a microcentrifuge at 4°C. Proteins were quantified using the Coomassie dye-binding method (500-0006; Bio-Rad). For immunoblot analyses, total protein extracts (20 µg) were subjected to 15% SDS-PAGE gels and then transferred to nitrocellulose membranes (162-0115; Bio-Rad). Primary antibodies raised against *C. reinhardtii* CrATG8 (Pérez-Pérez *et al.*, 2010) and secondary anti-rabbit (A6154; Sigma) antibodies were diluted 1 : 3000 and 1 : 10 000, respectively, in PBS containing 0.1% (v/v) Tween-20 (A4974; Applichem, Barcelona, Spain) and 5% (w/v) milk powder (A0830; Applichem). The Luminata Crescendo Millipore immunoblotting detection system (WBLUR0500; Millipore) was used to detect the proteins. Red Ponceau-staining membranes from the same Western blot analysis were used as protein loading control.

Chlorophyll extraction and quantification

Chlorophyll was extracted from *C. urium* and *C. reinhardtii* cells and analyzed according to Porra *et al.* (1989). The absorption at 750 nm (OD₇₅₀) was used as a reference. Chl*a* and Chl*b* were then photometrically quantified using the equation of Porra *et al.* (1989).

Chlorophyll fluorescence

Chlamydomonas urium and *C. reinhardtii* cells growing autotrophically at the exponential phase ($c. 2 \times 10^6$ cells ml⁻¹) in HSM medium were used to calculate maximum fluorescence (F_m), F_v/F_m parameter, the relative ETR (rETR) and maximum oxidizable P700 (P_m) using a DUAL-PAM-100 (Walz). To calculate the minimum fluorescence (F_0), cells were dark-adapted for 10 min with constant stirring. To determine the maximum fluorescence (F_m), DCMU was added to a final concentration of

20 μM on red light ($25 \mu\text{mol photons m}^{-2} \text{s}^{-1}$) background. To calculate rETR at growth light intensity, cells were dark-adapted for 10 min with constant stirring and then exposed to $50 \mu\text{mol photons m}^{-2} \text{s}^{-1}$ for 5 min. To determine rETR at different light intensities, cells were dark-adapted for 10 min with constant stirring and then exposed to the indicated light intensities for 3 min. The P_m value was measured by the application of a saturating red-light pulse ($5000 \mu\text{mol photons m}^{-2} \text{s}^{-1}$, duration 200 ms) on far-red light (75 W m^{-2}) background. F_m and P_m measurements were performed on equal amounts of chlorophyll ($5 \mu\text{g ml}^{-1}$). Three biological replicates were analyzed for each condition.

Oxygen evolution

Chlamydomonas urium and *C. reinhardtii* cells growing autotrophically at the exponential phase ($c. 2 \times 10^6 \text{ cells ml}^{-1}$) in HSM medium were used to perform a light response curve. To this end, 2 ml of cells ($c. 2 \times 10^6 \text{ cells ml}^{-1}$) were used to determine oxygen evolution at 25°C with continuous stirring in a Clark-type electrode (Chlorolab 2+ System; Hansatech, Norfolk, UK). Cells were dark-adapted for 10 min with constant stirring, then exposed to $50 \mu\text{mol photons m}^{-2} \text{s}^{-1}$ for 5 min, and finally exposed to darkness for 5 min. For the light curves, cells were exposed to the indicated light intensities for 3 min. O_2 production was calculated as the difference between oxygen production in the light and oxygen consumption in the dark. Three biological replicates were analyzed for each condition.

Results and Discussion

Isolation and characterization of a new extremophilic microalga

Río Tinto (Nerva, Spain) is a well-characterized extremely acidic (mean pH 2.3) river with a high content of heavy metals (Fe, Cu, Zn, As, etc.) and an unusual high microbial diversity (Aguilera, 2013; Amils, 2016). Early studies revealed that microalgae contribute at least 60% of the total biomass in the Río Tinto (Amaral Zettler *et al.*, 2002; Angeles *et al.*, 2006), and some acidophilic species from the *Chlorella*, *Chlamydomonas* and *Euglena* genus have been isolated from this extreme environment (Aguilera *et al.*, 2006, 2007). We have isolated several microalgae from samples taken from the water source of Río Tinto located at Peña de Hierro (Nerva, Spain), a natural ecosystem with the characteristic acidity and metal content of this river (Fig. 1a). Axenic cultures of one of the isolated microalgae were obtained through serial dilution (see the Materials and Methods section). Examination of this microalga by light and electron microscopy revealed a morphology and cell size similar to members from the genus *Chlamydomonas*. Cells were $c. 10 \mu\text{m}$ in diameter and had two apical cilia and a large cup-shaped chloroplast with a prominent pyrenoid and numerous starch granules (Fig. 1b,c). Based on morphological observations and a phylogenetic analysis (to be described later), we named this new microalga *C. urium* since *urium* was the original name of Río Tinto coined by the Romans.

Another extreme acidophilic microalga, *Chlamydomonas acidophila*, was isolated from Río Tinto (Aguilera *et al.*, 2006) and an acid lake from Japan (Nishikawa & Tominaga, 2001). *Chlamydomonas acidophila* strains exhibit high resistance to metals and acidic pH but are unable to efficiently grow at neutral pH values (Nishikawa & Tominaga, 2001).

We investigated the growth rate of *C. urium* under standard laboratory conditions at 25°C in autotrophic minimal medium, which has been widely used among *Chlamydomonas* species (Harris, 2009). In consonance with its extreme original habitat, *C. urium* cells were able to grow at low pH or in the presence of toxic concentrations of metals (Fig. S1a,b). However, unlike *C. acidophila* (Nishikawa & Tominaga, 2001), *C. urium* is able to grow at neutral pH. Notably, the growth of *C. urium* and *C. reinhardtii* cells was similar in minimal medium at pH 7 (Figs 1d, S1a, S2), indicating that this extremophilic microalga exhibits a high growth rate likely associated with a stable carbon assimilation in standard conditions. To investigate the photosynthetic efficiency of *C. urium* cells under laboratory conditions (25°C and $50 \mu\text{mol photons m}^{-2} \text{s}^{-1}$), we determined some photosynthesis-related parameters using pulse amplitude-modulated (PAM) fluorometry and a Clark electrode. The analysis of the relative electron transport rate (rETR), the maximum photochemical efficiency of PSII (F_v/F_m) and O_2 evolution indicated that the photosynthetic activity of *C. urium* is comparable to *C. reinhardtii* at nonsaturating light intensity (Fig. 1e–g). We also analyzed the total chlorophyll (Chl) content of *C. urium* cells at standard growth conditions and both strains displayed a similar Chla : Chlb ratio, although *C. urium* contained lower levels of total chlorophyll (Fig. 1h). Given that algal and plant cells lose chlorophyll during nitrogen deprivation, we monitored the chlorophyll content of *C. urium* and *C. reinhardtii* under nitrogen stress. Both microalgae downregulated their chlorophyll level with similar kinetics (Fig. S3). Nevertheless, the different total chlorophyll content of both microalgae led us to perform a more detailed photosynthetic study. We monitored the photosynthetic response of *C. urium* and *C. reinhardtii* cells at different light intensities. Oxygen production rates and rETR of *C. urium* were similar to *C. reinhardtii* at low light intensities, including growth light ($50 \mu\text{mol photons m}^{-2} \text{s}^{-1}$). However, *C. urium* exhibited higher oxygen production rates and rETR at light intensities exceeding $150 \mu\text{mol photons m}^{-2} \text{s}^{-1}$ (Figs 1i,j, S4a). Accordingly, the growth of *C. urium* cells was faster than *C. reinhardtii* cells under high light conditions (Fig. S2). The significant differences detected in photosynthetic rates at saturating light intensities in *C. urium* and *C. reinhardtii* together with the lower total chlorophyll content and similar Chla : Chlb ratio of *C. urium* suggested that PSII and PSI might differ in these two microalgae. Indeed, we found that the maximum fluorescence of PSII (F_m) was higher in *C. urium*, whereas the total amount of photo-oxidizable P700 at PSI (P_m) was reduced in the acidophilic microalga (Figs 1k,l, S4b,c). As part of the photosynthetic characterization of *C. urium*, we determined the respiration rates in darkness and directly after light exposure. No significant differences were found between *C. urium* and *C. reinhardtii* under standard growth conditions (Fig. S4d).

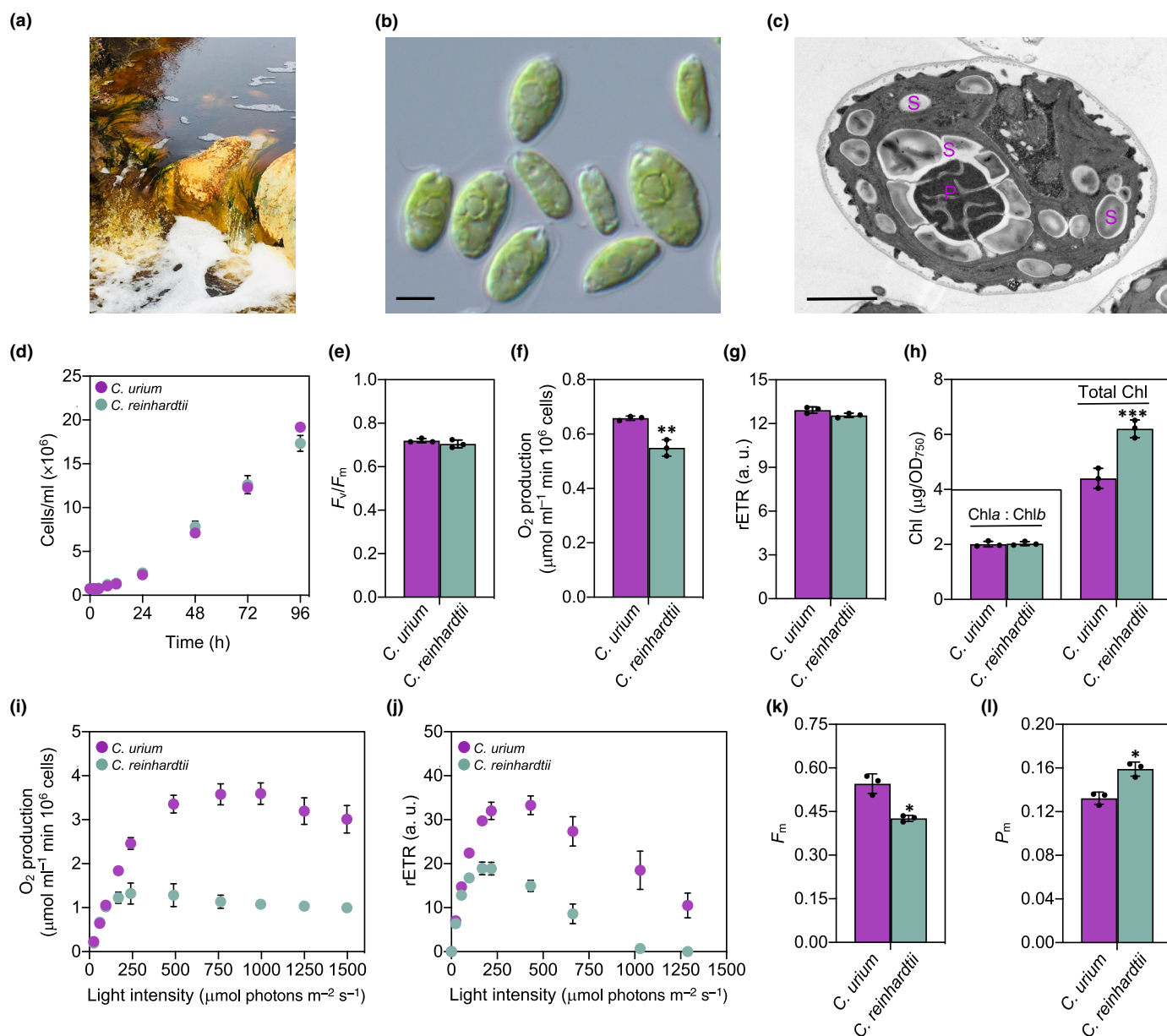


Fig. 1 *Chlamydomonas urium*, a newly identified green microalga isolated from the Río Tinto. (a) Natural environment of Río Tinto (Nerva, Spain). (b) Optical microscopy image of *C. urium* from axenic cultures grown autotrophically at the exponential phase in high salt medium (HSM) medium. Bar, 5 μm . (c) Electron microscopy image of *C. urium* grown as described in (b). Bar, 1 μm . S, starch granule; P, pyrenoid. (d) Growth curve of *C. urium* cells (pink) and *Chlamydomonas reinhardtii* cells (green) in HSM medium. Four biological replicates were taken, and the cell number ml^{-1} was measured. Photosynthetic parameters of both *Chlamydomonas* species including F_v/F_m ratio (e), O_2 production (f) and relative electron transport rate (rETR) (g). (h) Chlorophyll content of *C. urium* and *C. reinhardtii* cells. Inset panel shows the Chla : Chlb ratio. Oxygen production (i) and rETR (j) of *C. urium* and *C. reinhardtii* in response to different light intensities. (k) Maximum fluorescence (F_m) of both *Chlamydomonas* strains. (l) Maximum amount of photo-oxidizable P700 (P_m) of both *Chlamydomonas* strains. At least three biological replicates were measured. Error bars indicate SD. For panels (d–h), (k) and (l), cells were grown in HSM medium at 25°C and $50 \mu\text{mol m}^{-2} \text{ s}^{-1}$ of light intensity. A.u. indicates arbitrary units. Asterisks represent significant differences according to two-tailed Student's *t*-test: ***, $P < 0.001$; **, $P < 0.01$; *, $P < 0.05$. Not significant ≥ 0.05 . The statistical analysis is detailed in Supporting Information Table S3.

We also investigated the capacity of *C. urium* to use organic compounds such as acetate or glucose as carbon source. In contrast to *C. reinhardtii*, *C. urium* was unable to metabolize acetate in dark conditions and the presence of this organic carbon in the medium had a negative effect on *C. urium* cell growth in the light

(Fig. S1c). As described previously for *C. reinhardtii* (Xenie & Jean, 2013), we found that *C. urium* does not use glucose as carbon source (Fig. S1d). The natural acidic environment of *C. urium* does not preserve well the organic matter, which is mostly generated by photosynthetic and chemolithoautotrophic

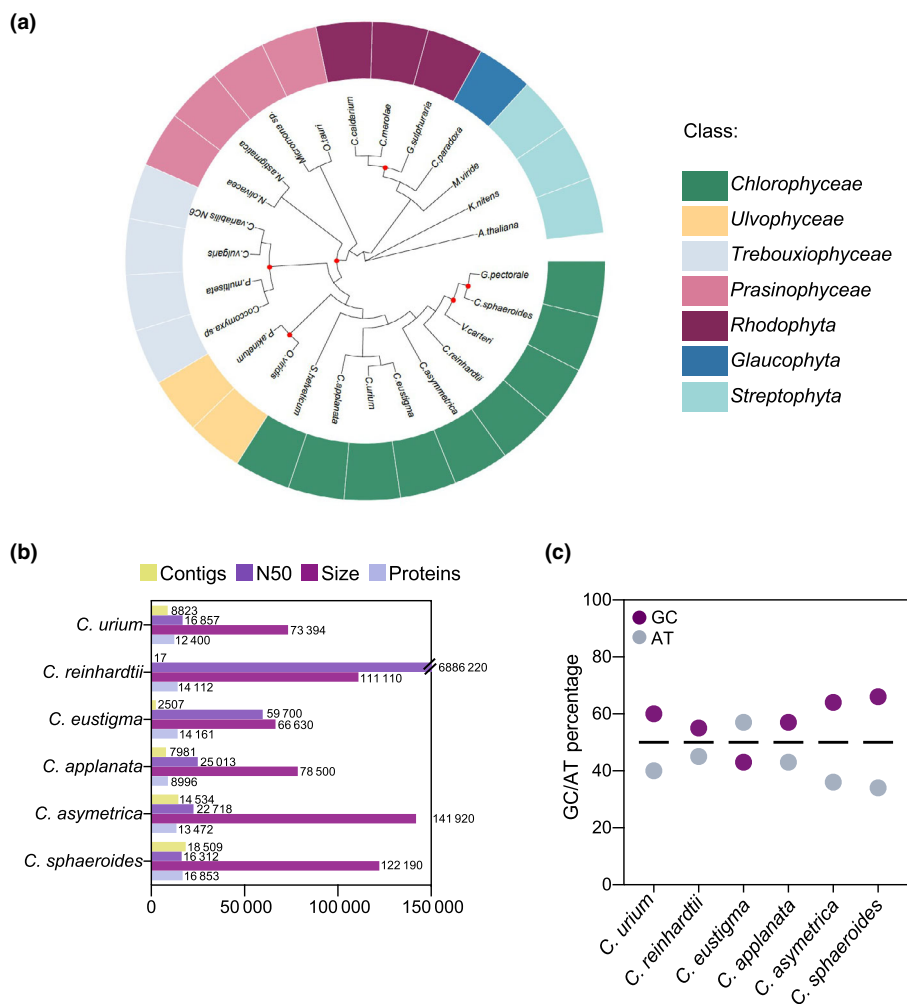


Fig. 2 Genome comparison of *Chlamydomonas urium* and other organisms. (a) Molecular phylogeny of different photosynthetic organisms based on the sequences of 16S and 23S ribosomal RNA genes. The different classes are indicated with a color code on the right. Bootstrap values below 70 are indicated by red dots. (b) Parameters of the genomes including contigs, N50, genome size and number of proteins from *C. urium* and other *Chlamydomonas* species. (c) AT and GC content (in %) of *C. urium* genome compared to other *Chlamydomonas* species. A, adenine; T, thymine; C, cytosine; G, guanine. The 50% value is indicated with a dashed line. *Chlamydomonas* species used in this analysis: *C. urium*; *C. reinhardtii*; *C. eustigma*; *C. applanata*; *C. asymetrica*; *C. sphaeroides*.

activity (López-Archilla *et al.*, 2001). Thus, it is likely that *C. urium* did not acquire the capacity to transport and/or metabolize organic compounds.

Analysis of the *C. urium* nuclear genome

To investigate the phylogenetic relationships of *C. urium*, we sequenced the genome of this microalga. Illumina NextSeq 500 reads of genomic DNA were obtained and processed for quality control. The sequences of 16S and 23S ribosomal RNA genes were identified and used to perform a molecular phylogenetic study. This evolutionary analysis indicated that *C. urium* belongs to the *Chlorophyceae* class and is closely related to *Chlamydomonas eustigma*, an acidophilic microalga isolated from sulfuric acid mine drainage (Hirooka *et al.*, 2017) (Fig. 2a). In the phylogenetic tree, *C. urium* is more distant to its neutrophilic relative *C. reinhardtii* although both microalgae evolved from a common ancestor (Fig. 2a). In close agreement, whole-genome comparisons between neutrophilic and acidophilic green algae indicate that acidophiles evolved from neutrophilic ancestors (Hirooka *et al.*, 2017). The sequenced *C. urium* DNA reads were assembled into 8823 contigs (N50 = 16.8 kb) with a total length

of 73.4 Mb (Fig. 2b). The GC content of the *C. urium* genome is 60%, which is similar to other members of the order *Chlamydomonadales* but significantly higher than its closest relative *C. eustigma* (45%) (Fig. 2c). A total of 12 400 protein-coding genes were identified in the assembled *C. urium* draft genome using AUGUSTUS software (Fig. 2b).

Autophagy is conserved in *C. urium*

Autophagy has been described in green algae and core ATG proteins are well conserved in these organisms (Díaz-Troya *et al.*, 2008; Pérez-Pérez *et al.*, 2010; Shemi *et al.*, 2015; Mallén-Ponce *et al.*, 2023). However, this major degradative pathway has not been yet investigated in extremophiles, which prompted us to analyze this catabolic process in *C. urium*. First, we searched for homologs of ATG genes in the assembled *C. urium* draft genome. Our survey identified ATG genes encoding proteins that regulate the initiation of autophagy, including the ATG1 kinase, proteins involved in early steps of autophagosome formation such as ATG6, ATG9 and ATG14, and proteins from the ATG8 lipidation system including ATG3, ATG7 and ATG8 (Fig. 3a). Core ATG genes were also identified in the genome of *C. eustigma* and

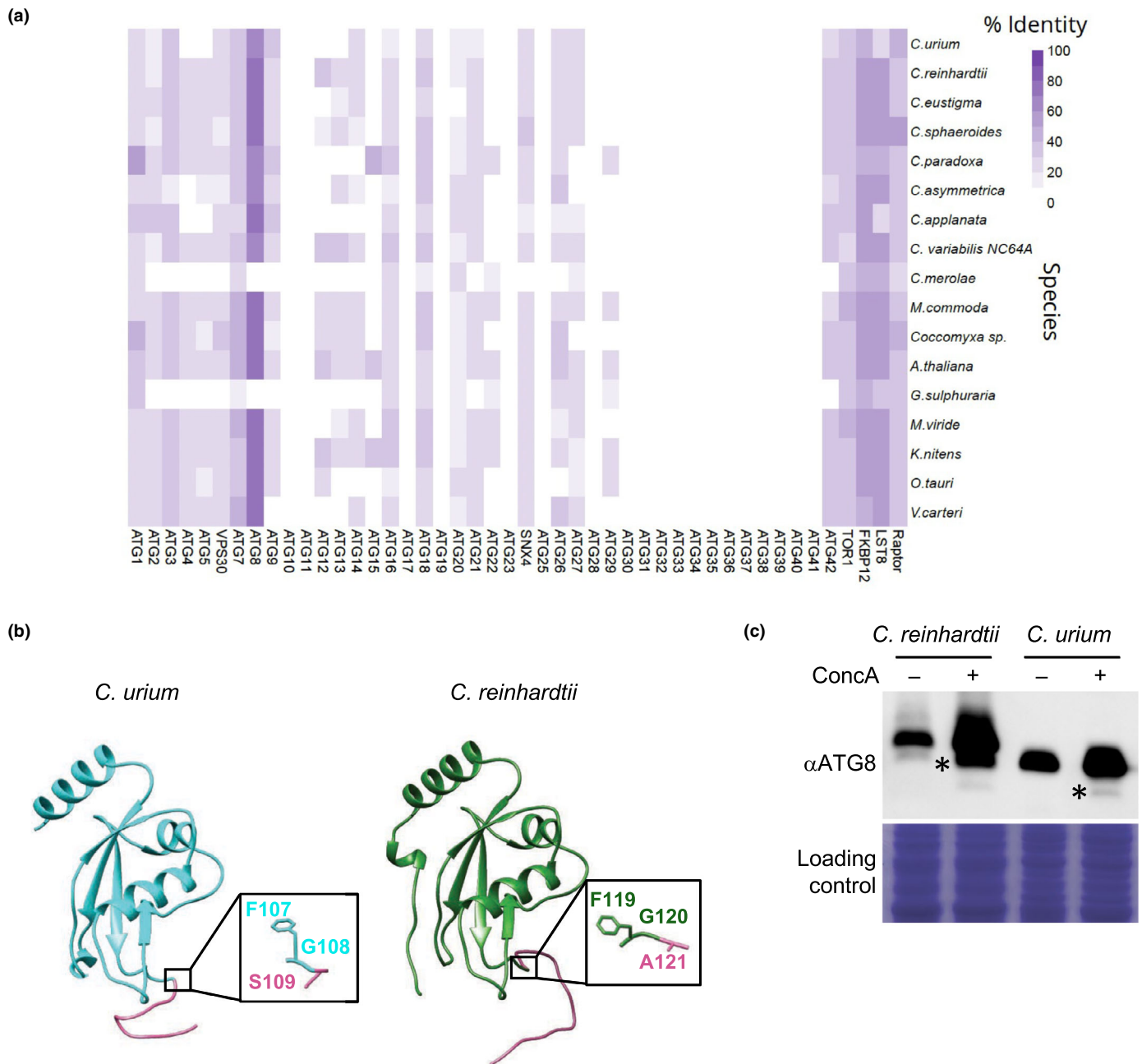


Fig. 3 Autophagy in the extremophilic microalga *C. urium*. (a) Conservation of ATG genes in *C. urium* and other organisms. Species abbreviations: *G. sulphuraria*, *Galdieria sulphuraria*; *C. merolae*, *Cyanidioschyzon merolae*; *M. commoda*, *Micromonas commoda*; *A. thaliana*, *Arabidopsis thaliana*; *K. nitens*, *Klebsormidium nitens*; *Coccomyxa* sp., *Coccomyxa* sp.; *C. sphaeroides*, *Chlamydomonas sphaeroides*; *C. reinhardtii*, *Chlamydomonas reinhardtii*; *C. variabilis* NC64A, *Chlorella variabilis* NC64A; *O. tauri*, *Ostreococcus tauri*; *M. viride*, *Mesostigma viride*; *C. eustigma*, *Chlamydomonas eustigma*; *V. carteri*, *Volvox carteri*; *C. eustigma*, *Chlamydomonas eustigma*; *C. paradoxa*, *Cyanophora paradoxa*; *C. asymmetrica*, *Chlamydomonas asymmetrica*; *C. applanata*, *Chlamydomonas applanata*; *C. urium*, *Chlamydomonas urium*. (b) Structural modeling of *C. urium* and *C. reinhardtii* ATG8 proteins. The C terminus of both proteins is colored in pink, and the highly conserved Gly (Gly108 from *C. urium* and Gly120 from *C. reinhardtii*) are highlighted. (c) Immunoblot analysis of ATG8 from *C. urium* and *C. reinhardtii* in the absence (–) or presence (+) of 0.2 μ M Concanamycin A (ConcA). Lipidated ATG8 (ATG8-PE) is indicated with asterisks. Coomassie-stained gel was used as loading control.

C. applanata (Fig. 3a), strongly suggesting that autophagy might be conserved in acidophilic green algae. This contrasts markedly with extremophilic unicellular species of red algae such as *Cyanidioschyzon merolae* or *Galdieria sulphuraria*, which lack ATG

genes (Shemi *et al.*, 2015). The absence of core autophagy components in red algae suggests that a divergent evolution in ATG genes could take place in Chlorophyta and Rhodophyta. In addition to ATG proteins, we found that all components of the

TORC1 complex (TOR1, LST8 and Raptor), a main negative regulator of autophagy in all eukaryotes (Mallén-Ponce *et al.*, 2022b), are conserved in *C. urium* (Fig. 3a).

Among the identified ATG proteins, ATG8 displayed the highest conservation in green algae (Figs 3a, S5a). ATG8 plays a central role in autophagosome formation, selective cargo recruitment and vacuolar fusion of autophagosomes (Nakatogawa, 2020). This protein is cleaved by the ATG4 protease at a highly conserved Gly located at the C-terminus, which is then conjugated to phosphatidylethanolamine (PE) in a process called ATG8 conjugation or ATG8 lipidation (Nakatogawa, 2020). Modified ATG8 (ATG8-PE) interacts with proteins from the core autophagy machinery as well as with autophagy adaptors and receptors. This interaction takes place through conserved hydrophobic pockets on ATG8 known as AIM and UIM for ATG8- and ubiquitin-interacting motif, respectively (Xie *et al.*, 2016; Kellner *et al.*, 2017; Gatica *et al.*, 2018; Marshall *et al.*, 2022). The *ATG8* gene from *C. urium* encodes a protein with 118 amino acids and a predicted molecular mass of 13.5 kDa. Similar to other microalgae (Mallén-Ponce *et al.*, 2023), structural modeling of *C. urium* ATG8 revealed a characteristic ubiquitin-like folding with conserved α -helices and β -strands (Fig. 3b), two hydrophobic pockets that bind to the AIM motif and a hydrophobic patch that binds to the UIM motif (Fig. S5b). As described for ATG8 proteins from other microalgae including *C. reinhardtii* (Pérez-Pérez *et al.*, 2010; Mallén-Ponce *et al.*, 2023), the C-terminus of *C. urium* ATG8 includes an extension after the conserved Gly108 that must be processed for its conjugation to autophagosomal membrane (Figs 3b, S5a).

To confirm the presence of ATG8 in *C. urium*, we used a polyclonal antibody raised against *C. reinhardtii* ATG8 that cross-reacts with ATG8 proteins from other microalgae and plants (Pérez-Pérez *et al.*, 2010; Álvarez *et al.*, 2012). In agreement with the predicted size of the protein, a single band of lower size than *C. reinhardtii* ATG8 was detected in total extracts from log-phase *C. urium* cells grown under standard conditions (Fig. 3c). Next, we investigated whether autophagy might operate in *C. urium* cells under these conditions. Basal autophagy can be monitored in microalgae by blocking autophagic flux with ConCA (Couso *et al.*, 2018), a specific inhibitor of vacuolar ATPase that prevents the degradative capacity of this compartment (Dröse & Alten-dorf, 1997). As described previously in *C. reinhardtii* (Couso *et al.*, 2018; Fig. 3c), treatment of *C. urium* cells with ConCA resulted in an increase in the abundance of ATG8 and the detection of ATG8-PE (Fig. 3c). Taken together, our observations strongly suggested that an active autophagy machinery is present in the extremophilic microalga *C. urium*.

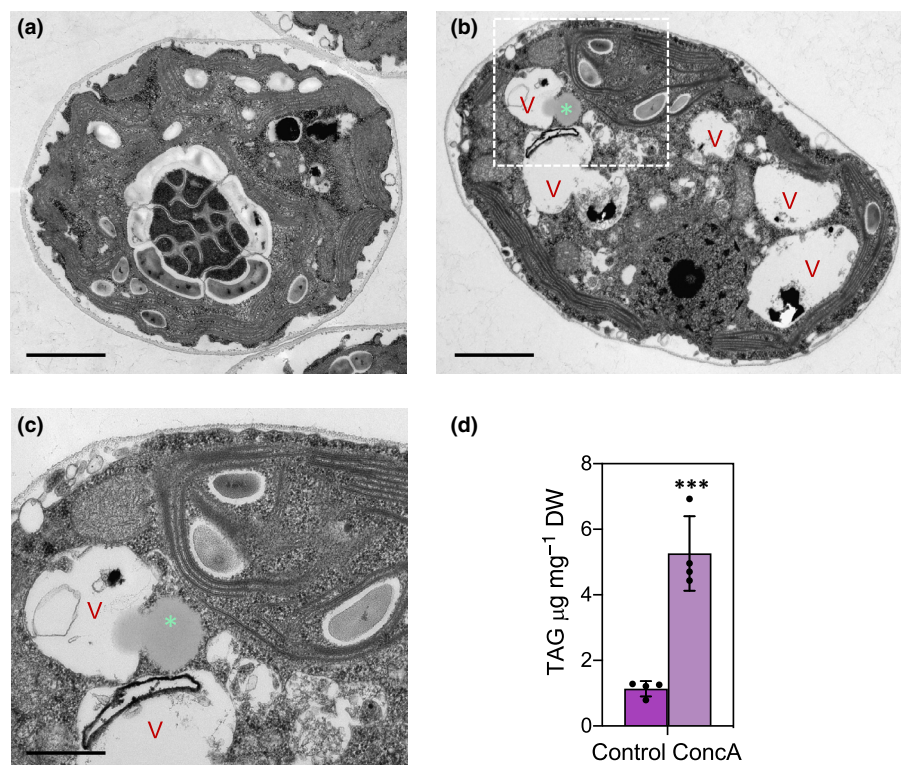
Inhibition of autophagic flux reveals the conservation of lipophagy in *C. urium*

To further investigate the effect of inhibiting autophagic flux in *C. urium*, we performed an ultrastructural analysis by electron microscopy. It has been reported that inhibition of autophagic flux by ConCA in *C. reinhardtii* results in a higher degree of

vacuolization and a pronounced increase in vacuole size (Couso *et al.*, 2018). Some of the most prominent structures at the electron microscope in *C. urium* cells under standard growth conditions were the pyrenoid and starch granules localized in the chloroplast, whereas vacuoles were occasionally found between the nucleus and the concave surface of the chloroplast (Figs 1c, 4a). However, treatment with ConCA had a profound effect on the size and number of vacuoles in *C. urium*. Large vacuoles with internal material and small vesicles inside were readily detected in *C. urium* cells upon autophagic flux inhibition (Fig. 4b,c). A similar effect has already been reported in *C. reinhardtii* cells following ConCA treatment (Couso *et al.*, 2018), supporting the notion that this drug inhibits autophagic flux in *C. urium*. Remarkably, we detected LDs in close contact with vacuoles or engulfed by these organelles in *C. urium* cells treated with ConCA (Figs 4b,c, S6a–d). LDs were even detected inside the vacuole in some cells (Fig. S6c), suggesting that these lipid storage organelles were likely enclosed by the vacuole via a lipophagy-like process. It is worth noting that LDs were rarely found in untreated *C. urium* cells, indicating that the detection of these organelles was a consequence of autophagic flux inhibition. The effect of ConCA in LD formation found in *C. urium* does not seem to take place in *C. reinhardtii* (Couso *et al.*, 2018). Thus, our results suggested that these two microalgae likely differ in the mechanisms regulating LD turnover, at least under standard growth conditions.

LDs are mainly composed of TAGs surrounded by a monolayer of phospholipids and specific proteins (Goold *et al.*, 2015). Therefore, we speculated that an increase in the number of LDs in *C. urium* cells treated with ConCA might also result in an increase in the level of TAGs. To test this hypothesis, we determined the TAG content of *C. urium* in response to ConCA. Our results showed a significant increase in TAGs in *C. urium* cells treated with ConCA (Fig. 4d), in agreement with the detection of LDs in these cells. Given that ConCA is an effective inhibitor of autophagic flux in multiple organisms including algae (Couso *et al.*, 2018), the most plausible explanation for the detection of LDs in contact with vacuoles in *C. urium* is that ConCA blocks the degradation of these lipid storage organelles in the vacuole. These results strongly suggest that the extremophilic microalga *C. urium* exhibits an active basal autophagy process for the recycling of TAGs that can be readily detected upon blockage of vacuolar function. Our results are in line with a study connecting TAG metabolism and autophagy in the marine microalga *Nannochloropsis oceanica*. Chemical inhibition of the phosphatidylinositol kinase VPS34, which regulates autophagy initiation (Nakatogawa, 2020), results in increased TAG level in *N. oceanica*, suggesting that TAGs might be degraded via autophagy in this marine microalga (Zienkiewicz *et al.*, 2020). In addition to lipophagy, algae and plants also mobilize lipids through lipolysis and fatty acid β -oxidation (Kong *et al.*, 2018; Li-Beisson *et al.*, 2021). A number of enzymes involved in the lipolysis of acyl-lipids and the β -oxidation of fatty acids have been described in algal genomes (Li-Beisson *et al.*, 2015). We identified in the genome of *C. urium* genes participating in lipolysis and β -oxidation, including acyl-CoA oxidases, dehydrogenases,

Fig. 4 Ultrastructural analysis of *Chlamydomonas urium* cells upon autophagic flux inhibition. Electron microscopy images of *C. urium* cells in the absence (a) or presence (b) of 0.2 μ M Concanamycin A (ConcA). Bars, 1 μ m. (c) Enlargement of (b) showing vacuole-lipid droplet (LD) contact sites. Vacuoles (V) and LDs (*) are indicated in the images. Bar, 500 nm. (d) Quantification of triacylglycerols (TAGs) from *C. urium* cells in the absence or presence of 0.2 μ M ConcA. DW indicates dry weight. Three biological replicates were analyzed for each condition. Error bars indicate SD. Asterisks represent significant differences according to two-tailed Student's *t*-test: ***, $P < 0.001$. The statistical analysis is detailed in Supporting Information Table S3.



hydrolases and lipases (Table S2). Therefore, these lipid catabolic pathways may likely contribute to lipid degradation besides lipophagy in *C. urium* under specific conditions.

Nitrogen starvation boosts lipophagy

Algae tend to upregulate the synthesis of TAGs and LDs upon exposure to different stress conditions, particularly nitrogen starvation (Wang *et al.*, 2009). In *C. reinhardtii*, nitrogen limitation triggers autophagy, allowing the recycling of cellular material to support cell survival (Pérez-Pérez *et al.*, 2010). We analyzed the efficiency of *C. urium* to generate TAGs and LDs under nitrogen deprivation. A 10-fold increase in the level of TAGs was detected in nitrogen-starved *C. urium* cells (Fig. 5a). In agreement with the high TAG content, electron microscopy analysis of nitrogen-starved *C. urium* cells showed the presence of a variable number of LDs per cell (Fig. 5b). This ultrastructural study also revealed close contacts between LDs and vacuoles (Fig. 5b–e) similar to the ones detected in ConcA-treated cells (Fig. 4b,c). These results suggested that there might be an interplay between LDs and vacuoles under nitrogen starvation likely mediated through lipophagy. To test this hypothesis, we blocked autophagic flux with ConcA in nitrogen-starved *C. urium* cells and analyzed the LDs by electron microscopy. Inhibition of autophagic flux resulted in a pronounced detection of large LDs that were frequently localized inside or in close contact with vacuoles (Figs 5f–i, S6). We also analyzed the TAG content in nitrogen-starved and ConcA-treated cells. Interestingly, the level of TAGs in these cells was similar to the one detected in nitrogen-starved cells (Fig. 5a), indicating that the inhibition of autophagic flux

did not further increase the TAG content under nitrogen stress. Taken together, our results indicated that LDs generated under nitrogen starvation are recycled in the vacuole via lipophagy in *C. urium*. Lipophagy-like processes have also been described in other microalgae under nutrient-limiting conditions. Carbon starvation leads to the degradation of lipids by the vacuole in the freshwater microalgae *Microsterias denticulata* (Schwarz *et al.*, 2017) and *Auxenochlorella protothecoides* (Zhao *et al.*, 2014). Nitrogen deprivation assays revealed direct contacts between LDs and vacuoles in the green oleaginous microalga *Lobosphaera incisa* (Kokabi *et al.*, 2020) and the marine microalga *Nannochloropsis oceanica* (Zienkiewicz *et al.*, 2020). Mounting evidence indicates that autophagy also participates in TAG hydrolysis and LD turnover in *C. reinhardtii*. Direct interaction between autophagosomes and LDs has been described at early stages of nitrogen starvation (Tran *et al.*, 2019). Moreover, a *C. reinhardtii atg8* insertional mutant displays a delay in TAG hydrolysis in nitrogen resupply assays (Kajikawa *et al.*, 2019), suggesting that autophagy participates in LD catabolism in this microalga.

Chlamydomonas urium maintains an active central metabolism upon autophagic flux inhibition

The capability of *C. urium* to accumulate large amounts of TAGs in response to ConcA suggested that the lytic activity of the vacuole regulates lipid homeostasis in this extremophilic alga. Because lipids constitute an important carbon sink in algae (Li-Beisson *et al.*, 2019), we speculated that autophagic flux inhibition could lead to a metabolic shift toward other cellular

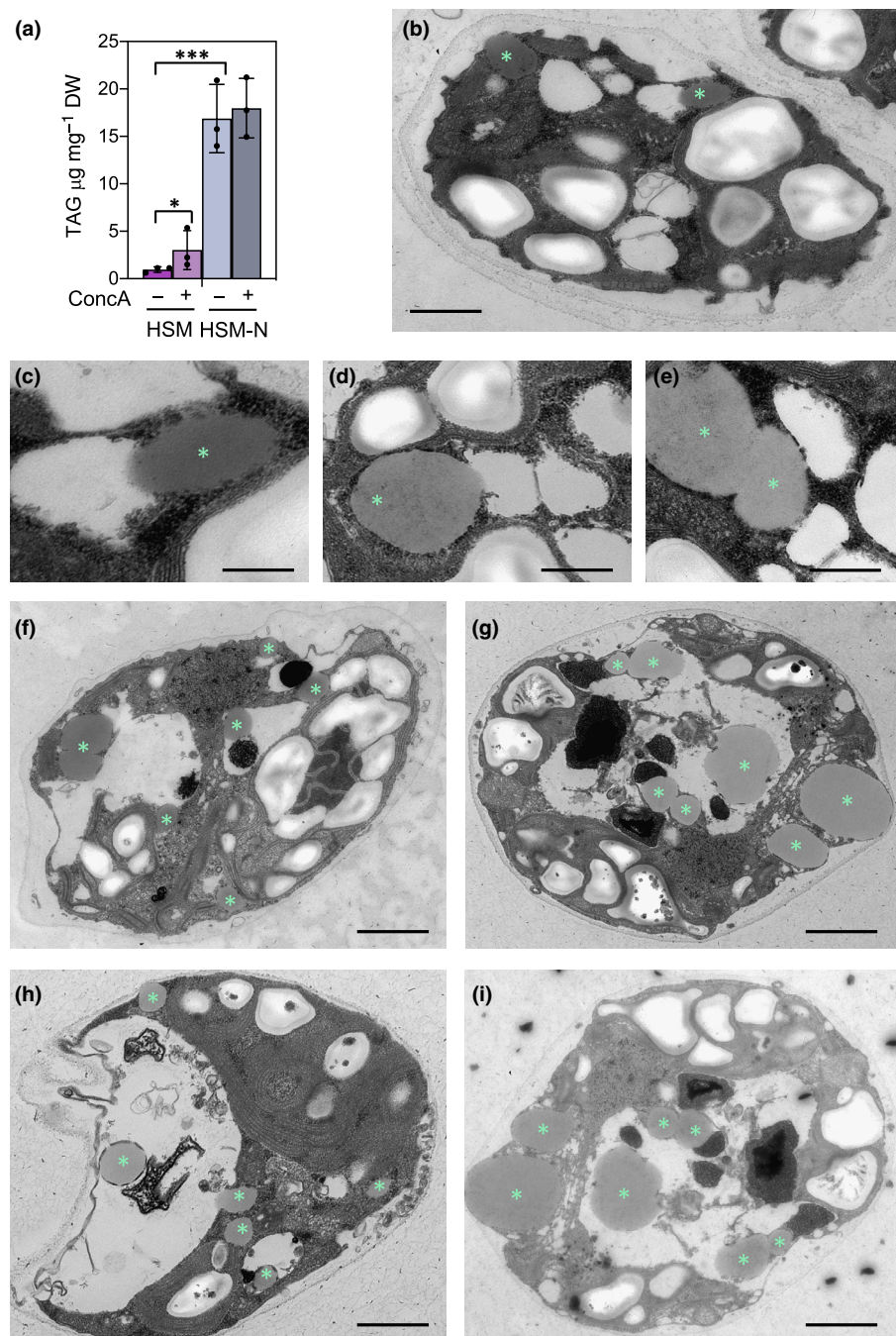


Fig. 5 Ultrastructural analysis of *Chlamydomonas urium* cells upon nitrogen starvation and autophagic flux inhibition. (a) Production of triacylglycerols (TAG) in *C. urium* cells subjected to N-starvation in the absence or presence of 0.2 μ M Concanamycin A (ConcA). DW indicates dry weight. Three biological replicates were analyzed for each condition. Error bars indicate SD. (b) Electron microscopy image of nitrogen-starved *C. urium*. Bar, 2 μ m. (c–e) Images showing lipid droplets (LDs) in close contact with vacuoles in nitrogen-starved cells. (c) Enlargement of (b). Bars, 300 nm. (f–i) Electron microscopy images of N-starved *C. urium* cells in the presence of 0.2 μ M ConcA. Bars, 1 μ m. Lipid droplets are labeled with an asterisk. Asterisks represent significant differences according to two-tailed Student's *t*-test: ***, $P < 0.001$; *, $P < 0.05$. The statistical analysis is detailed in Supporting Information Table S3.

pathways. To test this hypothesis, we performed a metabolomic analysis of *C. urium* in response to ConcA. Under normal growth, the abundance of some intermediates from the Calvin–Benson–Bassham (CBB) cycle such as RuBP, 3PGA, DHAP and Ru5P/X5P were higher ($\text{Log}_2\text{FC} \geq 1$, ≤ -1 and P -value of < 0.05) in *C. urium* while Acetyl-CoA and CoA were significantly lower in this extremophilic microalga in comparison with the levels detected in *C. reinhardtii* (Fig. S7a). The total amino acid content was higher in *C. urium* due to the larger levels of Gly, Ala, Ser, Asp and Lys (Fig. S7b,c). In consonance with these results, it has been recently proposed that higher metabolite levels might confer an increased metabolic flexibility to the

extremophilic microalga *Chlorella ohadii* to cope with extreme stress (Treves *et al.*, 2022).

The addition of ConcA had different effects in both microalgae, with a strong impact on CBB and TCA cycle intermediates, central metabolites and some amino acids. Inhibition of autophagic flux in *C. reinhardtii* led to a general drop of all intermediates from the CBB cycle, some intermediates from the TCA cycle and central metabolites connecting both cycles such as PEP and pyruvate (Fig. 6a). Moreover, the level of Acetyl-CoA, a precursor for the biosynthesis of fatty acids, strongly decreased in *C. reinhardtii* (Fig. 6a). By contrast, treatment of *C. urium* cells with ConcA had a lower effect on the CBB cycle while causing a substantial increase

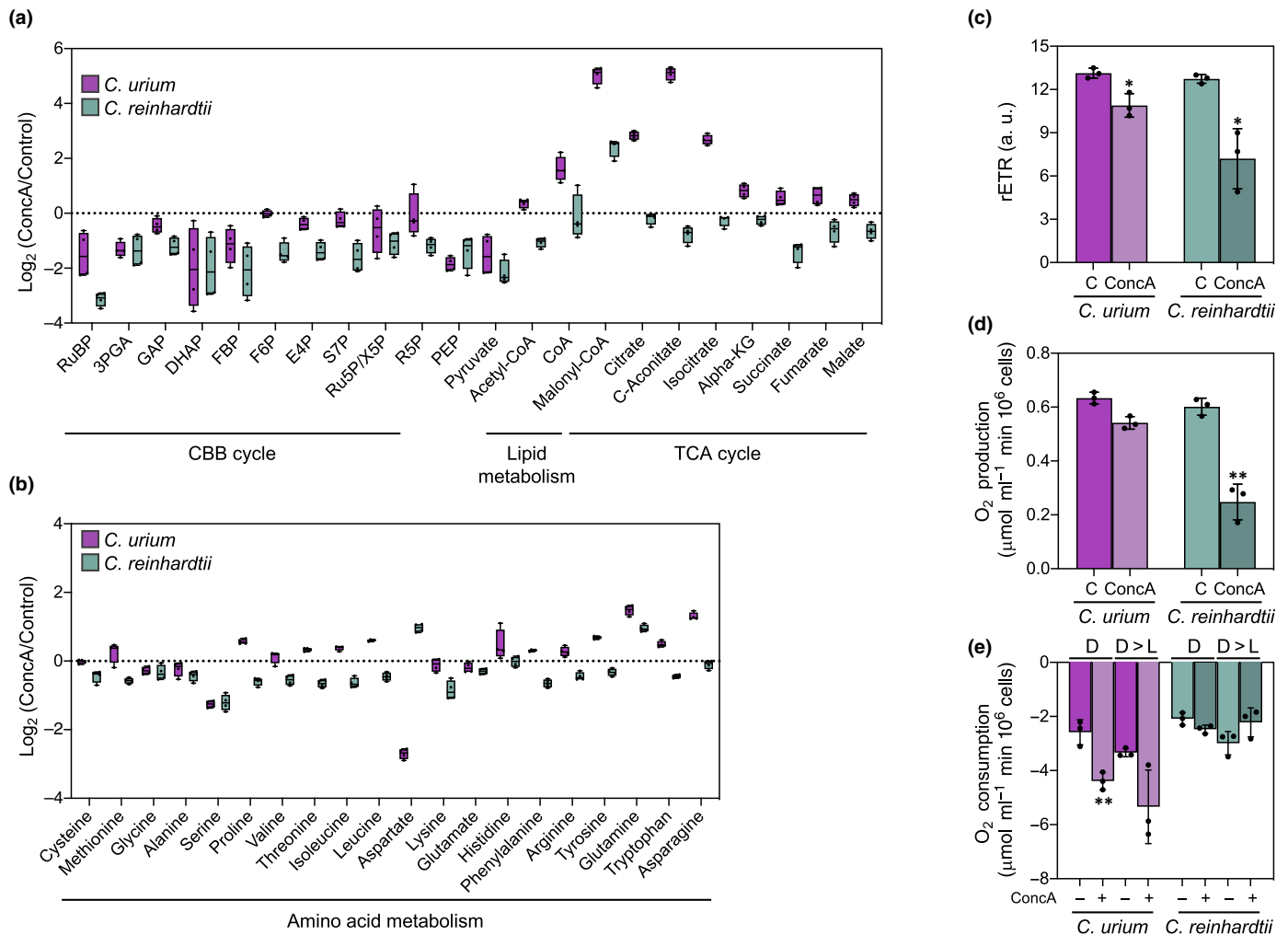


Fig. 6 Effect of autophagic flux inhibition on carbon metabolism. (a) Metabolomic analysis of *Chlamydomonas urium* and *Chlamydomonas reinhardtii* cells grown in high salt medium (HSM) medium and treated with 0.2 μM Concanamycin A (ConcA). Relative abundance of metabolites from the CBB cycle, lipid metabolism and TCA cycle. (b) Relative abundance of individual amino acids. The metabolite levels from ConcA-treated cells were related to untreated cells ($\text{log}_2 \text{ConcA}/\text{Control}$). Four biological replicates were analyzed for each condition. Error bars represent SD of the mean values. Boxplot elements in (a, b): enter lines represent median; box limits indicate upper and lower quartiles; and whiskers indicate Min to Max values. (c) Relative electron transport rate (rETR) from *C. urium* and *C. reinhardtii* cells in the absence or presence of 0.2 μM ConcA. (d) Oxygen production from *C. urium* and *C. reinhardtii* cells in the absence or presence of 0.2 μM ConcA. (e) Oxygen consumption from both *Chlamydomonas* strains treated with 0.2 μM ConcA. Respiration rates were determined after 5 min of dark (D) or after reillumination for 10 min and then in the dark for 5 min (D > L). Three biological replicates were analyzed for each condition. Error bars represent SD of the mean values. Asterisks represent significant differences according to two-tailed Student's *t*-test: **, $P < 0.01$; *, $P < 0.05$; not significant ≥ 0.05 . The statistical analysis is detailed in Supporting Information Table S3.

in TCA cycle intermediates, particularly citrate, aconitate and isocitrate (Fig. 6a). We also detected a substantial increase in the abundance of the fatty acid precursor malonyl in *C. urium* cells treated with ConcA (Fig. 6a), in close agreement with the high level of TAGs and LDs found in these cells (Fig. 4). Finally, the abundance of some amino acids including Gln, Arg, Leu, Val, Ile, Asn, Phe, Tyr and Trp was also upregulated in *C. urium* but not in *C. reinhardtii* upon autophagic flux inhibition (Fig. 6b).

We hypothesized that the production of TAGs and LDs in *C. urium* cells with impaired vacuolar function must be sustained by a robust carbon assimilation. Thus, we determined the photosynthetic capacity of *C. urium* upon autophagic flux inhibition. At nonsaturating light intensity (50 $\mu\text{mol photons m}^{-2} \text{ s}^{-1}$),

ConcA had only a mild impact on O_2 production and rETR in *C. urium* while the effect was much stronger in *C. reinhardtii* (Fig. 6c,d). The effect of ConcA on these photosynthetic parameters was more pronounced at high light intensities in both microalgae but *C. urium* exhibited higher capacities (Fig. S8). As organic acids from the TCA cycle are consumed by respiration, we also analyzed the O_2 consumption of both microalgae in response to ConcA. In line with the higher level of TCA cycle intermediates detected in *C. urium* cells treated with ConcA, respiration was upregulated in darkness and directly after light exposure in these cells (Fig. 6e). In *C. reinhardtii*, cells displayed lower respiration rates and no effect was observed upon ConcA treatment (Fig. 6e). These results indicated that the inhibition of

autophagic flux does not abrogate the capacity of *C. urium* cells to assimilate carbon via photosynthesis and thus generate carbon storage compounds such as TAGs and LDs.

Together, our results illustrate the different impacts of ConcA on the photosynthetic metabolism of *C. urium* and *C. reinhardtii*, and provide the metabolic basis for the capacity of an extremophilic alga to catabolize TAGs and LDs through lipophagy. LDs are highly dynamic structures that may also serve to buffer the levels of potentially toxic fatty acids, which are very sensitive to reactive oxygen species (ROS) damage. Excessive lipids in the cytoplasm or chloroplast may be detrimental to cells, generating ROS and causing organelle damage (Van Breusegem & Dat, 2006; Mullineaux & Baker, 2010; Yin *et al.*, 2011). Given that lipids are an important carbon sink in microalgae, especially those inhabiting extreme environments (Li-Beisson *et al.*, 2019; Treves *et al.*, 2022), we propose that the elevated level of basal lipophagy found in *C. urium* might serve as a mechanism to adjust lipid levels according to the cellular requirements. It is therefore likely that acidophilic microalgae such as *C. urium* utilize lipophagy to get the metabolic flexibility required for the adaptation of extremophilic organisms to their challenging environment. Neutrophilic microalgae including *C. reinhardtii* may activate lipophagy in response to stress but this lipid catabolic process is not active or operates at a low rate under optimal growth conditions. Whether other extremophilic microalgae utilize lipophagy to overcome extreme conditions remains to be investigated.

Acknowledgements

This work was supported in part by the *Ministerio de Ciencia, Innovación y Universidades* (grants PID2021-123500NB-I00 to JLC, PID2019-110080GB-I00 to MEPP and TED2021-130912B-I00 to JLC and MEPP), CSIC (grant 2023AEP102 to MEPP) and *Junta de Andalucía* (grant P20_00057 to JLC), a *Juan de la Cierva* postdoctoral contract (FJC2021-048000-I) to MJMP, and a predoctoral contract (PRE2022-102797) to YOG. We thank C3UPO for the HPC support, Carlos Parejo for technical assistance with the analysis of metabolites profiles and Florentino Pérez-Navarro for technical assistance collecting samples from the water source of Río Tinto.

Competing interests

None declared.

Author contributions

MEP-P and JLC designed and supervised the study. MEP-P, MJM-P and YO-G performed most of the experiments and analyzed the data. AR and AJP-P performed the genome assembling, annotation and analysis. JJS and EM-F carried out the TAG content determination. MEP-P, MJM-P, YO-G and AR prepared the figures. MEP-P and JLC wrote the manuscript with input of all co-authors. All authors revised the manuscript and gave final approval for the publication. MEP-P and MJM-P contributed equally to this work.

ORCID

José L. Crespo  <https://orcid.org/0000-0003-3514-1025>
Yosu Odriozola-Gil  <https://orcid.org/0000-0001-7728-5495>

Data availability

The data that support the *C. urium* genome assembly were deposited in GenBank (BioProject PRJNA1037726: <https://www.ncbi.nlm.nih.gov/bioproject/1037726>). Other data that support the findings of this study are available in the [Supporting Information](#).

References

- Aguilera A. 2013. Eukaryotic organisms in extreme acidic environments, the Río Tinto case. *Life* 3: 363–374.
- Aguilera A, Gómez F, Lospitao E, Amils R. 2006. A molecular approach to the characterization of the eukaryotic communities of an extreme acidic environment: methods for DNA extraction and denaturing gradient gel electrophoresis analysis. *Systematic and Applied Microbiology* 29: 593–605.
- Aguilera A, Souza-Egipsy V, Gómez F, Amils R. 2007. Development and structure of eukaryotic biofilms in an extreme acidic environment, Río Tinto (SW, Spain). *Microbial Ecology* 53: 294–305.
- Altschul SF, Madden TL, Schäffer AA, Zhang J, Zhang W, Lipman DJ. 1997. Gapped BLAST and PSI-BLAST: a new generation of protein database search programs. *Nucleic Acids Research* 25: 3389–3402.
- Álvarez C, García I, Moreno I, Pérez-Pérez ME, Crespo JL, Romero LC, Gotor C. 2012. Cysteine-generated sulfide in the cytosol negatively regulates autophagy and modulates the transcriptional profile in Arabidopsis. *Plant Cell* 24: 4621–4634.
- Amaral Zettler LA, Gómez F, Zettler E, Keenan BG, Amils R, Sogin ML. 2002. Eukaryotic diversity in Spain's River of Fire. *Nature* 417: 137.
- Amils R. 2016. Lessons learned from thirty years of geomicrobiological studies of Río Tinto. *Research in Microbiology* 167: 539–545.
- Angeles A, Manrubia SC, Felipe G, Nuria R, Ricardo A. 2006. Eukaryotic community distribution and its relationship to water physicochemical parameters in an extreme acidic environment, Río Tinto (Southwestern Spain). *Applied and Environmental Microbiology* 72: 5325–5330.
- Barros JAS, Siqueira JAB, Cavalcanti JHF, Araújo WL, Avin-Wittenberg T. 2020. Multifaceted roles of plant autophagy in lipid and energy metabolism. *Trends in Plant Science* 25: 1141–1153.
- Bolger AM, Lohse M, Usadel B. 2014. TRIMMOMATIC: a flexible trimmer for Illumina sequence data. *Bioinformatics* 30: 2114–2120.
- Brock TD. 1973. Lower pH limit for the existence of blue-green algae: evolutionary and ecological implications. *Science* 179: 480–483.
- Capella-Gutiérrez S, Silla-Martínez JM, Gabaldón T. 2009. TRIMAL: a tool for automated alignment trimming in large-scale phylogenetic analyses. *Bioinformatics* 25: 1972–1973.
- Casimiro-Soriguer CS, Muñoz-Mérida A, Pérez-Pulido AJ. 2017. SMA3S: a universal tool for easy functional annotation of proteomes and transcriptomes. *Proteomics* 17: 1700071.
- Couso I, Pérez-Pérez ME, Martínez-Force E, Kim H-S, He Y, Umen JG, Crespo JL. 2018. Autophagic flux is required for the synthesis of triacylglycerols and ribosomal protein turnover in Chlamydomonas. *Journal of Experimental Botany* 69: 1355–1367.
- Díaz-Troya S, Pérez-Pérez ME, Florencio FJ, Crespo JL. 2008. The role of TOR in autophagy regulation from yeast to plants and mammals. *Autophagy* 4: 851–865.
- Dolinsky TJ, Nielsen JE, McCammon JA, Baker NA. 2004. PDB2PQR: an automated pipeline for the setup of Poisson–Boltzmann electrostatics calculations. *Nucleic Acids Research* 32: W665–W667.

- Dröse S, Altendorf K. 1997. Bafilomycins and concanamycins as inhibitors of V-ATPases and P-ATPases. *Journal of Experimental Biology* 200: 1–8.
- Eddy SR. 1998. Profile hidden Markov models. *Bioinformatics* 14: 755–763.
- Fan J, Yu L, Xu C. 2019. Dual role for autophagy in lipid metabolism in Arabidopsis. *Plant Cell* 31: 1598–1613.
- Fernández-Moya V, Martínez-Force E, Garcés R. 2000. Identification of triacylglycerol species from high-saturated sunflower (*Helianthus annuus*) mutants. *Journal of Agricultural and Food Chemistry* 48: 764–769.
- Field CB, Behrenfeld MJ, Randerson JT, Falkowski P. 1998. Primary production of the biosphere: integrating terrestrial and oceanic components. *Science* 281: 237–240.
- Gatica D, Lahiri V, Klionsky DJ. 2018. Cargo recognition and degradation by selective autophagy. *Nature Cell Biology* 20: 233–242.
- Goodenough U, Heiss AA, Roth R, Rusch J, Lee J-H. 2019. Acidocalisomes: ultrastructure, biogenesis, and distribution in microbial eukaryotes. *Protist* 170: 287–313.
- Goold H, Beisson F, Peltier G, Li-Beisson Y. 2015. Microalgal lipid droplets: composition, diversity, biogenesis and functions. *Plant Cell Reports* 34: 545–555.
- Harris EH. 1989. In: Harris EHBT-TCS, ed. *Culture and storage methods*. San Diego, CA, USA: Academic Press, 25–63.
- Harris EH. 2009. Chapter 8 – Chlamydomonas in the laboratory. In: Harris EH, Stern DB, Witman GB, eds. *The Chlamydomonas sourcebook*, 2nd edn. London, UK: Academic Press, 241–302.
- Hirooka S, Hirose Y, Kanesaki Y, Higuchi S, Fujiwara T, Onuma R, Era A, Ohbayashi R, Uzuka A, Nozaki H *et al.* 2017. Acidophilic green algal genome provides insights into adaptation to an acidic environment. *Proceedings of the National Academy of Sciences, USA* 114: E8304–E8313.
- Jackman SD, Vandervalk BP, Mohamadi H, Chu J, Yeo S, Hammond SA, Jahesh G, Khan H, Coombe L, Warren RL *et al.* 2017. ABySS 2.0: resource-efficient assembly of large genomes using a Bloom filter. *Genome Research* 27: 768–777.
- Juruss E, Engel D, Star K, Monson B, Brandt J, Felberg LE, Brookes DH, Wilson L, Chen J, Liles K *et al.* 2018. Improvements to the APBS biomolecular solvation software suite. *Protein Science* 27: 112–128.
- Kajikawa M, Yamauchi M, Shinkawa H, Tanaka M, Hatano K, Nishimura Y, Kato M, Fukuzawa H. 2019. Isolation and characterization of Chlamydomonas autophagy-related mutants in nutrient-deficient conditions. *Plant and Cell Physiology* 60: 126–138.
- Katoh K, Standley DM. 2013. MAFFT multiple sequence alignment software version 7: improvements in performance and usability. *Molecular Biology and Evolution* 30: 772–780.
- Kellner R, De la Concepcion JC, Maqbool A, Kamoun S, Dagdas YF. 2017. ATG8 expansion: a driver of selective autophagy diversification? *Trends in Plant Science* 22: 204–214.
- Kokabi K, Gorelova O, Zorin B, Didi-Cohen S, Itkin M, Malitsky S, Solovchenko A, Boussiba S, Khozin-Goldberg I. 2020. Lipidome remodeling and autophagic response in the arachidonic-acid-rich microalga *Lobosphaera incisa* under nitrogen and phosphorous deprivation. *Frontiers in Plant Science* 11: 614846.
- Kong F, Romero IT, Warakanont J, Li-Beisson Y. 2018. Lipid catabolism in microalgae. *New Phytologist* 218: 1340–1348.
- Kurusu T, Koyano T, Hanamata S, Kubo T, Noguchi Y, Yagi C, Nagata N, Yamamoto T, Ohnishi T, Okazaki Y *et al.* 2014. OsATG7 is required for autophagy-dependent lipid metabolism in rice postmeiotic anther development. *Autophagy* 10: 878–888.
- Li-Beisson Y, Beisson F, Riekhof W. 2015. Metabolism of acyl-lipids in *Chlamydomonas reinhardtii*. *The Plant Journal* 82: 504–522.
- Li-Beisson Y, Kong F, Wang P, Lee Y, Kang B-H. 2021. The disassembly of lipid droplets in Chlamydomonas. *New Phytologist* 231: 1359–1364.
- Li-Beisson Y, Thelen JJ, Fedosejevs E, Harwood JL. 2019. The lipid biochemistry of eukaryotic algae. *Progress in Lipid Research* 74: 31–68.
- López-Archilla AI, Marin I, Amils R. 2001. Microbial community composition and ecology of an acidic aquatic environment: the Tinto River, Spain. *Microbial Ecology* 41: 20–35.
- Malavasi V, Soru S, Cao G. 2020. Extremophile microalgae: the potential for biotechnological application. *Journal of Phycology* 56: 559–573.
- Mallén-Ponce MJ, Gámez-Arcas S, Pérez-Pérez ME. 2023. Redox partner interactions in the ATG8 lipidation system in microalgae. *Free Radical Biology and Medicine* 203: 58–68.
- Mallén-Ponce MJ, Pérez-Pérez ME, Crespo JL. 2022a. Photosynthetic assimilation of CO₂ regulates TOR activity. *Proceedings of the National Academy of Sciences, USA* 119: e2115261119.
- Mallén-Ponce MJ, Pérez-Pérez ME, Crespo JL. 2022b. Deciphering the function and evolution of the target of rapamycin signaling pathway in microalgae. *Journal of Experimental Botany* 73: 6993–7005.
- Marshall RS, Hua Z, Mali S, McLoughlin F, Vierstra RD. 2022. ATG8-binding UIM proteins define a new class of autophagy adaptors and receptors. *Cell* 185: 1101–1102.
- Marshall RS, Vierstra RD. 2018. Autophagy: the master of bulk and selective recycling. *Annual Review of Plant Biology* 69: 173–208.
- Masclaux-Daubresse C, d'Andrea S, Bouchez I, Cacas J-L. 2020. Reserve lipids and plant autophagy. *Journal of Experimental Botany* 71: 2854–2861.
- Melo F, Sánchez R, Sali A. 2002. Statistical potentials for fold assessment. *Protein Science* 11: 430–448.
- Mullineaux PM, Baker NR. 2010. Oxidative stress: antagonistic signaling for acclimation or cell death? *Plant Physiology* 154: 521–525.
- Nakatogawa H. 2020. Mechanisms governing autophagosome biogenesis. *Nature Reviews Molecular Cell Biology* 21: 439–458.
- Nishikawa K, Tominaga N. 2001. Isolation, growth, ultrastructure, and metal tolerance of the green alga, *Chlamydomonas acidophila* (Chlorophyta). *Bioscience, Biotechnology, and Biochemistry* 65: 2650–2656.
- Olzmann JA, Carvalho P. 2019. Dynamics and functions of lipid droplets. *Nature Reviews Molecular Cell Biology* 20: 137–155.
- Pérez-Martín M, Blaby-Haas CE, Pérez-Pérez ME, Ascensión A-G, Blaby IK, Merchant SS, Crespo JL. 2015. Activation of autophagy by metals in *Chlamydomonas reinhardtii*. *Eukaryotic Cell* 14: 964–973.
- Pérez-Pérez ME, Florencio FJ, Crespo JL. 2010. Inhibition of target of rapamycin signaling and stress activate autophagy in *Chlamydomonas reinhardtii*. *Plant Physiology* 152: 1874–1888.
- Porra RJ, Thompson WA, Kriedemann PE. 1989. Determination of accurate extinction coefficients and simultaneous equations for assaying chlorophylls a and b extracted with four different solvents: verification of the concentration of chlorophyll standards by atomic absorption spectroscopy. *Biochimica et Biophysica Acta (BBA) – Bioenergetics* 975: 384–394.
- Sali A, Blundell TL. 1993. Comparative protein modelling by satisfaction of spatial restraints. *Journal of Molecular Biology* 234: 779–815.
- Schmollinger S, Chen S, Strenkert D, Hui C, Ralle M, Merchant SS. 2021. Single-cell visualization and quantification of trace metals in Chlamydomonas lysosome-related organelles. *Proceedings of the National Academy of Sciences, USA* 118: e2026811118.
- Schwarz V, Andosch A, Geretschlager A, Affenzeller M, Lütz-Meindl U. 2017. Carbon starvation induces lipid degradation via autophagy in the model alga Microcystis. *Journal of Plant Physiology* 208: 115–127.
- Seo AY, Lau P-W, Feliciano D, Sengupta P, Le Gros MA, Cinquin B, Larabell CA, Lippincott-Schwartz J. 2017. AMPK and vacuole-associated Atg14p orchestrate μ -lipophagy for energy production and long-term survival under glucose starvation. *eLife* 6: e21690.
- Shemi A, Ben-Dor S, Vardi A. 2015. Elucidating the composition and conservation of the autophagy pathway in photosynthetic eukaryotes. *Autophagy* 11: 701–715.
- Shen M, Sali A. 2006. Statistical potential for assessment and prediction of protein structures. *Protein Science* 15: 2507–2524.
- Singh R, Kaushik S, Wang Y, Xiang Y, Novak I, Komatsu M, Tanaka K, Cuervo AM, Czaja MJ. 2009. Autophagy regulates lipid metabolism. *Nature* 458: 1131–1135.
- Soto-Burgos J, Zhuang X, Jiang L, Bassham DC. 2018. Dynamics of autophagosome formation. *Plant Physiology* 176: 219–229.
- Spurr AR. 1969. A low-viscosity epoxy resin embedding medium for electron microscopy. *Journal of Ultrastructure Research* 26: 31–43.
- Stamatakis A. 2014. RAxML v.8: a tool for phylogenetic analysis and post-analysis of large phylogenies. *Bioinformatics* 30: 1312–1313.
- Stanke M, Morgenstern B. 2005. AUGUSTUS: a web server for gene prediction in eukaryotes that allows user-defined constraints. *Nucleic Acids Research* 33: W465–W467.
- Stephani M, Dagdas Y. 2020. Plant selective autophagy – still an uncharted territory with a lot of hidden gems. *Journal of Molecular Biology* 432: 63–79.

- Tran Q-G, Yoon HR, Cho K, Lee S-J, Crespo JL, Ramanan R, Kim H-S. 2019. Dynamic interactions between autophagosomes and lipid droplets in *Chlamydomonas reinhardtii*. *Cells* 8: 992.
- Treves H, Küken A, Arrivault S, Ishihara H, Hoppe I, Erban A, Höhne M, Moraes TA, Kopka J, Szymanski J *et al.* 2022. Carbon flux through photosynthesis and central carbon metabolism show distinct patterns between algae, C3 and C4 plants. *Nature Plants* 8: 78–91.
- Tsai C-H, Uygun S, Roston R, Shiu S-H, Benning C. 2018. Recovery from N deprivation is a transcriptionally and functionally distinct state in *Chlamydomonas*. *Plant Physiology* 176: 2007–2023.
- Van Breusegem F, Dat JF. 2006. Reactive oxygen species in plant cell death. *Plant Physiology* 141: 384–390.
- Wang ZT, Ullrich N, Sunjoo J, Waffenschmidt S, Goodenough U. 2009. Algal lipid bodies: stress induction, purification, and biochemical characterization in wild-type and starchless *Chlamydomonas reinhardtii*. *Eukaryotic Cell* 8: 1856–1868.
- Waterhouse A, Bertoni M, Bienert S, Studer G, Tauriello G, Gumienny R, Heer FT, de Beer TAP, Rempfer C, Bordoli L *et al.* 2018. SWISS-MODEL: homology modelling of protein structures and complexes. *Nucleic Acids Research* 46: W296–W303.
- Xenie J, Jean A. 2013. Central carbon metabolism and electron transport in *Chlamydomonas reinhardtii*: metabolic constraints for carbon partitioning between oil and starch. *Eukaryotic Cell* 12: 776–793.
- Xie K, Tian L, Guo X, Li K, Li J, Deng X, Li Q, Xia Q, Zhong Y, Huang Z *et al.* 2016. BmATG5 and BmATG6 mediate apoptosis following autophagy induced by 20-hydroxyecdysone or starvation. *Autophagy* 12: 381–396.
- Yin H, Xu L, Porter NA. 2011. Free radical lipid peroxidation: mechanisms and analysis. *Chemical Reviews* 111: 5944–5972.
- Zhao L, Dai J, Wu Q. 2014. Autophagy-like processes are involved in lipid droplet degradation in *Auxenochlorella protothecoides* during the heterotrophy-autotrophy transition. *Frontiers in Plant Science* 5: 400.
- Zienkiewicz A, Zienkiewicz K, Poliner E, Pulman JA, Du Z-Y, Stefano G, Tsai C-H, Horn P, Feussner I, Farre EM *et al.* 2020. The microalga nannochloropsis during transition from Quiescence to autotrophy in response to nitrogen availability. *Plant Physiology* 182: 819–839.
- van Zutphen T, Todde V, de Boer R, Kreim M, Hofbauer HF, Wolinski H, Veenhuis M, van der Klei IJ, Kohlwein SD. 2013. Lipid droplet autophagy in the yeast *Saccharomyces cerevisiae*. *Molecular Biology of the Cell* 25: 290–301.
- Fig. S1** Exposure of *Chlamydomonas urium* and *Chlamydomonas reinhardtii* cells to low pH, toxic concentrations of heavy metals or organic carbon.
- Fig. S2** Growth rate of *Chlamydomonas urium* and *Chlamydomonas reinhardtii* cells grown in HSM liquid medium at pH 7 under normal light or high light.
- Fig. S3** Total chlorophyll levels of *Chlamydomonas urium* and *Chlamydomonas reinhardtii*.
- Fig. S4** Photosynthetic parameters of *Chlamydomonas urium* and *Chlamydomonas reinhardtii* cells.
- Fig. S5** ATG8 proteins from *Chlamydomonas urium* and *Chlamydomonas reinhardtii*.
- Fig. S6** Electron microscopy images of *Chlamydomonas urium* cells subjected to nitrogen starvation in the presence of ConCA.
- Fig. S7** Comparative metabolic analysis of *Chlamydomonas urium* and *Chlamydomonas reinhardtii* cells grown in HSM medium under normal conditions.
- Fig. S8** Oxygen production and relative electron transport rate in *Chlamydomonas urium* and *Chlamydomonas reinhardtii* in the absence or presence of ConCA.
- Table S1** List of species used in the study.
- Table S2** Genes involved in lipid degradation in *Chlamydomonas reinhardtii* and *Chlamydomonas urium*.
- Table S3** Statistical analysis from main figures.

Supporting Information

Additional Supporting Information may be found online in the Supporting Information section at the end of the article.

Photosynthetic assimilation of CO₂ regulates TOR activity

Manuel J. Mallén-Ponce^a , María Esther Pérez-Pérez^a , and José L. Crespo^{a,1} 

^aInstituto de Bioquímica Vegetal y Fotosíntesis, Consejo Superior de Investigaciones Científicas–Universidad de Sevilla, Sevilla 41092, Spain

Edited by Michael Hall, Biozentrum, Universität Basel, Basel, Switzerland; received August 18, 2021; accepted November 29, 2021

The target of rapamycin (TOR) kinase is a master regulator that integrates nutrient signals to promote cell growth in all eukaryotes. It is well established that amino acids and glucose are major regulators of TOR signaling in yeast and metazoan, but whether and how TOR responds to carbon availability in photosynthetic organisms is less understood. In this study, we showed that photosynthetic assimilation of CO₂ by the Calvin–Benson–Bassham (CBB) cycle regulates TOR activity in the model single-celled microalga *Chlamydomonas reinhardtii*. Stimulation of CO₂ fixation boosted TOR activity, whereas inhibition of the CBB cycle and photosynthesis down-regulated TOR. We uncovered a tight link between TOR activity and the endogenous level of a set of amino acids including Ala, Glu, Gln, Leu, and Val through the modulation of CO₂ fixation and the use of amino acid synthesis inhibitors. Moreover, the finding that the *Chlamydomonas* starch-deficient mutant *sta6* displayed disproportionate TOR activity and high levels of most amino acids, particularly Gln, further connected carbon assimilation and amino acids to TOR signaling. Thus, our results showed that CO₂ fixation regulates TOR signaling, likely through the synthesis of key amino acids.

TOR kinase | CO₂ | amino acids | *Chlamydomonas*

The target of rapamycin (TOR) kinase is a fundamental regulator of cell growth and metabolism that integrates nutrient and energy signals to the cell growth machinery (1, 2). TOR associates to other proteins to constitute two functionally and architecturally distinct complexes, termed TOR complexes 1 and 2 (TORC1 and TORC2) (3). The core components of TORC1 include the TOR kinase, Raptor/Kog1 and LST8, whereas TORC2 is composed of TOR, LST8, Sin1/Avo1, and Rictor/Avo3. Like TOR itself, TORC1 and TORC2 are highly conserved in eukaryotes, although TORC2-specific components have not been identified in the green lineage (Viridiplantae).

TOR promotes cell growth in response to the availability of nutrients, activating anabolism and inhibiting catabolism under favorable conditions. Amino acids are main activators of TORC1 signaling in yeast and metazoans, although activation of this pathway in multicellular organisms requires additional input from growth factors (4, 5). In mammals, amino acid abundance is mainly signaled to mTORC1 via the small GTPases RAGs and RHEB and the lysosomal Ragulator complex, while amino acid signaling to TOR is partially conserved in yeast (4, 6). It is currently unknown how many different amino acids are sensed by TORC1 in yeast and mammals, but leucine and arginine are key regulators of mTORC1 activity, and yeast TORC1 responds preferentially to glutamine (4).

TORC1 is structurally and functionally conserved in plants. In *Arabidopsis thaliana*, TORC1 promotes cell growth by regulating fundamental processes, including ribosome biogenesis, transcription, cell expansion, autophagy, metabolism, and nutrient assimilation (7–9). However, upstream regulators of yeast and mammalian TORC1 such as RAGs and RHEB are not conserved in plants, suggesting that different regulatory mechanisms may operate in these organisms. Plant TOR integrates hormone and stress signals, but the underlying mechanisms are poorly understood. The plant hormones auxin and ABA have

been identified as positive and negative regulators, respectively, of TOR signaling in *Arabidopsis* (10, 11).

Energy and nutrients are also key regulators of TOR activity in plants. An original study performed in *Arabidopsis* seedlings demonstrated that exogenous glucose activates TOR kinase activity through glycolysis-mitochondria-mediated energy and metabolic relays (12). Neither hormones nor amino acids can substitute for glucose, suggesting that different inputs may act on plant TOR (12). Mounting evidence indicates that amino acid availability modulates TOR activity in plants. Inhibition of branched chain amino acid biosynthesis by genetic or chemical approaches led to TOR inhibition (13, 14), whereas addition of glutamine or isoleucine to leaf discs from *Arabidopsis* stimulates TOR activity (15). In plants, nitrogen is taken up by roots, and studies performed in TOR-overexpressing seedlings correlated root elongation with TOR function under excess nitrate, suggesting that nitrogen is an important nutrient for TOR signaling (16). Supporting this hypothesis, it has been shown that nitrate, ammonium, and glutamine promote TOR activity via activation of the small GTPase ROP2 (17).

TORC1 components are widely conserved in algal genomes, including freshwater and marine species (18, 19). Studies performed in the model green alga *Chlamydomonas reinhardtii* (hereafter *Chlamydomonas*) provided new insights into TOR signaling in photosynthetic eukaryotes (20). Biochemical evidence revealed the presence of *Chlamydomonas* TOR in a high-molecular-mass complex that associates with microsomal

Significance

Photosynthetic organisms are responsible for the incorporation of inorganic carbon in the biosphere through a fundamental process known as carbon fixation. This reaction allows the reduction of inorganic carbon, mostly atmospheric CO₂, to organic compounds such as carbohydrates and amino acids. Despite the biological relevance of carbon fixation in nature, how photosynthetic cells sense carbon availability remains poorly understood. Using the model microalga *Chlamydomonas reinhardtii*, we found that the photosynthetic assimilation of CO₂ regulates the activity of the target of rapamycin (TOR) kinase, a master regulator of cell growth and nutrient sensor widely conserved in all eukaryotes. Our study revealed that inorganic carbon fixation and photosynthesis regulate TOR activity, likely through the synthesis of central amino acids in carbon metabolism.

Author contributions: M.J.M.-P., M.E.P.-P., and J.L.C. designed research; M.J.M.-P. and M.E.P.-P. performed research; M.J.M.-P., M.E.P.-P., and J.L.C. analyzed data; and J.L.C. wrote the paper.

The authors declare no competing interest.

This article is a PNAS Direct Submission.

This open access article is distributed under [Creative Commons Attribution-NonCommercial-NoDerivatives License 4.0 \(CC BY-NC-ND\)](https://creativecommons.org/licenses/by-nc-nd/4.0/).

¹To whom correspondence may be addressed. Email: crespo@ibvf.csic.es.

This article contains supporting information online at <http://www.pnas.org/lookup/suppl/doi:10.1073/pnas.2115261119/-DCSupplemental>

Published January 7, 2022.

membranes (21). The sensitivity of *Chlamydomonas* to rapamycin has been exploited to dissect TOR signaling in this alga (22). Chemical inhibition of *Chlamydomonas* TORC1 with rapamycin blocks translation (23), induces the synthesis and storage of triacylglycerol (24), and triggers autophagy (25). Transcriptomic and metabolomic studies of *Chlamydomonas* cells treated with rapamycin uncovered TOR as a central regulator of primary metabolism (26, 27). Moreover, quantitative phosphoproteomic analysis following TOR inhibition identified proteins involved in translation, carotenoid biosynthesis, autophagy, and cell signaling (28, 29).

Despite recent progress on the study of TOR signaling in algae, little is known about upstream regulation of this pathway by nutrients and the underlying mechanisms. The similar response of TOR inhibition and nitrogen starvation suggested that this nutrient might regulate TOR signaling in *Chlamydomonas* (22, 24, 25, 27, 30). The TOR kinase has also been connected to inositol polyphosphate metabolism in *Chlamydomonas*, but the precise role of these molecules in TOR signaling is currently unknown (31). A recent study demonstrated that phosphorus availability regulates TOR activity via LST8 in *Chlamydomonas*. Phosphorus starvation results in a sharp decrease in LST8 abundance and down-regulation of TOR activity (32). The transcription factor PSR1, a global regulator of the phosphorus starvation response in *Chlamydomonas* (33), has been linked to the control of TOR signaling, as neither LST8 level nor TOR activity is properly regulated in PSR1-defective cells (32).

Photosynthetic organisms are able to fix inorganic carbon species like CO₂ to more reduced organic forms, a fundamental process that sustains life on Earth. This reaction is driven by the Calvin-Benson-Bassham (CBB) cycle in the chloroplast of plant and algal cells. Although nutrients such as nitrogen, phosphorus, sulfur, amino acids, and glucose have been shown to regulate TOR in different organisms, it is currently unknown whether this signaling pathway responds to inorganic carbon. In this study, we aimed to investigate whether carbon availability regulates TOR signaling using *Chlamydomonas* as model system. Our results demonstrated that the carbon source is a main regulator of TOR activity. We found that the photosynthetic assimilation of CO₂ efficiently activates TOR, probably through the synthesis of central amino acids.

Results

The Carbon Source Modulates TOR Activity. Given the fundamental role of TOR in coupling nutrient availability to cell growth, we investigated whether the carbon source regulates TOR in *Chlamydomonas*. To this aim, we monitored TOR activity in wild-type cells with atmospheric CO₂ as the sole carbon source (high saline medium, HSM) or using acetate as an additional carbon source [Tris-acetate-phosphate (TAP) medium], which sustains robust growth and biomass productivity in *Chlamydomonas* (ref. 34; Fig. 1A). The analysis of RPS6 phosphorylation, an established readout of TOR activity in *Chlamydomonas* (32), revealed a twofold increase in TOR activity in TAP-grown cells (Fig. 1B), which is consistent with a previous report showing stimulation of TOR activity under mixotrophic conditions in *Chlamydomonas* (30). The abundance of TOR and LST8 proteins was similar in cells grown either with acetate or atmospheric CO₂ (Fig. 1B), indicating that the carbon source might influence TOR activity without altering the level of TORC1 proteins.

Amino acids are main regulators of TOR signaling (4, 5), and a significant portion of assimilated carbon is invested in the synthesis of amino acids in *Chlamydomonas* (34). Thus, to understand why TAP-grown cells displayed higher TOR activity compared to HSM-grown cells, we analyzed the concentration of all amino acids in both conditions. The total amino acid

content was around 40% higher in cells using acetate as additional carbon source (SI Appendix, Fig. S1A), and the level of eight amino acids increased significantly (Fig. 1C). This subset of up-regulated amino acids included Glu, Gln, Ala, Val, Leu, Met, Gly, and Pro, some of which (Ala, Leu, Glu, Gln) are among the most abundant amino acids in *Chlamydomonas* (SI Appendix, Fig. S1B). Taken together, these results showed that the carbon source controls TOR activity in *Chlamydomonas* and pinpoint amino acids as potential TOR regulators.

CO₂ Fixation Promotes TOR Activity. To investigate the link between TOR and carbon assimilation in *Chlamydomonas*, we analyzed the effect of HCO₃[−] on RPS6 phosphorylation under autotrophic growth conditions. In aquatic systems, microalgae like *Chlamydomonas* actively transport and efficiently use HCO₃[−] as the carbon source for photosynthesis (ref. 35; Fig. 2A). Accordingly, it is well established that the addition of HCO₃[−] to *Chlamydomonas* cells potentially augments photosynthesis (ref. 36; Fig. 2B). In this study, we found that HCO₃[−] boosted RPS6 phosphorylation within 30 min, indicating that the assimilation of HCO₃[−] triggers TOR activity in *Chlamydomonas* (Fig. 2C). The impact of HCO₃[−] on TOR activity mirrored the stimulation of photosynthesis as both RPS6 phosphorylation and O₂ production gradually decreased following the 30-min HCO₃[−] boost (Fig. 2B and C). We also analyzed whether HCO₃[−] might change the abundance of TOR and LST8 proteins, but no significant effect was detected (Fig. 2C). To demonstrate that TOR mediates the increased phosphorylation of RPS6 in response to HCO₃[−], we examined RPS6 phosphorylation upon HCO₃[−] addition in rapamycin-treated cells. Indeed, inhibition of TOR by rapamycin fully prevented the HCO₃[−]-induced phosphorylation of RPS6 (Fig. 2D).

We next investigated the mechanism by which HCO₃[−] promotes TOR activity in *Chlamydomonas*. For its assimilation, HCO₃[−] must be converted to CO₂ through the carbonic anhydrase CAH3 localized in the thylakoid lumen, and then rubisco catalyzes the formation of 3-phosphoglycerate (3PG) from ribulose-1,5-bisphosphate (RuBP) and CO₂, a key reaction in the CBB cycle (ref. 34; Fig. 2A). To study the possible effect of disrupting CO₂ fixation on TOR, we used glycolaldehyde (GLA), a specific inhibitor of phosphoribulokinase (PRK) activity that interrupts the CBB cycle and inactivates photosynthesis (37). We indeed confirmed that GLA blocks PSII activity in our experimental setup within 30 to 60 min (SI Appendix, Fig. S2). GLA treatment led to a strong decrease of RPS6 phosphorylation that was detectable within 2 h following GLA addition (Fig. 2E). Moreover, we found that the inhibition of the CBB cycle by GLA abolished the HCO₃[−]-mediated up-regulation of TOR activity (Fig. 2F), indicating that disruption of CO₂ fixation inhibits TOR activity in *Chlamydomonas*.

Photosynthetic carbon assimilation constitutes a major source of intermediates for the synthesis of amino acids. We thus analyzed whether HCO₃[−]-induced stimulation of photosynthesis might change the amino acid content in *Chlamydomonas*. Excluding Ser and Gly, the level of all amino acids increased within 30 min of HCO₃[−] addition (Fig. 2G). Some amino acids (Val, Leu, Ile, Thr, Pro, Met, Phe, Tyr) remained high, while others (Ala, Glu, Gln, Cys, Asp, Asn, Lys, His, Arg, Trp) gradually decreased in the time course of the experiment. Among the transiently up-regulated amino acids, Ala, Glu, Gln, Asp, and Asn displayed a similar trend to TOR activity, peaking at 30 min after HCO₃[−] addition. Moreover, Ala and Glu were the amino acids most highly induced by HCO₃[−] at 30 min (Fig. 2G). We also studied the effect of GLA on the amino acid content in *Chlamydomonas*. In contrast to HCO₃[−], inhibition of CO₂ fixation by GLA caused a progressive decline of most amino acids (Fig. 2H). The negative effect of GLA on the amino acid content and TOR activity was evident after 2 to 4

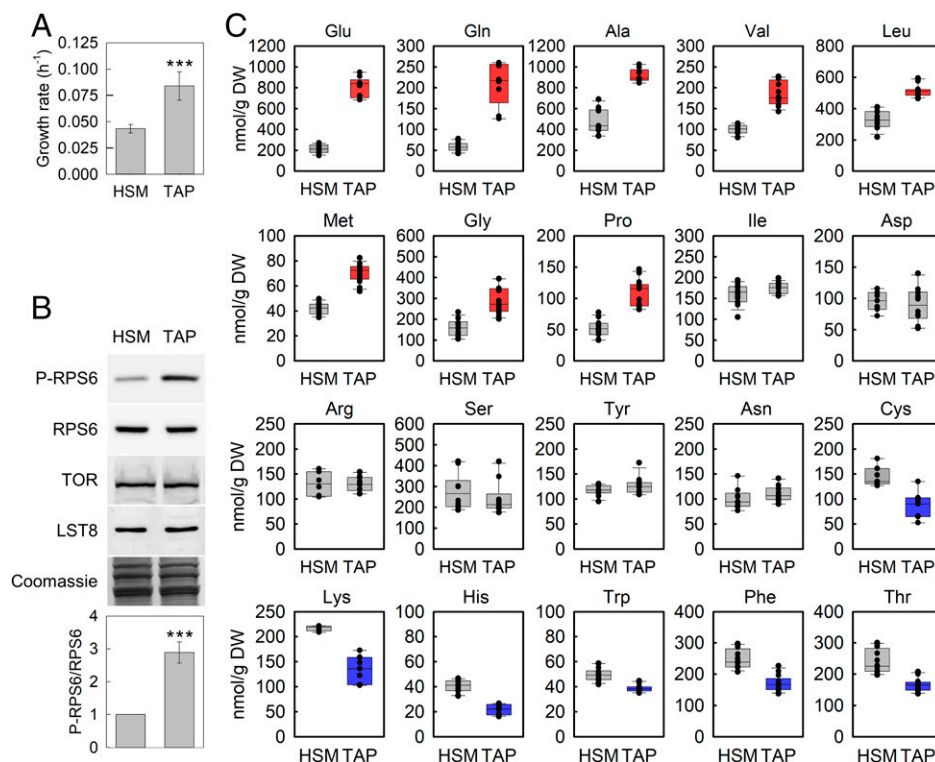


Fig. 1. Carbon source modulates TOR activity in *Chlamydomonas*. (A) Growth rate of wild-type 4A+ *Chlamydomonas* cells under autotrophic (HSM) or mixotrophic (TAP) conditions. Growth rate is expressed in h⁻¹, and it was calculated as the increase in cell number during a time period (see *Materials and Methods*). Five biological replicates were analyzed for each condition. (B) Immunoblot analysis of phosphorylated RPS6 (P-RPS6), RPS6, TOR, and LST8 proteins in cells growing exponentially in HSM or TAP medium. TOR activity was determined as the ratio of phosphorylated to total RPS6 protein from three biological replicates (a. u., arbitrary units). Coomassie brilliant blue-stained gels were used as protein loading control. (C) Amino acid content of *Chlamydomonas* in HSM or TAP medium. Amino acids up-regulated and down-regulated in the presence of acetate (TAP) are shown in red and blue, respectively. Amino acids with no significant change in both media are shown in gray. Each condition included at least eight biological replicates. Error bars represent SD of the mean values. Asterisks represent significant differences according to two-tailed Student's *t* test, ****P* < 0.001. DW, dry weight.

h since the absolute levels of amino acids at the 1-h time point might still be sufficient to activate TOR, despite a reduction in the relative amount (Fig. 2 *E* and *H*). Actually, the level of some amino acids that might be important for TOR activation such as Gln, Leu, and Val were not decreased after 1 h GLA treatment (Fig. 2*H*). Gln was the only amino acid that remained high in GLA-treated cells, probably because of a decrease in the C/N ratio upon photosynthesis inhibition and the availability of NH₄⁺ under these conditions (SI Appendix, Fig. S2). These results revealed a tight link between TOR activity and the endogenous level of some amino acids including Ala, Glu, Gln, Leu, and Val in response to the stimulation or inhibition of CO₂ fixation.

Inhibition of Photosynthesis Down-Regulates TOR Activity. Photosynthesis provides ATP and NADPH required for carbon fixation. Based on the regulatory role that CO₂ fixation plays on TOR activity (Fig. 2), we speculated that the disruption of photosynthesis might disturb TOR signaling in *Chlamydomonas*. To test this hypothesis, we monitored TOR activity in air-grown cells subjected to darkness or treated with 3-(3,4-dichlorophenyl)-1,1-dimethylurea (DCMU), an inhibitor of photosynthetic electron transport at PSII level. Our results showed that the inhibition of photosynthesis by darkness or DCMU (SI Appendix, Fig. S2) led to a gradual and pronounced decrease of TOR activity (Fig. 3 *A* and *B*). To characterize the regulation of TOR by light, we analyzed the effect of a dark-to-light transition on TOR activity. Interestingly, reillumination of dark-adapted cells resulted in a fast and strong reactivation of TOR (Fig. 3*C*).

Moreover, we found that inhibition of CO₂ fixation by GLA fully prevented the reactivation of TOR by light (Fig. 3*C*), further supporting the regulation of TOR by carbon fixation.

We also determined the amino acid content in *Chlamydomonas* cells subjected to darkness or treated with DCMU. Two clusters of amino acids with similar patterns were detected under both conditions. About half of the amino acids declined, following a similar trend to TOR activity, while the other half increased in response to photosynthesis inhibition (Fig. 3*D*). The subset of down-regulated amino acids included Ala, Glu, Gln, Leu, and Val, whose levels were also found to correlate with TOR activity under different carbon sources (Fig. 1) and in response to the stimulation or inhibition of CO₂ fixation (Fig. 2).

The Abundance of Intracellular Amino Acids Regulates TOR Activity.

We aimed to establish a direct role of amino acids in the control of TOR signaling by carbon fixation. Given the inability of *Chlamydomonas* cells to transport amino acids other than Arg (38), in order to show a direct link between intracellular amino acids and TOR, we blocked the synthesis of central amino acids. For this purpose, we treated *Chlamydomonas* cells with sulfometuron methyl (SMM), an inhibitor of acetolactate synthase that catalyzes the first common step in the biosynthesis of Leu and Val (ref. 39; Fig. 4*A*), and aminooxyacetate (AOA), which blocks Ala formation by inhibiting alanine aminotransferase (ref. 40; Fig. 4*A*). The analysis of the amino acid profile of SMM- and AOA-treated cells confirmed the efficiency of the two inhibitors. As expected, SMM caused a sharp drop of Leu

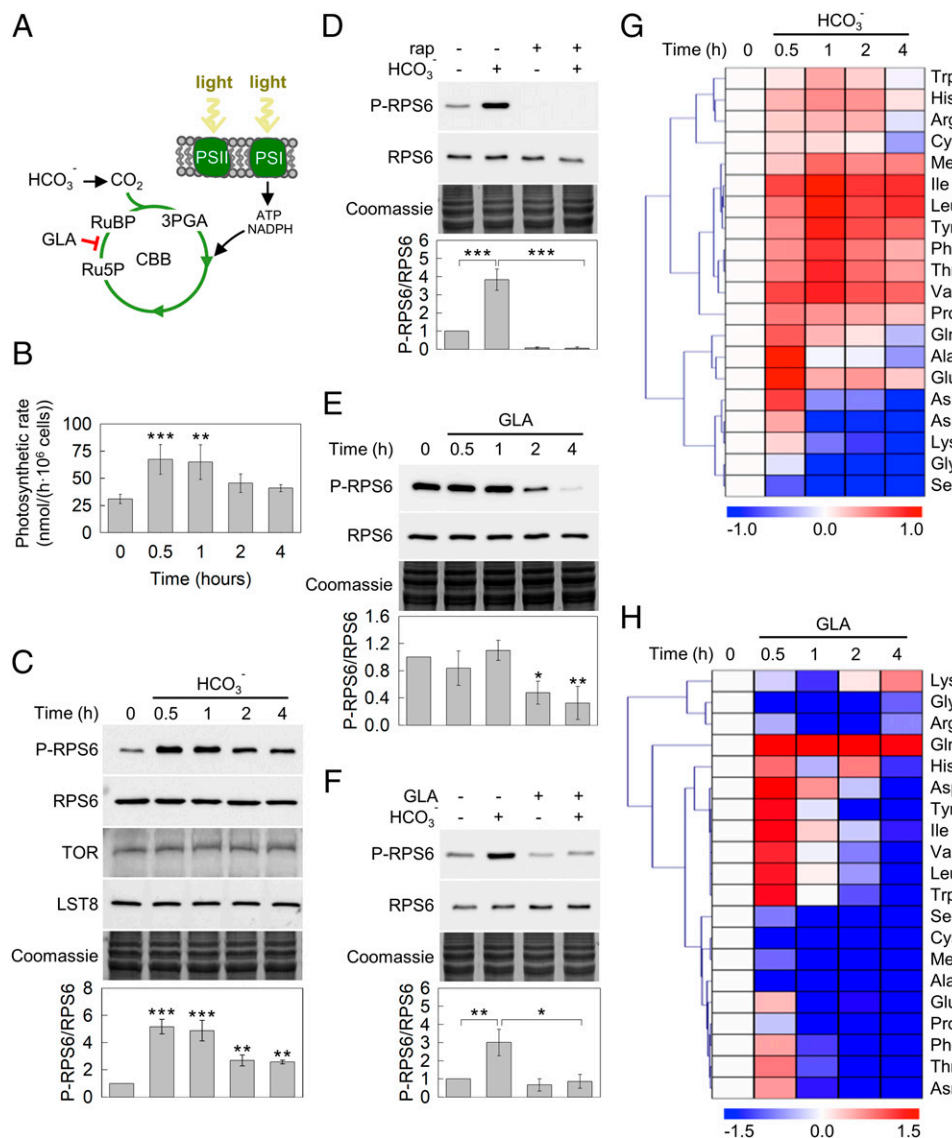


Fig. 2. CO₂ fixation activates TOR signaling in *Chlamydomonas*. (A) Schematic representation of photosynthesis and CO₂ fixation. The incorporation of HCO₃⁻ to the CBB cycle and the inhibitory effect of GLA are indicated. (B) Photosynthetic rate of *Chlamydomonas* cells growing in the presence of 10 mM HCO₃⁻ (0, 0.5, 1, 2, and 4 h) in HSM. Three biological replicates were analyzed for each time point. (C) Immunoblot analysis of P-RPS6, RPS6, TOR, and LST8 of *Chlamydomonas* cells grown as described in B. (D) Western blot analysis of P-RPS6 and RPS6 in *Chlamydomonas* cells treated (+) or not (-) with 1 μM rap for 2 h and then 10 mM HCO₃⁻ for 0.5 h. (E) Western blot analysis of P-RPS6 and RPS6 of *Chlamydomonas* cells treated with 10 mM GLA for 0, 0.5, 1, 2, and 4 h. (F) Western blot analysis of P-RPS6 and RPS6 in *Chlamydomonas* cells treated (+) or not (-) with 10 mM GLA for 2 h and then 10 mM HCO₃⁻ for 0.5 h. Coomassie brilliant blue-stained gels were used as protein loading control. For TOR activity determination in C to F, the P-RPS6/RPS6 ratio was calculated from three biological replicates (a.u., arbitrary units). Untreated cells were used as control. Error bars represent SD of the mean values. Asterisks in B, C, and E represent significant differences according to one-way ANOVA and Bonferroni's test: **P* < 0.05, ***P* < 0.01, and ****P* < 0.001. Asterisks in D and F represent significant differences according to two-tailed Student's *t* test: ***P* < 0.01 and ****P* < 0.001. (G, H) Hierarchical clustering analysis showing the relative abundance of each amino acid over the time course in HCO₃⁻ (G) or GLA (H) treatment after normalization to untreated (0 h) sample using log₂ transformation. Four biological replicates were analyzed for each treatment.

and Val, whereas AOA led to a pronounced decrease of Ala (Fig. 4B). However, the down-regulation of Leu, Val, and Ala synthesis by SMM and AOA also resulted in a strong increase of some amino acids, probably because of the redirection of fixed carbon to the synthesis of other amino acids and/or the activity of transaminases. Indeed, SMM boosted the level of Gln, Glu, and Ala among other amino acids while AOA markedly raised Leu, Val, Gln, Glu, Asp, Asn, and Pro abundance (Fig. 4B). We next analyzed the effect of SMM and AOA on TOR activity. Notably, TOR activity was up-regulated in cells treated with these inhibitors, indicating that TOR responds to changes in amino acid abundance (Fig. 4C). Moreover, we

found that the inhibition of carbon fixation by GLA fully prevented the up-regulation of TOR induced by SMM and AOA (Fig. 4D). Thus, our results revealed that carbon fixation is the primary regulator of TOR activity in SMM- and AOA-treated cells and demonstrated a direct link between the abundance of intracellular amino acids and TOR in *Chlamydomonas*.

Starch Deficiency Up-Regulates TOR Activity. Starch biosynthesis is an essential outlet of photosynthetic electron transport. In *Chlamydomonas*, it has been shown that the disruption of starch synthesis results in a pronounced drop in photosynthetic capacity and the redirection of photosynthetically fixed carbon

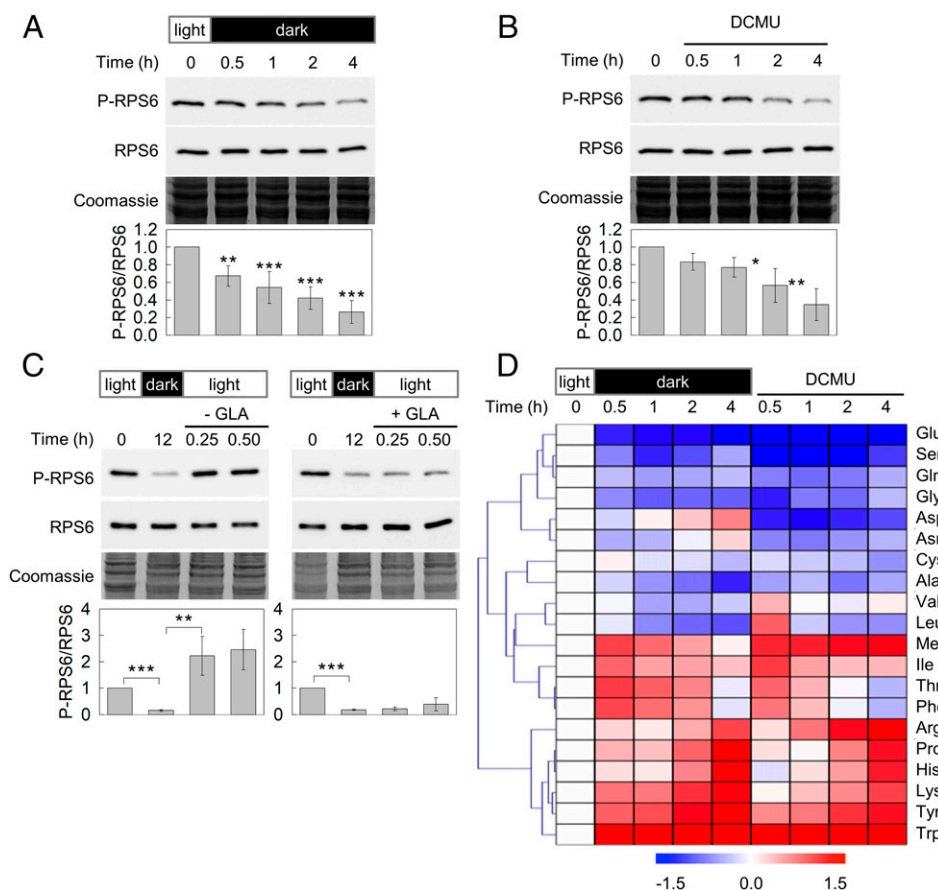


Fig. 3. Inhibition of photosynthesis down-regulates TOR activity in *Chlamydomonas*. (A) Western blot analysis of P-RPS6 and RPS6 in wild-type *Chlamydomonas* cells in HSM transferred from standard light illumination (0 h) to darkness for 0.5, 1, 2, and 4 h. (B) Western blot analysis of P-RPS6 and RPS6 in *Chlamydomonas* cells grown in HSM and treated with 20 μ M DCMU for 0, 0.5, 1, 2, and 4 h. TOR activity in A and B was determined as described in Fig. 1B. (C) Hierarchical clustering analysis showing the relative abundance of each amino acid over the time course in cells shifted from light to dark or treated with 20 μ M DCMU after normalization to 0 h sample using log2 transformation. Four biological replicates were analyzed for each treatment in B and C. (D) Cells growing in the light were shifted to dark for 12 h and then reilluminated for 15 or 30 min. Prior to the dark-to-light transition, cells were treated with 10 mM GLA for 30 min. P-RPS6 and RPS6 were detected by Western blot in these conditions. Coomassie brilliant blue-stained gels were used as protein loading control. For TOR activity quantification in A, B, and D, the P-RPS6/RPS6 ratio was calculated from five, four, and three biological replicates, respectively. Untreated cells were used as control. Error bars represent SD of the mean values. Asterisks in A and B represent significant differences according to one-way ANOVA and Bonferroni's test: * $P < 0.05$, ** $P < 0.01$, and *** $P < 0.001$. Asterisks in C represent significant differences according to two-tailed Student's t test: ** $P < 0.01$ and *** $P < 0.001$.

under autotrophic conditions (41). Thus, to further explore the connection between TOR and carbon fixation in *Chlamydomonas*, we analyzed TOR activity in the *sta6* mutant, which is unable to synthesize starch because of the lack of the enzyme ADP glucose pyrophosphorylase (42). Since the *sta6* mutant was generated in the cell wall-deficient *cw15* background (42), first of all we confirmed that *cw15* and wild-type cells display the same basal TOR activity in our experimental setup (SI Appendix, Fig. S3A). Actually, we also determined the amino acid profile in both strains, and no significant differences were detected for any amino acid (SI Appendix, Fig. S3B). Remarkably, the analysis of RPS6 phosphorylation in *sta6* cells revealed a much higher TOR activity in this mutant compared to the *cw15* strain (Fig. 5A), indicating that the inability to synthesize starch up-regulates TOR. To exclude that the up-regulation of TOR activity in *sta6* cells might be related to additional mutations reported in this strain (43), we also monitored RPS6 phosphorylation in a *sta6*-rescued strain (44). As anticipated, the complemented *sta6* strain exhibited the same level of RPS6 phosphorylation as *cw15* cells (SI Appendix, Fig. S4A).

Given the tight connection found between TOR activity and the amino acid content in *Chlamydomonas*, we determined the

amino acid abundance of *sta6* cells under autotrophic growth. The total amino acid content was around 60% higher in the *sta6* mutant (SI Appendix, Fig. S4B). All amino acids other than Ile, Tyr, Thr, Trp, and Phe were up-regulated in *sta6* cells (Fig. 5B), although the most remarkable increase was detected in the Gln content, which was eight times higher (SI Appendix, Fig. S4C). To further investigate the misregulation of TOR in the starch-deficient *sta6* mutant, we determined TOR activity and amino acid abundance in this strain under conditions that either increase or diminish the activity of TOR. On the one hand, addition of HCO_3^- to *cw15* and *sta6* cells stimulated TOR activity in both strains, although to a different range. Like in wild-type cells (Fig. 2B), HCO_3^- led to a sevenfold raise of TOR activity in *cw15* cells, whereas this increase was less pronounced in the *sta6* mutant (Fig. 5C). The effect of HCO_3^- in the amino acid content of *cw15* and *sta6* cells was similar, but some amino acids like Gln did not increase in the *sta6* mutant (Fig. 5B), probably because of the massive concentration of this amino acid before HCO_3^- addition (SI Appendix, Fig. S4C). On the other hand, inhibition of CO_2 fixation or photosynthesis down-regulated TOR activity in *sta6* cells to levels comparable to the ones detected in *cw15* cells despite the much higher

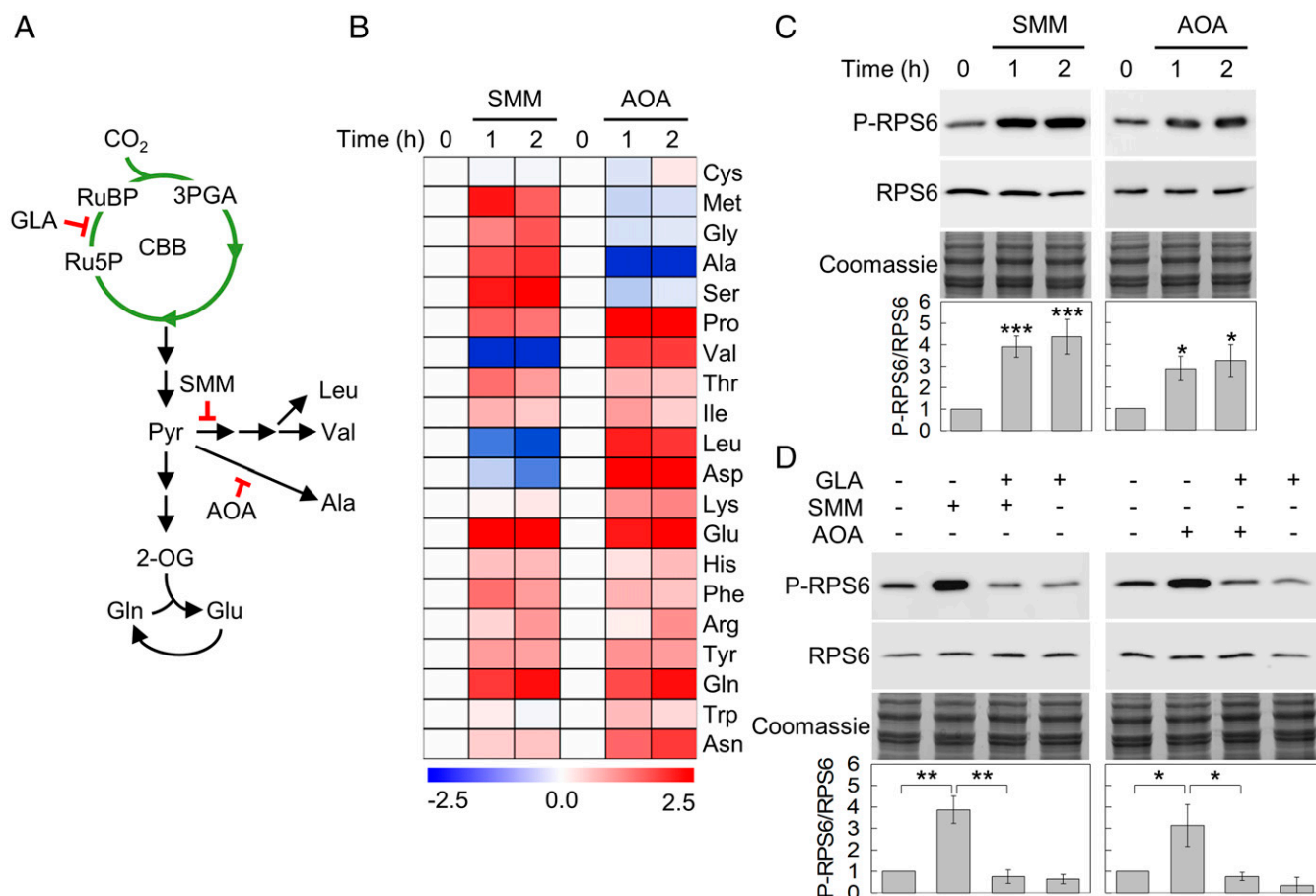


Fig. 4. TOR activity responds to the intracellular abundance of amino acids. (A) Schematic representation of CO₂ fixation and the metabolic pathways for the synthesis of Val, Leu, Ala, Glu, and Gln. The inhibitory effect of GLA, SMM, and AOA is indicated. (B) Heat map showing the relative abundance of each amino acid over the time course in SMM or AOA treatment after normalization to untreated (0 h) sample using log₂ transformation. (C) Western blot analysis of P-RPS6 and RPS6 in *Chlamydomonas* cells grown in HSM and treated with 5 μ M SMM or 1 mM AOA for 1 and 2 h, respectively. (D) Western blot analysis of P-RPS6 and RPS6 in *Chlamydomonas* cells treated (+) or not (–) with 10 mM GLA for 2 h and 5 μ M SMM or 1 mM AOA for 1 h. Coomassie brilliant blue–stained gels were used as protein loading control. For TOR activity determination in C and D, the P-RPS6/RPS6 ratio was calculated from three biological replicates (a.u.). Untreated cells were used as control. Error bars represent SD of the mean values. Asterisks in C and D represent significant differences according to Bonferroni's test and one-way ANOVA, respectively: * P < 0.05, ** P < 0.01, and *** P < 0.001.

TOR activity inherent to the starchless mutant (Fig. 5 D–F). The analysis of the amino acid content under these conditions revealed similar effects for most amino acids except Ile, Tyr, Thr, Trp, and Phe, which were less abundant in the *sta6* mutant and markedly increased in response to the inhibition of CO₂ fixation or photosynthesis (Fig. 5B). Taken together, these results suggested that the higher TOR activity of the *sta6* mutant might be due to the elevated concentration of key amino acids such as Gln, which activates TOR signaling in yeast and mammalian cells (4).

Discussion

The CBB cycle catalyzes the incorporation of inorganic CO₂ into organic molecules, an essential process performed by photosynthetic organisms that keeps life on Earth. In this study, we found that CO₂ fixation promotes the activity of the cell growth master regulator TOR in the green alga *Chlamydomonas*. The TOR pathway integrates different nutrient signals including the availability of organic carbon compounds like glucose. In non-photosynthetic eukaryotes, glucose is the major carbon source and TOR perceives glucose deficiency through the AMPK/Snf1 kinase (4). In plants, it has been shown that exogenous glucose taken up by root glucose transporters activates TOR kinase

activity (12). Glucose-TOR signaling seems to be a main channel for the regulation of central metabolism in plants, as profound transcriptional reprogramming takes place in metabolic networks upon glucose stimulation of TOR (12). Chemical targeting of mitochondria demonstrated that glucose-mediated activation of plant TOR depends on mitochondrial electron transport chain and oxidative phosphorylation (12).

In the absence of exogenous carbon supply, CO₂ fixation provides carbon skeletons for all reactions in photosynthetic cells. In order to sustain cell growth, a significant portion of fixed carbon is invested in the synthesis of amino acids (34). In close agreement, we found that HCO₃[–] addition to *Chlamydomonas* cells quickly increased the level of all amino acids except Gly and Ser, which are likely down-regulated due to a decrease of rubisco oxygenase activity and photorespiration (Fig. 2G). Conversely, inhibition of CO₂ fixation resulted in a sharp drop of most amino acids (Fig. 2H), corroborating the role of fixed carbon in the synthesis of amino acids. Our results also demonstrated that carbon fixation regulates TOR activity in *Chlamydomonas*. Stimulation of CO₂ fixation with HCO₃[–] boosted TOR activity, whereas inhibition of this fundamental process led to a strong decline of TOR activity (Fig. 2). Moreover, the amino acid profile of *Chlamydomonas* cells subjected to different carbon sources or treated with inhibitors of carbon fixation,

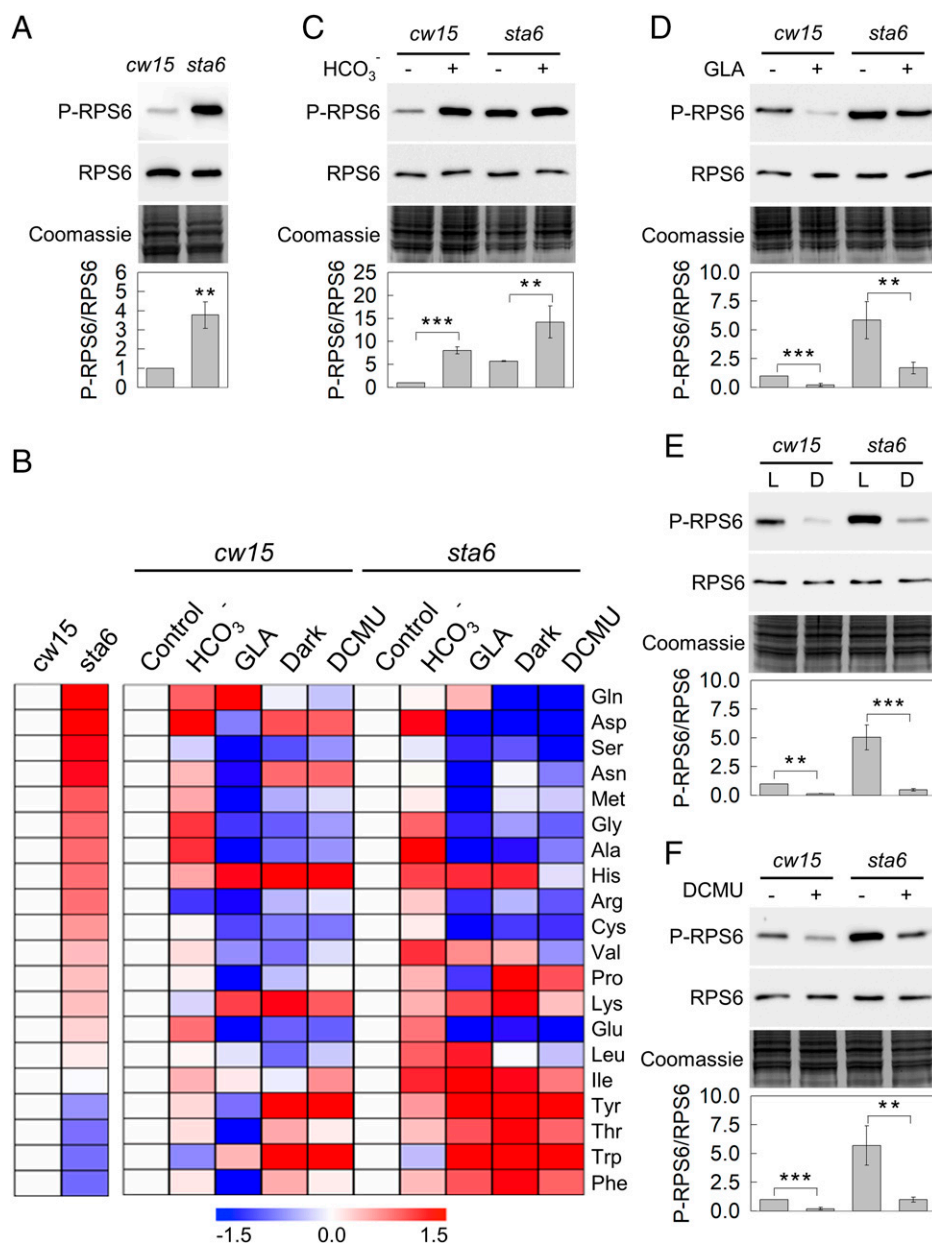


Fig. 5. TOR activity is up-regulated in the *Chlamydomonas* starchless mutant *sta6*. (A) Western blot analysis of P-RPS6 and RPS6 in *cw15* and *sta6* *Chlamydomonas* strains growing exponentially in HSM. Three biological replicates were analyzed in both strains. (B) Heat map showing the relative abundance of each amino acid in *cw15* and *sta6* cells under the following conditions: control, HCO_3^- (10 mM, 30 min), GLA (10 mM, 2 h), dark (2 h), and DCMU μM , 2 h). On the *Left*, each amino acid level is shown normalized to *cw15* cells. On the *Right*, each amino acid level is displayed under the different treatments normalized to untreated cells in both strains. The normalization was calculated using log2 transformation. Four biological replicates were analyzed for each treatment in both strains. (C–F) Western blot analysis of P-RPS6 and RPS6 in *cw15* and *sta6* cells grown in HSM and subjected to the different conditions shown in B. L and D in E refer to light and dark, respectively. Coomassie brilliant blue–stained gels were used as protein loading control in all cases. For TOR activity measurements, the P-RPS6/RPS6 ratio was calculated from three biological replicates. Untreated cells were used as control. Error bars represent SD of the mean values. Asterisks in A and C to F represent significant differences according to two-tailed Student's *t* test: $**P < 0.01$ and $***P < 0.001$.

photosynthesis, or amino acid synthesis uncovered a close link between the kinase activity of TOR and the abundance of Ala, Glu, Gln, Leu, and Val (Fig. 6). Thus, in close agreement with the established and evolutionarily conserved role of amino acids as TOR regulators (4), our study strongly suggests that the modulation of TOR activity by fixed carbon in *Chlamydomonas* is ultimately governed by the intracellular abundance of a subset of key amino acids (Fig. 6).

In yeast and mammalian cells, Leu and Gln regulate TORC1 signaling via the RAG family of small GTPases (4). Recent studies performed in *Arabidopsis* indicated that amino acids are also key

upstream signals for plant TOR activation. Accumulation of branched chained amino acids, particularly Val, in a mutant defective in Leu biosynthesis leads to up-regulation of TOR activity (13). Moreover, the same study showed that exogenous feeding of plants with Val, Leu, and Ile stimulated TOR activity (13). Similarly, incubation of *Arabidopsis* leaf discs in Ile or Gln up-regulated TOR activity (15). An in-depth analysis of TOR regulation by nitrogen and amino acids in *Arabidopsis* revealed an efficient activation of TOR by exogenously supplied amino acids, although with different capacities (17). A group of amino acids composed by Ala, Gln, Gly, Cys, Ser, Glu, Asp, and Leu exhibited

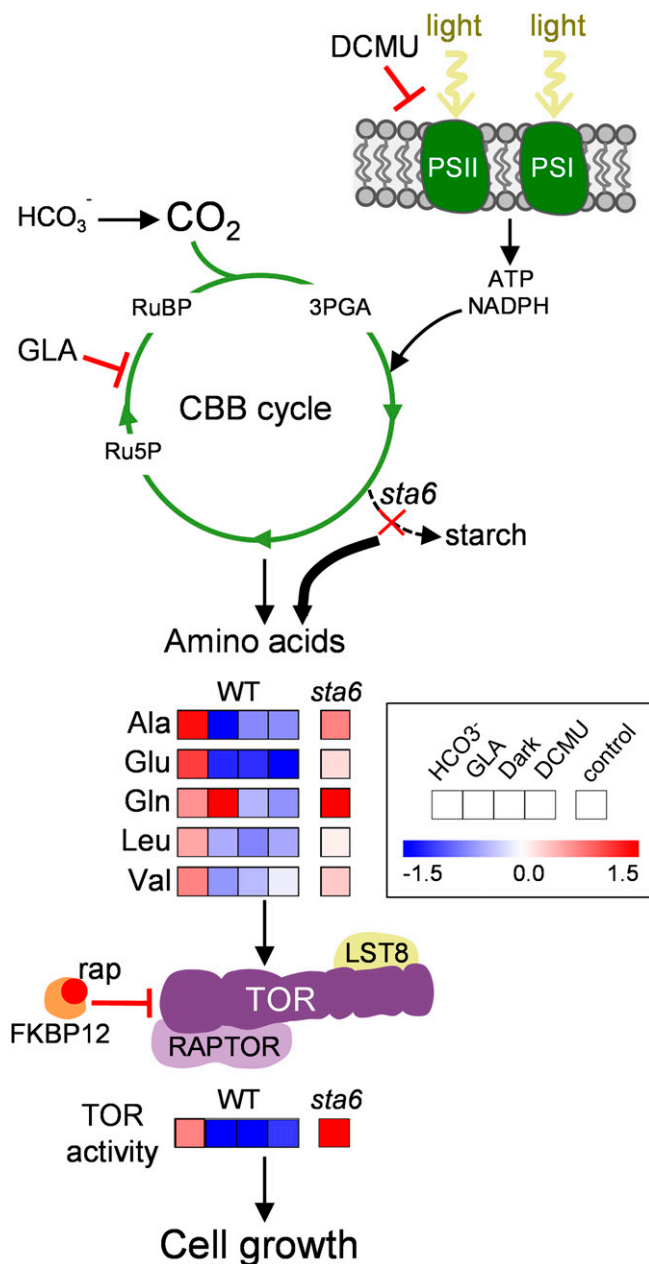


Fig. 6. Proposed model for the regulation of TOR activity by inorganic carbon in *Chlamydomonas*. The CBB cycle catalyzes the incorporation of inorganic CO_2 into organic molecules such as amino acids and starch, a main carbon sink in photosynthetic cells. Photosynthesis provides ATP and NADPH to fuel chemical reactions from the CBB cycle. The availability of fixed carbon modulates the endogenous level of Ala, Glu, Gln, Leu, and Val, increasing with HCO_3^- and decreasing upon inhibition of CO_2 fixation (GLA) or photosynthesis (DCMU, dark). These amino acids regulate TOR activity, which couples carbon sufficiency to cell growth. The inability of the *sta6* mutant to synthesize starch redirects part of the fixed carbon to the synthesis of amino acids, particularly Gln, leading to a massive increase of TOR activity. Heat maps show the relative levels of amino acids and TOR activity in *Chlamydomonas* cells under the conditions indicated in Figs. 2, 3, and 5. Inhibitors of CO_2 fixation (GLA), photosynthesis (DCMU), and TOR (rap) are indicated.

high potency for *Arabidopsis* TOR activation, while other amino acids had little or no regulatory effect on TOR activity (17).

Despite the evolutionary distance between plants and algae, our study in *Chlamydomonas* also connected TOR activity regulation to a similar set of amino acids. Fluctuations in carbon

availability resulted in profound changes in TOR activity and the endogenous level of Ala, Glu, Gln, Leu, and Val, reinforcing the tight relationship among carbon fixation, amino acids, and TOR in photosynthetic organisms (Fig. 6). Furthermore, experiments performed with amino acid synthesis inhibitors demonstrated a direct connection between intracellular amino acid abundance and TOR. Blocking the synthesis of Ala or the branched chain amino acids Val and Leu resulted in a marked increase of other central amino acids and the up-regulation of TOR activity (Fig. 4). The amino acids identified in *Chlamydomonas* as potential TOR regulators are generated from the central carbon-skeleton donors pyruvate (Ala, Leu, and Val) and α -ketoglutarate (Glu and Gln) (SI Appendix, Fig. S5). Remarkably, a similar conclusion was reached in *Arabidopsis* since addition of amino acids derived from pyruvate or the nitrogen-assimilation pathway exhibited the highest TOR-activating capacity (17). The same study also concluded that external supply of amino acids originating from glycolate (Gly, Ser) and sulfur-assimilation (Cys) pathways led to high activation of TOR (17). However, the endogenous levels of Gly, Ser, and Cys followed an opposite trend to TOR activation in *Chlamydomonas* (SI Appendix, Fig. S5), precluding these amino acids as potential regulators of TOR activity in response to carbon availability.

The molecular mechanisms by which TOR perceives amino acids have been reported only in yeast and mammals. Yeast TORC1 seems to sense Leu availability through the Leu-transfer RNA synthetase (45). In mammalian cells, the cytosolic proteins SESTRIN2 and CASTOR1 have been identified respectively as specific sensors of Leu and Arg acting upstream of mTORC1 (5). How mTORC1 perceives Gln is unclear, but it has been reported that activation of mTORC1 by Gln occurs via glutaminolysis (46). Neither orthologs of Leu and Arg sensors nor upstream mTORC1 regulators have been identified in plant and algal genomes, suggesting that the TOR pathway might have experienced specific evolutionary adaptations in the green lineage. Unlike yeast and mammals, algae and plants are autotrophic and can synthesize all amino acids using CO_2 as the sole carbon source. Thus, photosynthetic eukaryotes might have developed unique mechanisms to signal carbon and amino acid sufficiency to the TOR pathway.

The finding that the *Chlamydomonas* starchless mutant *sta6* displays excessive TOR activity provided a further connection of carbon assimilation and amino acids to TOR signaling. Our results indicate that the inability of *sta6* cells to synthesize starch redirects part of the assimilated carbon to the synthesis of amino acids (Fig. 5), as revealed by the higher abundance detected in the *sta6* mutant of most amino acids, notably Gln, which increased eight times. Given the direct link identified in this study between amino acids and TOR (Fig. 4), it is plausible that redirection of fixed carbon to the synthesis of amino acids boosted TOR activity in the *sta6* mutant (Fig. 6). Supporting this conclusion, we found that inhibition of carbon fixation or photosynthesis abolished the hyperactivation of TOR in *sta6* cells (Fig. 5). The TOR pathway has been shown to regulate starch metabolism in plants and algae. Mutations in the *LST8-1* gene or down-regulation of *AtTOR* expression triggers starch accumulation in *Arabidopsis* (47, 48). Similarly, treatment of *Chlamydomonas* or the unicellular red alga *Cyanidioschyzon merolae* with rapamycin increases the starch content (26, 49). However, the impact of starch deficiency on plant TOR signaling has not been explored yet. Our study suggests that starch might regulate cell growth in *Chlamydomonas* since starch deficiency activates TOR, the main growth-promoting pathway in the cell. This hypothesis is in agreement with a previous study in plants showing that starch acts as a major integrator in the regulation of plant growth (50).

In conclusion, we have shown that CO_2 fixation and photosynthesis activate TOR signaling in *Chlamydomonas*, likely

through the synthesis of key amino acids. The regulation of TOR and cell growth by inorganic carbon might have biotechnological implications in algae and plants. Photosynthetic organisms are responsible for converting sunlight and CO₂ into organic matter and are therefore visualized as a resource for the renewable fuel industry and a solution to mitigate the problem of raising concentrations of atmospheric CO₂ (51). Therefore, modulation of TOR activity by inorganic carbon might help to improve biomass productivity in algae and plants, directly influencing agricultural yield or biofuel production.

Materials and Methods

C. reinhardtii Strains and Growth Conditions. *C. reinhardtii* strains used in this study were wild-type 4A+, *cw15*, *sta6*, and complemented *sta6* (termed as C6) and are available as CC-4051, CC-4349, CC-4348, and CC-4567, respectively, from the Chlamydomonas Resource Center (<https://www.chlamycollection.org/>). *Chlamydomonas* cells were grown under standard illumination (~50 $\mu\text{E m}^{-2} \text{s}^{-1}$ from light-emitting diode lamps) in HSM or TAP medium (38) on an orbital shaker (100 rpm) at 25 °C. When required, cells in exponential growth phase (~2 $\times 10^6$ cells mL⁻¹) were treated with HCO₃⁻ (Sigma-Aldrich, 55761), GLA (Sigma-Aldrich, G-9376), rapamycin (rap; Cayman Chemical, 53123-88-9), DCMU (Sigma-Aldrich, D7763), SMM (Sigma-Aldrich, 34224), or AOA (Sigma-Aldrich, C-13408) at the indicated concentrations and time. For light-to-dark transition experiments, cells grown in HSM were transferred from standard illumination to complete darkness for the indicated time. Growth rates were estimated during exponential growth phase according to the formula $\mu = \ln(N/N_0)/t$, where N_0 and N represent the cell number at $t = 0$ h and $t = 24$ h, respectively. μ is expressed in h⁻¹. Cell number was determined using a Countess II FL Automated Cell Counter (Invitrogen).

Protein Preparation, Western Blot Assays, and TOR Activity Determination. Protein electrophoresis in denaturing conditions was performed as previously described (25). *Chlamydomonas* cells from liquid cultures were collected by centrifugation (4,000 $\times g$, 2 min), washed in lysis buffer [50 mM Tris-HCl (pH 7.5)], and resuspended in a minimal volume of the same buffer. Cells were lysed by two cycles of slow freezing to -80 °C followed by thawing at room temperature. The soluble protein cell extract was separated from the insoluble fraction by centrifugation (15,000 $\times g$, 20 min, 4 °C). Proteins were quantified using the Coomassie dye binding method (Bio-Rad, 500-0006) as described by the manufacturer.

For immunoblot analyses, total protein extracts (15 to 40 μg) were subjected to sodium dodecyl sulfate–polyacrylamide gel electrophoresis and then transferred to either polyvinylidene fluoride membrane (Millipore, IPVH00010) previously activated in methanol for P-RPS6 detection or nitrocellulose membrane (Amersham, 10600003) for detection of other proteins. Primary antibodies raised against *Chlamydomonas* P-RPS6 and RPS6 (32), TOR (21), and LST8 (21) proteins and secondary anti-rabbit (Sigma-Aldrich, A6154) were diluted 1:6,000, 1:6,000, 1:1,000, 1:6,000, and 1:10,000, respectively, in phosphate-buffered saline containing 0.1% (vol/vol) Tween-20 (Applichem, A4974) and 5% (wt/vol) milk powder (Applichem, A0830). Proteins were detected with the Luminata Crescendo Millipore immunoblotting detection system (Millipore, WBLUR0500) and visualized using a ChemiDoc Imaging System (Bio-Rad). Coomassie brilliant blue-stained gels were used as protein loading control.

For determination of the phosphorylation status of RPS6, phosphorylated (P-RPS6) and total RPS6 were quantified using the ImageLab

software (Bio-Rad), and the P-RPS6/RPS6 ratio was calculated as previously described (32).

Amino Acid Analysis. To determine the amino acid profile, *Chlamydomonas* cells growing exponentially (~2 $\times 10^6$ cells mL⁻¹) under the indicated treatment were collected by centrifugation (4,000 $\times g$, 2 min) and immediately frozen in liquid nitrogen. Cells were then lyophilized and 2 mg of dried weight for each condition were used to extract amino acids. Cells were resuspended with HCl 0.1 N, mixed by vortexing, and then incubated on ice for 1 h. After centrifugation (15,000 $\times g$, 15 min) at 4 °C to remove cells debris, the supernatant was transferred to a fresh tube and used to analyze the amino acid content by mass spectrometry (Sciex 6500+ QTRAP hybrid triple quadrupole liquid chromatography with tandem mass spectrometry). Amino acids were quantified using a standard amino acid mixture (Sigma-Aldrich). At least four biological replicates were analyzed for each condition.

Oxygen Evolution Measurement. *Chlamydomonas* cells growing autotrophically in HSM medium were incubated with bicarbonate, DCMU, or GLA for the indicated time, and then 2 mL of cells (~2 $\times 10^6$ cells mL⁻¹) was used to determine oxygen evolution at 25 °C with continuous stirring in a Clark-type electrode (Chlorolab 2+ System; Hansatech). Photosynthetic rate was calculated as the difference between oxygen production in the light and oxygen consumption in the dark. Oxygen production was analyzed for 5 min at 60 $\mu\text{mol photons m}^{-2} \text{s}^{-1}$. Cells were then exposed to darkness for 5 min to calculate oxygen consumption.

Chlorophyll Fluorescence Measurement. Chlorophyll fluorescence measurements were performed using a DUAL-PAM-100 (Walz). *Chlamydomonas* cells growing autotrophically in HSM medium were incubated with DCMU or GLA for the indicated time, and then 2 mL of cells (~2 $\times 10^6$ cells mL⁻¹) was used to determine relative electron transport rate (rETR) and maximum photochemical efficiency (Fv/Fm). Cells were dark adapted for 15 min with constant stirring to obtain the Fv/Fm ratio. Cells were then exposed to 50 $\mu\text{mol photons m}^{-2} \text{s}^{-1}$ for 5 min to quantify rETR values.

Statistics. Data from at least three independent experiments were analyzed using SigmaPlot 11 software. Two-tailed Student's *t* tests were used to compare different strains, different growing conditions, and different treatments. One-way ANOVA followed by Bonferroni's post hoc comparisons tests were used to analyze the temporal changes in the different treatments. $P < 0.05$ was taken as the threshold for statistical significance. Single (*), double (**), and triple (***) asterisks indicate a significant difference: $P < 0.05$, $P < 0.01$, and $P < 0.001$, respectively. For amino acid analysis, heat map showing the fold changes were generated using the MeV software. Amino acid correlations were clustered with hierarchical clustering using Pearson correlation for the distance measure and average linkage for the linkage method. A summary of the statistical analysis of experiments shown in main and supplementary figures can be found in *SI Appendix, Tables S1 and S2*, respectively.

Data Availability. All study data are included in the article and/or *SI Appendix*.

ACKNOWLEDGMENTS. This work was supported in part by Ministerio de Ciencia y Tecnología (Grants PGC2018-099048-B-I00 to J.L.C. and PID2019-110080GB-I00 to M.E.P.-P.) and Consejo Superior de Investigaciones Científicas (Grant 202040I006 to M.E.P.-P.). We thank Carlos Parejo for technical assistance with the analysis of amino acid profiles.

- M. Laplante, D. M. Sabatini, mTOR signaling in growth control and disease. *Cell* **149**, 274–293 (2012).
- S. Wullschlegel, R. Loewith, M. N. Hall, TOR signaling in growth and metabolism. *Cell* **124**, 471–484 (2006).
- R. Loewith *et al.*, Two TOR complexes, only one of which is rapamycin sensitive, have distinct roles in cell growth control. *Mol. Cell* **10**, 457–468 (2002).
- A. González, M. N. Hall, Nutrient sensing and TOR signaling in yeast and mammals. *EMBO J.* **36**, 397–408 (2017).
- R. L. Wolfson, D. M. Sabatini, The dawn of the age of amino acid sensors for the mTORC1 pathway. *Cell Metab.* **26**, 301–309 (2017).
- M. Binda *et al.*, The Vam6 GEF controls TORC1 by activating the EGO complex. *Mol. Cell* **35**, 563–573 (2009).
- L. Fu, P. Wang, Y. Xiong, Target of rapamycin signaling in plant stress responses. *Plant Physiol.* **182**, 1613–1623 (2020).
- C. Ingargiola, G. Turquetto Duarte, C. Robaglia, A. S. Leprince, C. Meyer, The plant target of rapamycin: A conduit TOR of nutrition and metabolism in photosynthetic organisms. *Genes (Basel)* **11**, 1285 (2020).
- Y. Mugume, Z. Kazibwe, D. C. Bassham, Target of rapamycin in control of autophagy: Puppet master and signal integrator. *Int. J. Mol. Sci.* **21**, 8259 (2020).
- M. Schepetilnikov *et al.*, TOR and S6K1 promote translation reinitiation of uORF-containing mRNAs via phosphorylation of eIF3h. *EMBO J.* **32**, 1087–1102 (2013).
- P. Wang *et al.*, Reciprocal regulation of the TOR kinase and ABA receptor balances plant growth and stress response. *Mol. Cell* **69**, 100–112.e6 (2018).
- Y. Xiong *et al.*, Glucose-TOR signalling reprograms the transcriptome and activates meristems. *Nature* **496**, 181–186 (2013).
- P. Cao *et al.*, Homeostasis of branched-chain amino acids is critical for the activity of TOR signaling in *Arabidopsis*. *eLife* **8**, e50747 (2019).
- M. Schaufelberger *et al.*, Mutations in the *Arabidopsis* ROL17/isopropylmalate synthase 1 locus alter amino acid content, modify the TOR network, and suppress the root hair cell development mutant *lrx1*. *J. Exp. Bot.* **70**, 2313–2323 (2019).
- B. M. O'Leary, G. G. K. Oh, C. P. Lee, A. H. Millar, Metabolite regulatory interactions control plant respiratory metabolism via target of rapamycin (TOR) kinase activation. *Plant Cell* **32**, 666–682 (2020).

16. D. Deprost *et al.*, The Arabidopsis TOR kinase links plant growth, yield, stress resistance and mRNA translation. *EMBO Rep.* **8**, 864–870 (2007).
17. Y. Liu *et al.*, Diverse nitrogen signals activate convergent ROP2-TOR signaling in Arabidopsis. *Dev. Cell* **56**, 1283–1295.e5 (2021).
18. S. Díaz-Troya, M. E. Pérez-Pérez, F. J. Florencio, J. L. Crespo, The role of TOR in autophagy regulation from yeast to plants and mammals. *Autophagy* **4**, 851–865 (2008).
19. A. Shemi, S. Ben-Dor, A. Vardi, Elucidating the composition and conservation of the autophagy pathway in photosynthetic eukaryotes. *Autophagy* **11**, 701–715 (2015).
20. M. E. Pérez-Pérez, I. Couso, J. L. Crespo, The TOR signaling network in the model unicellular green alga *Chlamydomonas reinhardtii*. *Biomolecules* **7**, 54 (2017).
21. S. Díaz-Troya, F. J. Florencio, J. L. Crespo, Target of rapamycin and LST8 proteins associate with membranes from the endoplasmic reticulum in the unicellular green alga *Chlamydomonas reinhardtii*. *Eukaryot. Cell* **7**, 212–222 (2008).
22. J. L. Crespo, S. Díaz-Troya, F. J. Florencio, Inhibition of target of rapamycin signaling by rapamycin in the unicellular green alga *Chlamydomonas reinhardtii*. *Plant Physiol.* **139**, 1736–1749 (2005).
23. S. Díaz-Troya *et al.*, Inhibition of protein synthesis by TOR inactivation revealed a conserved regulatory mechanism of the BiP chaperone in *Chlamydomonas*. *Plant Physiol.* **157**, 730–741 (2011).
24. S. Imamura *et al.*, Target of rapamycin (TOR) plays a critical role in triacylglycerol accumulation in microalgae. *Plant Mol. Biol.* **89**, 309–318 (2015).
25. M. E. Pérez-Pérez, F. J. Florencio, J. L. Crespo, Inhibition of target of rapamycin signaling and stress activate autophagy in *Chlamydomonas reinhardtii*. *Plant Physiol.* **152**, 1874–1888 (2010).
26. J. Jüppner *et al.*, The target of rapamycin kinase affects biomass accumulation and cell cycle progression by altering carbon/nitrogen balance in synchronized *Chlamydomonas reinhardtii* cells. *Plant J.* **93**, 355–376 (2018).
27. U. Mubeen, J. Jüppner, J. Alpers, D. K. Hinch, P. Giavalisco, Target of rapamycin inhibition in *Chlamydomonas reinhardtii* triggers de novo amino acid synthesis by enhancing nitrogen assimilation. *Plant Cell* **30**, 2240–2254 (2018).
28. V. Roustan, W. Weckwerth, Quantitative phosphoproteomic and system-level analysis of TOR inhibition unravel distinct organellar acclimation in *Chlamydomonas reinhardtii*. *Front. Plant Sci.* **9**, 1590 (2018).
29. E. G. Werth *et al.*, Investigating the effect of target of rapamycin kinase inhibition on the *Chlamydomonas reinhardtii* phosphoproteome: From known homologs to new targets. *New Phytol.* **221**, 247–260 (2019).
30. S. Upadhyaya, S. Agrawal, A. Gorakshakar, B. J. Rao, TOR kinase activity in *Chlamydomonas reinhardtii* is modulated by cellular metabolic states. *FEBS Lett.* **594**, 3122–3141 (2020).
31. I. Couso *et al.*, Synergism between inositol polyphosphates and TOR kinase signaling in nutrient sensing, growth control and lipid metabolism in *Chlamydomonas*. *Plant Cell* **28**, 2026–2042 (2016).
32. I. Couso *et al.*, Phosphorus availability regulates TORC1 signaling via LST8 in *Chlamydomonas*. *Plant Cell* **32**, 69–80 (2020).
33. D. D. Wykoff, A. R. Grossman, D. P. Weeks, H. Usuda, K. Shimogawara, Psr1, a nuclear localized protein that regulates phosphorus metabolism in *Chlamydomonas*. *Proc. Natl. Acad. Sci. U.S.A.* **96**, 15336–15341 (1999).
34. X. Johnson, J. Alric, Central carbon metabolism and electron transport in *Chlamydomonas reinhardtii*: Metabolic constraints for carbon partitioning between oil and starch. *Eukaryot. Cell* **12**, 776–793 (2013).
35. Y. Wang, D. J. Stessman, M. H. Spalding, The CO₂ concentrating mechanism and photosynthetic carbon assimilation in limiting CO₂: How *Chlamydomonas* works against the gradient. *Plant J.* **82**, 429–448 (2015).
36. G. Amoroso, D. Sultemeyer, C. Thyssen, H. P. Fock, Uptake of HCO₃ and CO₂ in cells and chloroplasts from the microalgae *Chlamydomonas reinhardtii* and *Dunaliella tertiolecta*. *Plant Physiol.* **116**, 193–201 (1998).
37. S. Takahashi, N. Murata, Interruption of the Calvin cycle inhibits the repair of Photosystem II from photodamage. *Biochim. Biophys. Acta* **1708**, 352–361 (2005).
38. E. H. Harris, *The Chlamydomonas Sourcebook*, (Academic Press, San Diego, 2009).
39. M. E. Hartnett, J. R. Newcomb, R. C. Hodson, Mutations in *Chlamydomonas reinhardtii* conferring resistance to the herbicide sulfometuron methyl. *Plant Physiol.* **85**, 898–901 (1987).
40. J. V. Moroney, B. J. Wilson, N. E. Tolbert, Glycolate metabolism and excretion in *Chlamydomonas reinhardtii*. *Plant Physiol.* **82**, 821–826 (1986).
41. S. Saroussi *et al.*, Alternative outlets for sustaining photosynthetic electron transport during dark-to-light transitions. *Proc. Natl. Acad. Sci. U.S.A.* **116**, 11518–11527 (2019).
42. C. Zabawinski *et al.*, Starchless mutants of *Chlamydomonas reinhardtii* lack the small subunit of a heterotetrameric ADP-glucose pyrophosphorylase. *J. Bacteriol.* **183**, 1069–1077 (2001).
43. I. K. Blaby *et al.*, Systems-level analysis of nitrogen starvation-induced modifications of carbon metabolism in a *Chlamydomonas reinhardtii* starchless mutant. *Plant Cell* **25**, 4305–4323 (2013).
44. Y. Li *et al.*, *Chlamydomonas* starchless mutant defective in ADP-glucose pyrophosphorylase hyper-accumulates triacylglycerol. *Metab. Eng.* **12**, 387–391 (2010).
45. G. Bonfils *et al.*, Leucyl-tRNA synthetase controls TORC1 via the EGO complex. *Mol. Cell* **46**, 105–110 (2012).
46. R. V. Durán *et al.*, Glutaminolysis activates Rag-mTORC1 signaling. *Mol. Cell* **47**, 349–358 (2012).
47. C. Caldana *et al.*, Systemic analysis of inducible target of rapamycin mutants reveal a general metabolic switch controlling growth in *Arabidopsis thaliana*. *Plant J.* **73**, 897–909 (2013).
48. M. Moreau *et al.*, Mutations in the *Arabidopsis* homolog of LST8/GβL, a partner of the target of Rapamycin kinase, impair plant growth, flowering, and metabolic adaptation to long days. *Plant Cell* **24**, 463–481 (2012).
49. I. Pancha *et al.*, Target of rapamycin-signaling modulates starch accumulation via glycogenin phosphorylation status in the unicellular red alga *Cyanidioschyzon merolae*. *Plant J.* **97**, 485–499 (2019).
50. R. Sulpice *et al.*, Starch as a major integrator in the regulation of plant growth. *Proc. Natl. Acad. Sci. U.S.A.* **106**, 10348–10353 (2009).
51. S. S. Merchant, J. Kropat, B. Liu, J. Shaw, J. Warakanont, TAG, you're it! *Chlamydomonas* as a reference organism for understanding algal triacylglycerol accumulation. *Curr. Opin. Biotechnol.* **23**, 352–363 (2012).